FACULTY OF HEALTH AND MEDICAL SCIENCES
UNIVERSITY OF COPENHAGEN

PhD thesis

Mette Kjølhede Nedergaard, MD

^{18}F-FET/PET to monitor tumour development and assess treatment response in Glioblastoma multiforme

- Multimodal imaging in orthotopic xenograft models

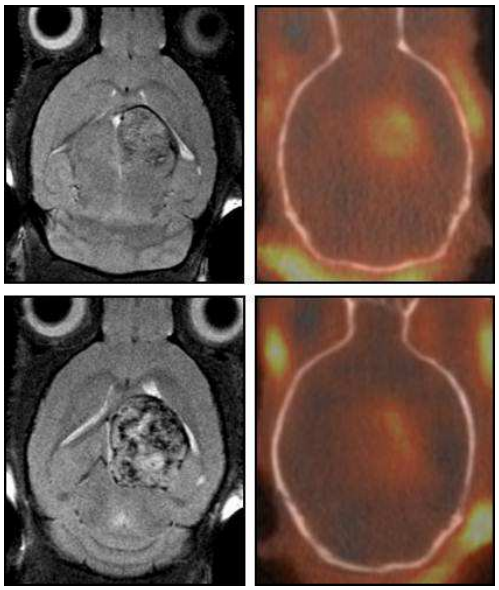

Academic advisors:
Professor Andreas Kjær, MD, PhD, DMSc
Ulrik Lassen, MD, PhD
Marie-Therésé Stockhausen, MSc, PhD

Submitted: July 18, 2014

PREFACE

This thesis has been submitted to the Graduate School at the Faculty of Health and Medical Sciences, University of Copenhagen, Denmark, in order to fulfil the requirements for obtaining the PhD degree in health and medical science.

The thesis is based on experimental work carried out from August 2011 to July 2014 under the supervision of principal supervisor Professor Andreas Kjær (MD, PhD, DMSc) and project supervisors Ulrik Lassen (MD, PhD) and Marie-Therésé Stockhausen (MSc, PhD). The majority of experiments were conducted at the Department of Clinical Physiology, Nuclear Medicine and Cluster for Molecular Imaging, Copenhagen University Hospital and Faculty of Health and Medical Sciences, University of Copenhagen. Establishment and maintenance of the cell cultures used for the *in vivo* experiments were performed at the Department of Radiation Biology, Copenhagen University Hospital, Denmark.

Financial support was received from: Danish Cancer Research Foundation; The Danish Cancer Society; Danish National Advanced Technology Foundation; AP Møller Foundation; The Lundbeck Foundation; Novo Nordisk Foundation; Svend Andersen Foundation; The John and Birgitte Meyer Foundation; Danish Research Council and Rigshospitalets Research Foundation.

ACKNOWLEDGEMENT

I would like to express my gratitude to a number of people who have been important to me during my PhD-project.

I am first of all very grateful to my team of supervisors for complementing each other in their guidance, valuable support and enthusiastic encouragement. I always left project-meetings full of energy, with concreate answers to my questions and with renewed and stronger confidence in the project. Professor Andreas Kjær, my principal supervisor, for sharing your huge scientific experience and for creating a research environment where it often appears as if "only the sky is the limit". Ulrik Lassen, my co-supervisor, for keeping the clinical perspective, for always answering urgent mails and for initiating project-meetings, which helped me stay focused. Marie-Therésé Stockhausen, my project supervisor, for your critical readings, your spot-on questions and our many motivating discussions. A special thanks to Professor Liselotte Højgaard for providing excellent research-facilities.

Thanks to my present colleagues at the Department of Radiation Biology for creating a positive and supportive atmosphere. Especially, Hans Skovgaard Poulsen for useful critique and mentoring. Mette Villingshøj and Pia Pedersen for their technical assistance and for their diligent introduction to work in the laboratory. Karina Kristoffersen for your positive attitude and for valuable collaboration in establishing the orthotopic GBM model. Signe Regner Michaelsen for in depth scientific discussions, for always helping with experimental work when needed, and for her critical readings and constructive suggestions on this thesis.

Furthermore, I am grateful to Tina Binderup for introducing me to both mice and humans at the Cluster for Molecular Imaging (CMI), and for her patience and support when teaching me how to perform MicroPET and image analysis. Henrik El-Ali for help with the technical aspects of MicroMRI, PET and CT. Anne Mette Fisker Hag for stepping in with practical assistance, Jytte Oxbøl for introducing me to gene expression analysis and for her assistance in the laboratory. I am also thankful to all my colleagues at CMI for contributing to a workplace atmosphere characterized by a helpful, humoristic and social attitude.

Also thanks to Babloo Lukram and Michelle Kaijer for assistance with immunohistochemistry and Chief radiochemist Jacob Madsen and staff at the Department of Clinical Physiology, Nuclear Medicine & PET for performing the radiochemical work and providing the PET radiotracers used in the thesis.

I am also very grateful for the financial support from the Danish Cancer Research Foundation; The Danish Cancer Society; Danish National Advanced Technology Foundation; AP Møller Foundation; The Lundbeck Foundation; Novo Nordisk Foundation; Svend Andersen Foundation; The John and Birgitte Meyer Foundation; Danish Research Council and Rigshospitalets Research Foundation.

The warmest thanks to my husband Søren for your support, for providing additional perspectives and for accepting that sometimes mice come before men. Finally, my daughters Emma and Rosa for lighting up every day.

LIST OF PAPERS

This Ph.D. thesis is based on the following manuscripts, which are included in the appendix and referred to in the text by their Roman numerals:

I Nedergaard MK, Kristoffersen K, Michaelsen SR, Madsen J, Poulsen HS, Stockhausen MT, Ulrik Lassen U and Kjaer A. The Use of Longitudinal ^{18}F-FET MicroPET Imaging to Evaluate Response to Irinotecan in Orthotopic human Glioblastoma Multiforme Xenografts.

PLoS One. 2014;9(2):e100009

II Nedergaard MK, Michaelsen SR, Perryman L, Erler, Poulsen HS, Lassen U, Stockhausen MT and Kjaer A. Comparison of ^{18}F-FET and ^{18}F-FLT MicroPET for the assessment of anti-VEGF efficacy in an orthotopic model of glioblastoma.

Submitted to *The Journal of Nuclear Medicine* June 02, 2014

III Nedergaard MK, Michaelsen SR, Urup T, Broholm H, El Ali H, Poulsen HS, Stockhausen MT, Kjaer A and Lassen U. ^{18}F-FET MicroPET and MicroMRI for anti-VEGF and anti-PlGF response assessment in an orthotopic murine model of human glioblastoma.

Submitted to *Neuro-Oncology* July 18, 2014

ABBREVIATIONS

BBB	Blood-brain-barrier
bCSC	Brain cancer stem-like cells
bFGF	Basic fibroblast growth factor
BLI	Bioluminescence imaging
Bq	Becquerel
^{11}C-MET	L-methyl-^{11}C-methionine
CD31	Cluster of differentiation 31
CT	Computer tomography
Cq	Quantification cycle
DWI	Diffusion-weighted imaging
DTI	Diffusion tensor imaging
EGF	Epidermal growth factor
EGFR	Epidermal growth factor receptor
^{18}F-FDG	2'-deoxy-2'-^{18}F-fluoro-D-glucose
^{18}F-FET	O-(2-^{18}F-fluoroethyl)-L-tyrosine
^{18}F-FLT	3'-deoxy-3'-^{18}F-flurothymidine
FWHM	Full-with-at-half-maximum
GBM	Glioblastoma multiforme
GOI	Gene of interest
IHC	Immunohistochemistry
i.p.	Intraperitoneal
i.v.	Intravenously
LAT	L-type amino acid transporter
LUC	Luciferase
MAP	Maximum a posteriori
MRI	Magnetic resonance imaging
MRS	Magnetic resonance spectroscopy

MVD	Micro-vessel density
NRQs	Normalized relative quantities
OS	Overall survival
PWI	Perfusion-weighted imaging
PET	Positron emission tomography
PlGF	Placental growth factor
PFS	Progression-free survival
PVE	Partial volume effect
qPCR	Quantitative real-time polymerase chain reaction
ROI	Region of interest
RT	Radiotherapy
SD	Standard deviation
SEM	Standard error of mean
SUV	Standardized uptake value
SUV_{max}	Maximum standardized uptake value
SUV_{mean}	Mean standardized uptake value
T/B	Tumour-to-background
TK1	Thymidine kinase 1
TP53	Tumor protein 53
VEGF	Vascular endothelial growth factor
VEGF-R	Vascular endothelial growth factor receptor

DANISH SUMMARY - DANSK RESUMÉ

Introduktion

Glioblastoma multiforme (GBM) er den hyppigste og mest aggressive form for hjernekræft hos voksne. På trods af intensiv behandling er prognosen for patienter diagnosticeret med GBM dårlig med en median overlevelse på under 1,5 år. Korrekt og tidlig vurdering af en behandlings-effekt er fundamentalt for at opnå bedst mulig sygdoms-kontrol for de fleste typer af kræft. Magnetisk resonans imaging (MRI) bruges til behandlings-monitorering af patienter med GBM. Da MRI primært måler ændringer i anatomisk tumorstørrelse, kan der først adskilles mellem responderende og ikke-responderende patienter efter typisk 1-2 måneders behandling. Derudover er det ved brug af MRI vanskeligt at bestemme effekten af både anti-angiogenese behandling og radioterapi, begge behandlinger der bruges til patienter med GBM. I kliniske studier har positron emission tomography (PET) med aminosyre analogen O-(2-^{18}F-fluoroethyl)-L-tyrosine (^{18}F-FET) i forhold til MRI vist sig at være bedre til at kunne skelne mellem tumorvæv og nekrose efter radioterapi. Ligeledes kunne ^{18}F-FET PET, tidligere end MRI måle en behandlingseffekt af anti-VEGF. Evidensen for brug af ^{18}F-FET PET til respons-monitorering er dog stadig begrænset, og mekanismerne for ^{18}F-FET optaget i hjernen er kun delvist belyst.

I denne afhandling blev anvendeligheden af ^{18}F-FET PET til evaluering af GBM yderligere undersøgt. Dette blev gjort vha. en præ-kliniske GBM model og ^{18}F-FET MicroPET, hvorved det var muligt at teste forskellige hypoteser vedrørende ^{18}F-FET optag i GBM.

Det specifikke formål med denne afhandling var dels at undersøge om ^{18}F-FET MicroPET kunne bruge til at monitorerer tumorvæksten i en intrakraniel (orthotop) GBM xenograft model, og dels at undersøge, om ^{18}F-FET MicroPET, sammenlignet med MRI og MicroPET med proliferations-traceren 3'-deoxy-3'-^{18}F-fluorothimidine (^{18}F-FLT), giver yderligere information om tumorvækst og behandlingseffekt i GBM.

Metoder

Humane GBM cancer celler blev injiceret ortotopisk ind i hjernen på mus og efter tumoranslag blev musene behandlet med kemoterapi (Irinotecan), angiogenese targeterende antistoffer (anti-VEGF eller anti-VEGF + anti-PLGF) eller kontrolbehandling. Tumorudviklingen og behandlingseffekten blev fulgt *in vivo* med ^{18}F-FET MicroPET og sammenlignet med andre billeddannende teknikker (MRI, bioluminescence og ^{18}F-FLT MicroPET). Desuden blev *in vivo* ^{18}F-FET optaget i hjernetumoren samt ^{18}F-FET behandlingseffekten sammenlignet med molekylær-biologiske ændringer i tumor vævet *ex vivo* vha. hhv. gen-ekspression analyse (for aminosyre transportørerne LAT1 og LAT2 samt proliferations markøren Ki67) og immunohistokemi (for kvantificering af micro-vessel density (MVD) og Ki67 proliferations-indekset).

Resultater og konklusion

I studie I fandt vi, at ^{18}F-FET MicroPET kan bruges til at monitorere tumorudviklingen samt til at vurdere en behandlingseffekt af Irinotecan i en ortotop xenograft GBM model. Derudover fandt vi, at ^{18}F-FET optaget var negativ korreleret med gene ekspressionen af LAT1 og LAT2 i xenograft tumorerne. I studie II fandt vi, at ^{18}F-FET og ^{18}F-FLT MicroPET giver forskellig information om tumorvækst og behandlingseffekt. I studie III fandt vi, at ^{18}F-FET MicroPET var bedre end MRI til at detekterer en behandlingseffekt. I alle 3 studier var behandling-effekten og ændringerne i ^{18}F-FET optaget ikke ledsaget af ændringer i Ki67 proliferations-indekset, men i studie II og III afspejlede ændringerne i ^{18}F-FET optaget ændringer i MVD. I studie II var der ingen overlevelses-gevinst i behandlingsgruppen, men i studie III blev ændringer i ^{18}F-FET optaget som et mål for anti-cancer effekt, underbygget af overlevelsesanalysen. ^{18}F-FET MicroPET kan således bruges til monitorering af tumorudviklingen samt til detektering af en behandlingseffekt i prækliniske ortotopiske GBM modeller. Yderligere studier er dog nødvendige for at bestemme, hvordan ^{18}F-FET optaget bedst måles, kvantificeres og bruges til præcis vurdering af anti-cancer effekt i ortotope GBM xenograft tumorer.

ENGLISH SUMMARY

Introduction

Glioblastoma multiforme (GBM) is the most common and aggressive type of brain-cancer in adults. Despite intensive treatment, the prognosis for patients diagnosed with GBM is poor with a median survival of less than 1.5 years. Accurate and early response assessment is fundamental to obtain optimal disease-control in most types of cancer. Magnetic resonance imaging (MRI) is used to monitor anti-cancer treatment in patients with GBM. As MRI primarily detects changes in anatomical tumour-size, differentiation between responding and non-responding patients requires typically 1-2 months of treatment. In addition, assessment of both anti-angiogenic treatment and radiotherapy (common treatments in GBM) is difficult using MRI. Compared to MRI, positron emission tomography (PET) with the amino-acid analogue O-(2-^{18}F-fluoroethyl)-L-tyrosine (^{18}F-FET) was in clinical studies superior to differentiate between tumour-tissue and necrosis caused by radiotherapy. Similarly, in GBM patients ^{18}F-FET PET detected anti-VEGF treatment-effects earlier than MRI. However, there is only limited evidence for the use of ^{18}F-FET PET to assess treatment response, and the mechanisms responsible for ^{18}F-FET uptake in GBM are only partly elucidated.

In the present thesis the feasibility of ^{18}F-FET PET to monitor GBM was further investigated. Using pre-clinical GBM models and ^{18}F-FET MicroPET, it was possible to test different hypothesis regarding ^{18}F-FET uptake in GBM.

The specific aim of the present thesis was partly to investigate if it was feasibly to use ^{18}F-FET MicroPET to monitor tumour-development in an intracranial GBM xenograft model, and partly to investigate if ^{18}F-FET MicroPET, as compared to MRI and MicroPET using the proliferation tracer 3'-deoxy-3'-^{18}F-fluorothimidine (^{18}F-FLT), reveal different information about tumour development and treatment response in GBM.

Methods

Human GBM cancer cells were orthotopically injected into the brain of mice, and at tumour take, mice were treated with chemotherapy (Irinotecan), antibodies targeting angiogenesis (anti-VEGF or anti-VEGF + anti-PLGF) or control-treatment. Tumour-development and treatment effect were monitored *in vivo* using ^{18}F-FET MicroPET and compared to other imaging modalities (MRI, bioluminescence and ^{18}F-FLT MicroPET). In addition, *in vivo* ^{18}F-FET uptake in the brain tumour and the ^{18}F-FET treatment response was compared to molecular changes in the tumour tissue *ex vivo* using gene expression analysis (for the amino-acid transporters LAT1 and LAT2 together with the proliferation-marker Ki67) and immunohistochemistry (assessing micro-vessel density (MVD) and the Ki67 proliferative index).

Results and conclusions

In study I, we showed that ^{18}F-FET MicroPET is feasible to monitor tumour-development and to assess a treatment response towards Irinotecan in an orthotopic xenograft GBM model. In addition, we found a negative correlation between ^{18}F-FET uptake and LAT1 and LAT2 expression in the xenograft tumours. In study II, we found that ^{18}F-FET MicroPET in comparison to ^{18}F-FLT MicroPET reveals different information about tumour-development and treatment-efficacy. In all studies, treatment effect and changes in the ^{18}F-FET uptake was undetectable when Ki67 proliferation was evaluated; however, in study II and III changes in ^{18}F-FET uptake reflected changes in MVD. In study II, no survival gain was observed in the treatment group; however, survival analysis confirmed changes in ^{18}F-FET uptake as a measure of anti-cancer efficacy in study III. In conclusion, ^{18}F-FET MicroPET is feasibly to monitor tumour-development and can be used to assess treatment-efficacy in pre-clinical orthotopic GBM xenografts. Still, further studies are necessary to elucidate how ^{18}F-FET uptake should be measured, quantified and used to most accurately assess anti-cancer activity in orthotopic GBM xenograft tumours.

TABLE OF CONTENTS

1 INTRODUCTION

Cancer patients often respond differently although they harbour the same type of tumour. With an increased understanding of human genetics, it has become apparent that equal primary cancers are heterogeneous in terms of genotypes and hence, respond differently to anti-cancer treatment. The search for biomarkers, that can predict how individual patients will respond to treatment, has therefore accelerated over the last years. Identification of genetic alterations and molecular characteristic specific to each patient could potentially predict drug efficacy and help selecting patients who most likely will benefit from a certain anti-cancer treatment. However, as resistance is inevitable with most anti-cancer treatments, biomarkers of treatment response are also needed to guide anti-cancer treatment and differentiate responding from non-responding patients. Thereby can non-responding patients avoid unnecessary side-effects from ineffective treatments, and other therapies can be pursued, and in addition can expensive anti-cancer medicine be spared. The most common and aggressive primary brain tumour is Glioblastoma multiforme (GBM) and the prognosis for patients diagnosed with GBM is poor[1]. Although some advancement in treatment outcome has been documented over the last two decades, therapies remain mainly palliative. As such, additional research, aiming to identify new treatments in GBM and strategies to identify biomarkers of response or resistance, are urgently needed. Positron emission tomography (PET) is used for non-invasive imaging of molecular processes *in vivo,* and depending on which radiotracer is used, PET can be used to assess treatment response and potentially as an early imaging biomarker of anti-cancer activity.

In animal models, new possible predictive biomarkers can be evaluated[2,3], and animal models are fundamental to validate and help prioritize the development of novel anti-cancer compounds. Further, in animal models it is possible to thoroughly investigate different molecular aspect of a new PET tracers (e.g. transport mechanisms) or new anti-cancer agents[2,4].

In the present thesis, tumour uptake of the PET radiotracer ^{18}F-FET was investigated preclinically in an intracranial (orthotopic) murine model of GBM. Primarily, we wanted to evaluate the feasibility of using ^{18}F-FET PET to monitor tumour development in mice with orthotopic human derived GBM. In addition, we wanted to evaluate ^{18}F-FET PET as a non-invasive imaging biomarker for early treatment response in GBM and further, to compare ^{18}F-FET uptake with the uptake of the proliferation tracer ^{18}F-FLT. When the present Ph.D. project was initiated, ^{18}F-FET PET was already used increasingly in clinical studies of GBM; however, there was no available literature describing ^{18}F-FET uptake longitudinally in orthotopic murine models of glioma[5-7].

2 AIMS AND HYPOTHESIS OF THE THESIS

The overall hypothesis of the present thesis is that ^{18}F-FET MicroPET can be used to monitor intracranial tumour development and furthermore, to evaluate response to anti-cancer treatments *in vivo* in an intracranial model of human GBM.

Three experimental studies with specific aims were conducted and included in the present thesis.

2.1 Specific aims

2.1.1 Study I

- To evaluate the feasibility of ^{18}F-FET MicroPET to monitor tumour development in an orthotopic xenograft GBM model.
- To evaluate ^{18}F-FET MicroPET as an early biomarker of treatment response of chemotherapy in an orthotopic xenograft GBM model.
- To evaluate if *in vivo* ^{18}F-FET tumour uptake in orthotopic GBM xenografts correlated with the gene expression of the proliferative marker Ki67 and with the amino acid transporters LAT1 and LAT2 in tumours *ex vivo*.

2.1.2 Study II

- To compare the potential of ^{18}F-FET and ^{18}F-FLT MicroPET as early biomarkers of treatment response towards anti-VEGF treatment in an orthotopic xenograft GBM model.
- To compare *in vivo* ^{18}F-FET tumour uptake in orthotopic GBM xenografts with the Ki67 proliferative index and micro-vessel density (MVD) in the xenograft tumours *ex vivo*.

2.1.3 Study III

- To use ^{18}F-FET MicroPET in combination with MicroMRI to evaluate treatment response of anti-VEGF monotherapy in an orthotopic xenograft GBM model.
- To use ^{18}F-FET MicroPET in combination with MicroMRI to evaluate combined treatment with anti-PlGF and anti-VEGF in an orthotopic xenograft GBM model.
- To compare *in vivo* ^{18}F-FET tumour uptake in orthotopic GBM xenografts with the Ki67 proliferative index and micro-vessel density (MVD) in the xenograft tumours *ex vivo*.
- To correlate treatment response of combined treatment with anti-PlGF and anti-VEGF with the gene expression of PlGF and VEGFR-1 in the xenograft tumours.

3 BACKGROUND

3.1 Glioblastoma multiforme

Brain tumours can be of primary (intracranial) or secondary (metastatic) origin, among which gliomas are the most frequent type of the primary brain tumours (PBT) accounting for approximately 50-70%[8]. Gliomas are classified and graded according to the World Health Organization (WHO) classification system[9]. The classification of gliomas is based on the histological appearance and the similarity with the different glial cells of the central nervous system (CNS), and it includes astrocytoma, oligodendroglioma, mixed oliogoastrocytoma and ependymomas. The grading of gliomas into either low-grade (WHO Grades I-II) or high-grade (WHO Grade III-IV) is dependent on histological criteria like nuclear atypia, mitotic activity, microvascular proliferation and necrosis (Figure 1). Grade III and IV tumours are considered as malignant gliomas, and GBM, which is the main focus of the presented studies, is classified as a grade IV astrocytoma, the most common and aggressive type of PBT in adults. In western countries, the yearly incidence of GBM is 3.5/100.000[8], and every year about 260 new cases of GBM are diagnosed in Denmark[10].

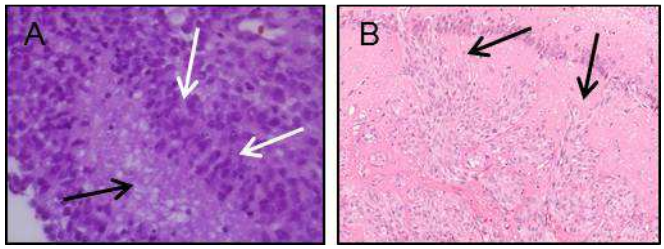

Figure 1: Histology of GBM. A) HE staining from a patient GBM tumour specimen showing necrosis (black arrow) and pseudo-palisading cells around the necrotic foci (white arrows). B) HE staining from a xenograft tumour showing infiltrative tumour cells (black arrows). Both histological features are common in GBM. Image A was kindly lend from Helle Broholm.

GBM arise either *de novo* as primary GBM or develops as secondary GBM from pre-existing lower grade gliomas, of which the majority is primary GBM that accounts for approximately 90%[8]. Despite a considerable heterogeneity of GBM in terms of pathology and gene expression, several common genetic alterations in the cellular pathways underlying GBM pathogenesis, growth and angiogenesis have been described. Amplification of the epidermal growth factor receptor (EGFR) gene and subsequent over-expression of EGFR is detected in about 40% of primary GBM, and it is the most frequent genetic alteration in primary GBM[11,12]. Additionally, mutation and inactivation in the phosphatase and tensin homolog (PTEN) gene and loss of heterozogosity (LOH) on chromosome 10 are the most common genetic mutation in primary GBM. Mutations in the tumour suppressor gene TP53 is most common in secondary GBM and isocitrate dehydrogenase 1 (IDH1) mutations has been identified as a molecular marker of secondary GBM[13,14]. Different treatment regimens are

aimed to target specific molecules in some of the molecular pathways involved in GBM[15,16]; however, because of the complex interconnection and cross-talk between different core oncogenic pathways the cancer cells are able to evade targeted therapy, and as written by Timothy Cloughesy and Paul Mischel: "Targeting the signal transduction pathways that a tumour needs to proliferate and survive is like trying to strike a moving target"[1].

The prognosis for patients diagnosed with GBM remains poor despite multimodal therapies, including maximal surgical resection and radiotherapy combined with chemotherapy as first-line treatment. The landmark phase III trial, published by Stupp *et al*. in 2005, demonstrated an improvement in median survival (14.6 vs. 12.1 months) and two-year survival rate (26.5% vs. 10.4%) in patients receiving concomitant and adjuvant temozolomide (TMZ, Temodal®) with radiotherapy (RT) over those receiving RT alone[17]. Subsequently, the "Stupp-regimen" became the new standard of care following debulking surgery for patients with newly diagnosed GBM. Recently, the anti-angiogenic agent Bevacizumab (Avastin®) has shown some promise with an increase in progression free survival in recurrent GBM; however, the effect on overall survival was only modest at best[18]. As such, advancements in the treatment of patients with GBM have occurred in the past decade, but they are modest and current therapies remain mainly palliative[18,19].

3.2 Targeting angiogenesis in GBM

It is widely accepted that the formation of new blood vessel, a process known as angiogenesis is, a fundamental process for tumour progression and metastasis. As GBM is one of the most vascularized solid tumours it has been an attractive target for anti-angiogenic therapy[20]. The regulation of angiogenesis is much more complex than it was initially thought[21]. However, in a simplified and classical model a scale illustrates the angiogenic balance and initiation of angiogenesis - the "angiogenic switch" - depends of the balance of pro-angiogenic molecules on one side and anti-angiogenic molecules on the other[21].

3.2.1 VEGF-A and PlGF signalling in GBM

One of the most analysed angiogenic growth factors is vascular endothelial growth factor A (VEGF-A), which is one of the five members of the VEGF gene family (VEGF-A, B, -C, -D and placental growth factor (PlGF)).The gene expression of VEGF-A is up-regulated in glioma tumour cells, and the level of VEGF-A production in astrocytomas correlate directly with the degree of malignancy[15,22,23]; therefore, VEGF-A is considered a major pro-angiogenic mediator in GBM[24]. Tumour cells are the main source of VEGF-A in GBM, and paracrine signalling, in which VEGF-A binds VEGF receptor 1 (VEGFR-1) and receptor 2 (VEGFR-2) located on endothelial cells, plays a crucial role in angiogenesis and progression of GBM[25]. Although VEGFR-1 and VEGFR-2 both are up-regulated in tumour endothelial cells in GBM[26-28], VEGFR-2 is considered the major receptor involved in angiogenesis and it binds all members of the VEGF gene family[26,29,30]. Recent studies have demonstrated co-expression of VEGF-A and VEGFRs in GBM cancer cells, which imply the existence of an autocrin loop in which tumour derived VEGF-A stimulates VEGFRs expressed by the tumour cells themselves[23,31]. Autocrine VEGFR-2 signalling in GBM may partly explain the limited

impact of anti-VEGF treatment in GBM patients as the stage of free extracellular VEGF-A (accessible by anti-VEGF treatment) potentially is bypassed[31].

In contrast to VEGFR-2, VEGFR-1 binds only VEGF-A, VEGF-B and PlG. The precise function of VEGFR-1 in angiogenesis and tumour growth is still under debate, and the downstream signalling events are not completely understood[32,33]. VEGFR-1 has been shown to mediate either anti- or pro-angiogenic signalling depending on different conditions and the activating ligand type[32]. Under physiological conditions, it has been suggested that VEGFR-1 acts primarily as a non-signalling "decoy" receptor for VEGF-A, and due to higher affinity of VEGF-A for VEGFR-1 than VEGFR-2, binding to VEGFR-1 results in less VEGF-A binding to VEGFR-2 and thus less pro-angiogenic signalling[32]. PlGF binds selectively to VEGFR-1 and its soluble isoform, termed sVEGFR-1. Under pathological conditions as cancer or wound healing, the expression of PlGF is up-regulated, and binding of PlGF to VEGFR-1 is in general considered as pro-angiogenic signalling[34,35]; however, under normal physiological conditions the role of PlGF is negligible, which is in contrast to the essential role of VEGF-A in both physiological and pathological angiogenesis[36].

PlGF is one of several growth factors that have been implicated in resistance to anti-angiogenic therapies in GBM, due to up-regulation of PlGF plasma levels in response to hypoxia and VEGF-A inhibition[37-39]. Tumour cells and some stromal cells express PlGF, whereas a variety of cells like endothelial cells, tumour cells, macrophages, bone marrow progenitors and stromal cells, such as fibroblasts express VEGFR-1[39]. As such, PlGF exerts multiple functions in malignant tumours; it is involved in migration and proliferation of VEGFR-1 expressing tumour cells, and it stimulates proliferation of endothelial cells and recruits VEGFR-1 expressing angiocompetent cells from the bone marrow, which promote neovascularization[39].

3.2.2 Anti-VEGF treatment

Several drugs that target the tumour vasculature have been introduced into clinical practice the past years. Bevacizumab is a humanized monoclonal antibody that by binding to VEGF-A prevents it from interacting with its receptors and as such neutralizes some of its biological effects. Bevacizumab is the first commercially available anti-angiogenic agent for the treatment of cancer and in combination with chemotherapy it has been approved for the treatment of different cancer types[40]. The US Food and Drug Administration (FDA) granted in May 2009 accelerated approval to Bevacizumab as a single agent for the treatment of recurrent GBM[41]. In contradiction, The European Medicines Agency (EMA) rejected the marketing application in November 2009 as they questioned the activity of Bevacizumab in recurrent GBM[42]. Two large phase III trials recently investigated the benefit of adding Bevacizumab to standard treatment as first-line therapy in GBM[43,44]. Although no significant effect on overall survival (OS) was observed, the progression-free survival (PFS) was increased. In addition, contradicting results regarding the impact of Bevacizumab on quality of life were reported. As such, future investigations are necessary to define when and how patients with GBM will benefit from Bevacizumab. Despite the controversy of Bevacizumab in GBM, H. A. Fine recently wrote in an editorial of the New England Journal of Medicine: "Bevacizumab remains the single most important therapeutic agent for glioblastoma since Temozolomide"[45]. However,

because it is only a fraction of patients that respond to Bevacizumab, and as resistance seems inevitable[29], there is a need for predictive and valid biomarkers that can identify responsive patients and detect emerging resistance. However, currently no predictive biomarkers have been validated[46]. Although VEGF pathway-targeting agents are the most clinically evaluated and developed of anti-angiogenic agents, and despite extensive pre-clinical research, the complex anti-tumour mechanisms of anti-VEGF agents, and the mechanisms of treatment resistance, are incompletely understood. Therefore, further studies are also needed to gain a better understanding of these mechanisms and to identify predictive biomarkers of treatment response[15,29].

3.2.3 Anti-PlGF treatment

Conflicting opinions exist on the value of neutralizing PlGF as a therapeutic target in oncology. Fischer *et al.* reported that anti-VEGF and anti-PlGF had an additive effect on tumour growth in several preclinical tumour models[37], and later results, regarding additive effect of anti-PLGF, were supported by a different group[47]. Conversely, other groups have found either no effect of PlGF antibodies on tumour growth[32], or even a suppressive effect of PlGF on tumour growth and angiogenesis[38,48-50]. Furthermore, it has been demonstrated that the expression of VEGFR-1 in cancer cells could determine the efficacy of anti-PlGF treatment; a hypothesis that was suggested as a possible explanation for the conflicting data in the literature[51]. Still, treatment efficacy of anti-PLGF in combination with anti-VEGF has not been evaluated in an orthotopic model of GBM.

3.3 Animal models of GBM

Drug development in cancer research is a multistep process that initially requires an understanding of the mechanisms and common genetic alteration in the cellular pathways underlying the human disease, followed by identification of possible targets for cancer therapy. *In vitro* models, using human cancer cell lines, are usually one of the first steps in this process. Still, the complex interactions between a tumour and its surrounding micro-environment are impossible to imitate under *in vitro* conditions, and as such, it can be argued that *in vivo* animal models better recapitulate the tumour-stroma relations.

In vivo models can be chemically induced, genetically engineered or be xenograft models. Rat and murine models of GBM are both used frequently and Barth and Kaur[52] have summarized the relative advantages and disadvantages of murine glioma models as compared to rat glioma models. The most important advantage of the intracranial rat model is, the larger brain size, which allows brain tumour imaging, with an acceptable resolution, using a less powerful and more accessible MRI scanner[53]. The murine models have other advantages which include that murine models are easier to genetically manipulate, and in addition, mice are cheaper to purchase and maintain.

For chemically induced brain tumour models, the rat has been the most widely used as brain tumours can be induced by exposure of N-nitroso compounds into the adult or pregnant rat[54]. In addition, cell lines derived from the chemically induced model subsequently can be used for the establishment of syngeneic, immunologically compatible models in immune-competent rats.

However, spontaneous rejection of the injected tumour cells, in addition to lack of the typical GBM histological characteristic like single cell invasion and microvascular proliferation, are some of the drawback of the chemically induced models in rats[53,54]. In contrast, a chemical induced murine model (GL261) demonstrate single-cell invasion and shared many histopathological markers with human GBM, which makes it a strong model for studying GBM therapies[53].

Genetically engineered models (GEMs) have primarily been studied in mice[2], as the ability to manipulate the rat genome has, until recently, been limited due to the available gene targeting technologies[55]. As such, available genetically engineered rat models are very few, and the experience with these models is sparse. To elucidate the molecular mechanisms, involved in the initiation and progression of GBM, several murine GEM, reflecting some of the common genetic mutations in GBM (e.g. EGFR amplification, TP53 and PTEN mutation) and more sophisticated models with multiple genetic aberrations, have been developed[2,54]. A major strength of the GEM and the chemical induced models is the use of immune-competent rodents as these models better recapitulates the complex interaction between the tumour and the host stroma cells, including the host immune-system. A drawback with GEM is that they are costly and more time intensive to produce and study[54]. In addition, they cannot in full recapitulate the unknown reasons for GBM development in humans as only known aberrations can by studied.

In xenograft models, human derived tumour cell lines or fresh human biopsies are injected or engrafted either orthotopically or subcutaneously into immune-deficient (nude or severe combined immunodeficiency (SCID) mice). A strength of the biopsy xenograft model is the ability to maintain the heterogeneity of the original patient tumour. However, these models are highly variable in terms of genetic alteration, growth rates and survival, which make standardization for experimental evaluation of new anti-cancer compounds difficult[54]. The prototypic xenograft model in GBM research was for many years to establish xenografts from the subcutaneous injection of 0.5-1.0 million glioma cells grown in serum-containing media. This often is a very reproducible and simple way to establish subcutaneous tumours. However, a major drawback of using serum-growing cancer cell lines is that the cancer cells lose important tumour hallmarks and may deviate from the original patient tumour after only a few *in vitro* passages[56]. Therefore, the traditional subcutaneous xenograft is not an optimal model to predict drug efficacy in humans[57].

As a consequence, new strategies of xenograft models have been investigated, and human glioma cells have been grown as spheres in well-defined serum-free media, with the addition of epidermal growth factor (EGF) and the basic fibroblast growth factor (bFGF). The so-called neurosphere cultures consist of both cells with stem-cell characteristic, known as brain cancer stem-like cells (bCSC), in addition to cells being more differentiated[58] and have, as compared to traditionally serum-cultured cell lines, been shown to more closely resemble the original patient tumour, both under *in vitro* and *in vivo* growth conditions[56]. According to the cancer-stem cell theory the bCSC are responsible for tumour initiation, progression and treatment resistance; although some controversy regarding the theory exist[59,60], and therefore, the bCSC represents a potential therapeutic target in GBM. Based on this, xenografts established with neurospheres (as compared to traditionally grown cell lines) is a more reliable model for preclinical investigations of new anti-cancer treatment as the tumour, according to the theory, is eradicated at its roots when the bCSC

are targeted[60]. One the major drawback with the xenograft models is the use of the immuno-compromised mice. The complex interaction between the cancer cells and the stromal micro-environment (including immune-cells) in patients is not mimicked in xenograft models, and hence, xenograft models are often considered unreliable in predicting treatment outcome in patients[54,57]. None of the currently available animal models fully recapitulates the genomic, histopatological and phenotypic signatures of human GBM[54], and each model has limitations. Therefore, depending on the nature of the experiments to be conducted, researchers must select the most appropriate model. However, whether it is a xenograft model or GEM mouse or rat model, orthotopic tumour models are considered better predictive models of drug efficacy than traditional subcutaneous models[61]. As such, more advanced imaging techniques like MRI and PET are necessary to monitor tumour development and response to anti-cancer treatment.

3.4 Imaging of GBM

3.4.1 Positron emission tomography (PET)

PET scanning in conjunction with administration of radiolabeled agents is a method for non-invasive assessment of metabolic processes or molecular targets, *in vivo*. Accordingly, PET is regarded as a "functional" imaging method, which is in contrast to the "anatomical" imaging using conventional magnetic resonance imaging (MRI). Radiolabeled agents, also termed radiotracers or tracers, are potential imaging biomarkers of treatment outcome, receptor status or different cellular processes depending on which molecules have been labelled. The radiotracers are used in a nano-molar amount to measure the biological target without disturbing the biological processes, which is a fundamental aspect of tracers[62].

Extensive research has been aimed at revealing disease specific targets, and subsequently, at developing tracers that are specific for these targets. Radiolabeled agents are composed of a short-lived positron emitting isotopes e.g. ^{18}F or ^{11}C attached to a biologically active molecule like in 2'-deoxy-2'-^{18}F-fluoro-D-glucose (^{18}F-FDG). Following intravenous injection, the tracer is distributed in the whole body and concentrated where the biologically active molecule is located. When the radiotracer undergoes decay a positron is emitted. Subsequently, the positron will travel a short distance (depending on the positron energy) and collide with an electron; creating a positron-electron annihilation. As a result of the annihilation, two 511 keV gamma photons at an angel of nearly 180° are emitted. The PET technique depends on the simultaneous detection of the two annihilation photons, which are registered by two opposing detectors in the PET scanner. The coincidence data are converted into sinograms and mathematically reconstructed into 3-dimensional images of tracer distribution[63].

The glucose analogue ^{18}F-FDG is the most widely used PET tracer; however, there are limitations when ^{18}F-FDG is used for imaging of brain tumours. A low tumour-to-background (T/B) uptake, due to the high physiological uptake in the brain, decreases the sensitivity of FDG, and uptake of glucose in inflammatory cells compromises the specificity of FDG in the brain[64]. Therefore, PET with radiolabeled amino acids like O-(2-^{18}F-fluoroethyl)-L-tyrosine (^{18}F-FET) and the radiolabeled

thymidine analogue 3'-deoxy-3'-^{18}F-fluorothimidine (^{18}F-FLT) are among the most promising radiotracers in clinical neuro-oncology as they overcome some of the limitations of ^{18}F-FDG PET[64].

3.4.1.1 ^{18}F-FET

The radiolabeled amino acid ^{18}F-FET has a low uptake in normal brain tissue, and therefore a high T/B ratio that increases the sensitivity and makes delineation of the tumour boundaries more precise[65]. Together with L-methyl-^{11}C-methionine (^{11}C-MET), ^{18}F-FET are at present the most widely used amino acid tracers for brain tumour imaging[64]. Multiple clinical studies have evaluated ^{11}C-MET PET for the visualization of brain tumours, and it has been successfully used in clinical neuro-oncology[66,67]. However, in clinical practice, ^{18}F-FET has logistic and economic advantages over ^{11}C-MET, due to the longer physical half-life of ^{18}Fcompared to ^{11}C (109.8 min vs. 20.4 min). From several clinical studies, there is increasing evidence for the use of ^{18}F-FET PET as an addition to MRI, as ^{18}F-FET PET adds complementary information about tumour growth and response to therapy[68-71]. However, as ^{18}F-FET only has become clinical available in recent years, data are still sparse and ^{18}F-FET PET needs validation[66]. Despite that ^{18}F-FET PET is widely used in the clinic, only a few animal studies (mostly in rats) have evaluated the bio-distribution and tumour accumulation of ^{18}F-FET in GBM xenografts[5-7,72].

In order to interpret results from ^{18}F-FET PET, it is essential to understand the mechanisms and the major factors that influence the transport and tumour uptake of ^{18}F-FET. Accumulation of ^{18}F-FET in brain tumour cells is presumable linked to high expression of the L-type amino acid transporters (LATs), which are the major transport system for large neutral amino acid[72,73]; however, the transport mechanisms of ^{18}F-FET have not been thoroughly investigated[73,74].

3.4.1.2 ^{18}F-FLT

Several preclinical and clinical studies, in many different cancer types, have evaluated the thymidine analogue ^{18}F-FLT for detection of cell proliferation and anti-cancer activity. In a recent meta-analysis, it was concluded that there is evidence for a strong correlation between Ki67 proliferative index and FLT uptake in lung, breast and brain cancer[75-78]. Dividing cells are supplied with nucleosides for DNA synthesis by two distinct pathways: the salvage pathway and the *de novo* pathway[78]. In the thymidine salvage pathway, plasma-membrane nucleoside transporters facilitate the transport of nucleosides including ^{18}F-FLT and thymidine across the cell membrane[79]. Phosphorylation of thymidine by thymidine kinase 1 (TK1) is followed by incorporation of thymidine into DNA whereas phosphorylation of ^{18}F-FLT results only in intracellular trapping. In the *de novo* synthesis pathway, thymidine is produced from deoxyuridine monophosphate (dUNM) and subsequently incorporated into DNA[78]. As ^{18}F-FLT only enters the cells through the thymidine salvage pathway, ^{18}F-FLT uptake potentially underestimate proliferations in *de novo* pathway dependent tumours[78].

In brain tumour imaging, ^{18}F-FLT has low accumulation in the normal brain and thereby a high T/B ratio, which potentially could increase the sensitivity. Therefore, several studies have evaluated the potential of ^{18}F-FLT PET in clinical neuro-oncology; as such, in malignant glioma ^{18}F-FLT PET has been used to differentiate between radiation necrosis and tumour recurrence[80] and for tumour grading[81,82]. In addition, a few small clinical studies have demonstrated that ^{18}F-FLT PET could serve as a potential early imaging biomarker of treatment response in glioma[83-86]. Similarly, in a few

preclinical studies in orthotopic glioma xenografts, ^{18}F-FLT MicroPET was an early marker of treatment efficacy[87-91]. However, a limited transport of FLT across the intact BBB has been demonstrated, which hampers the sensitivity of ^{18}F-FLT and potentially affects anti-angiogenic response assessment[92].

3.4.2 Magnetic Resonance Imaging (MRI)

Valid and reproducible response criteria are fundamental for clinicians to make decisions about continuation of effective therapy and conversely, modification or termination of ineffective treatment for individual patients and in clinical trials, as it enables response rates to be compared between different studies. Until recently, the "Macdonal criteria" have been the standard criteria for assessing GBM response, and the evaluation was based on magnetic resonance imaging (MRI) and relied on contrast enhancement and T1-weighted images as a proxy for tumour size. Because of important limitations in the Macdonal criteria, the Response Assessment Neuro-Oncology (RANO) working Group has developed new guidelines for treatment response in brain tumours. The new criteria also consider non-enhancement T2 and fluid-attenuated invasion recovery (FLAIR) images in addition to T1-weighted tumour size. Clinical status and corticosteroid dose are also considered in the criteria[93]. However, there are still difficulties in assessing true tumour response because contrast enhancing and non-enhancing regions are non-specific and are influenced by different processes, such as sub-acute radiation effects, postoperative changes, changes in glucocorticoid dosage as well as anti-angiogenic treatments that affect the permeability of the tumour vasculature [94,95]. In realization of the limitations of the RANO criteria, PET with various radiotracers (like ^{18}F-FET and ^{18}F-FLT) have been investigates, to more accurately determine "true" tumour response. In the present thesis, the main focus was on the PET technique; however, development and investigation of various functional MR imaging techniques, such as perfusion-weighted imaging (PWI), diffusion-weighted imaging (DWI), diffusion tensor imaging (DTI) or magnetic resonance spectroscopy (MRS), has emerged in parallel to the investigation of different PET tracers[96]. Although the potential of the advanced MRI techniques is promising, additional validation in large clinical trials, and reproducible analytical methods to quantify the different parameters, are required[97-99].

3.4.3 Bioluminescence Imaging (BLI)

Bioluminescence imaging (BLI) is an experimental imaging technique, which relies on the emission and detection of light (photons) from living organisms. Fundamental for the technique is the biochemical reaction in which the enzyme Luciferase catalyses the oxygenation of its substrate Luciferin with the production of light. In a typical experimental setup, *in vitro* cancer cells are transduced with the luciferase gene (luc), and subsequently injected in mice to create an *in vivo* xengraft model. Standard gene transfer methods are used for the gene transfection, and the North American firefly luciferase (Fluc), and its substrate D-luciferin, is the most used luciferase-luciferin pair for *in vivo* imaging[100]. D-luciferin has a low molecular weight (318.41 g/mol), and therefore, it diffuses freely across membranes including the blood-brain-barrier (BBB), and it can be

administered intraperitoneally prior to imaging[101]. When the low energy photons are emitted from the luciferase-luciferin reaction in the mouse, a highly sensitive charged coupled device (CCD) camera is used to detect and quantify the diffuse 2D signal emitted from the surface of the mouse. In contrast to e.g. cells, tissue from mammals is not transparent and most bioluminescent light is absorbed by haemoglobin and melanin. As Firefly luciferase emits a large portion of light above 600 nm it has an increased depth penetration, and it is therefore favourable for *in vivo* imaging[101]. However, due to absorption and scatter of the low energy photons, bioluminescence has limited spatial resolution (1-3 mm), and the intensity of the signal is dependent on the depth of the luciferase expressing cells[102]. With the ability to detect as few as 1,000 human tumour cells, BLI is among the most sensitive for small animal imaging (Figure 2). However, as the depth penetration of the emitted photons is only a few centimetres the use of BLI in patients is currently very limited[102]. In the present thesis, we used BLI to monitor tumour growth, and the BLI signal was used to quantify variable tumour cells.

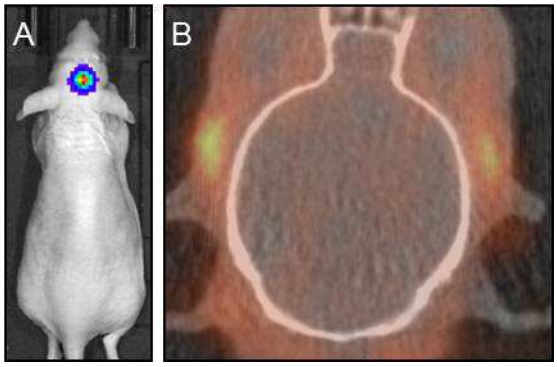

Figure 2: Sensitivity of BLI and ^{18}F-FET MicroPET. A) BLI image showing viable tumour-cells 14 days after intracranial tumour-cell injection in a mouse, while the same mouse had no measurable brain-tumour using ^{18}F-FET MicroPET in B).

4 METHODOLOGICAL CONSIDERATIONS

4.1 GBM tumour models and anti-cancer treatments

In this thesis we used human GBM cancer cells grown as neurospheres to create intracranial xenograft models. When the Ph.D. study was initiated, the neurosphere cells had only been used to establish subcutaneous xenografts; thus, establishment of the orthotopic GBM models was part of the present thesis. As the primary focus was to investigate the potential of ^{18}F-FET PET as an early biomarker of response, we only used two GBM neurosphere cell lines, established from to different patients with GBM at our hospital. Limited activity of Bevacizumab was observed when we used the cell culture GBM048 in study I and II; hence, we chose to shift to another model system and used the cell culture GBM017 in study III. Previous examinations of these cell cultures have revealed that they differ both in regard to *in vitro* growths pattern and in the expression of a number of genes (e.g. EGFR)[103]. As such, models with different genomic characteristic were evaluated; however, we did not compare treatment efficacy between the two models. If anti-cancer activity of new compounds is the focus of future studies, considerations regarding the most reliable animal model must be undertaken (as described in section 3.3 and in future perspectives).

In manuscript I, we used Irinotecan (CPT-11) as an example of a chemotherapeutic agent often used for anti-cancer treatment, in several types of cancers and in GBM. Hence, based on other preclinical studies in orthotopic GBM, we expected anti-cancer activity of Irinotecan[104,105]; thus, Irinotecan was not the focus of the manuscript. Still, in clinical studies in recurrent GBM, Irinotecan is mostly used in combination with other anti-cancer agents[106]. The active metabolite of Irinotecan (SN-38) inhibits the enzyme topoisomerase 1, which is an essential nuclear enzyme that ensures DNA relaxation during DNA transcription and replication[107].

In manuscript II, we used the anti-angiogenic agent B20-4.1, which is an antibody against vascular endothelial growth factor A (VEGF-A). Unlike Bevacizumab, B20-4.1 has affinity for both the human and the murine VEGF-A[108], and therefore, B20-4.1 activity in mice better reflects Bevacizumab activity in patients. As described in section 3.2.2, Bevacizumab has demonstrated activity in recurrent GBM, and anti-cancer activity of B20-4.1 has similarly been demonstrated in several xenograft tumours[32,109].

In manuscript III, we combined B20-4.1 with RO5323441 or TB403, which is a humanized monoclonal antibody that binds both PlGF-1 and PlGF-2 and has affinity for both the murine and the human PlGF-2[110]. The present Ph.D. thesis was initiated in parallel to a phase I-II clinical trial of Bevacizumab in combination with TB403 in patients with recurrent GBM as the preclinical investigation potentially could add additional information about response- or resistance-mechanisms of TB403 and B20-4.1.

4.2 Small-animal PET/CT

In manuscript I, the MicroPET/CT acquisition and image analysis is described in detail. In study I and II, we chose to express tracer uptake as a T/B ratios instead of absolute SUVs, as this is most commonly used in recent literature on GBM[111-113]. In study III, we additionally included FET uptake calculated as SUV_{max} values in the tumour region as results were highly significant and in line with quantification of the T/B ratio. In a recent study, SUV_{max} was as a prognostic parameter in patients with different glioma grade; however, T/B ratios of ^{18}F-FET have mostly been used to evaluate treatment response[114]. Clinical studies often calculate T/B ratios, different from the quantification of T/B ratios in the present thesis, using the SUV_{max} and SUV_{mean} values of the brain tumour and the SUV_{mean} value of the background; although different ratios have been calculated and different methodologies applied[115,116]. As such, standardization of ^{18}F-FET PET protocols and reporting of ^{18}F-FET PET results are therefore needed[114]. In clinical studies, a cut-off value of ≥ 1.6 in T/B ratio is often used to differentiate tumour from non-tumour tissue, which is based on results from a biopsy-controlled study[117]. In the present thesis, the aim was to evaluate ^{18}F-FET PET to detect a treatment response in a murine model, and therefore, we wanted to detect tumours early to make the treatment window as wide as possible. Based on pilot studies, we initially established a threshold T/B ratio ≥ 1.3 for tumour take, as this threshold had 100% specificity for TT with at least a 30% increase in the T/B ratio at the following ^{18}F-FET PET. Results from study I allowed us to lower the threshold value to a T/B ratio ≥ 1.2 to increase the treatment window in study II and III; however, as treatment groups were matched according to the T/B ratio at TT, the threshold value is less important.

The spatial resolution of the MicroPET scanner used in the present thesis is 1.2 mm full-width-at-half-maximum (FWHM) using the MAP algorithm. Due to the limited spatial resolution of the PET system, small objects appear to have lower activity in comparison to larger objects with equal activity; which is described as the partial volume effect (PVE)[118]. Spillover is another phenomenon caused by the limited spatial resolution, and it causes an overestimation of the activity due to activity spillover from surrounding areas. As the tumour to brain contrast of ^{18}F-FET is high, spillover is not considered an important bias in the presented studies. In contrast, PVE is only considered negligible, if the tumour size is approximately twice the FWHM. In study III, we used MRI to evaluate tumour volume, and a few small tumours (2 mm^3) were included, which potentially could bias our results due to PVE. However, as mice with small tumours were equally represented in the different treatment group, bias introduced due to partial volume effect or spillover were similar between treatment groups, and therefore, results regarding quantification of activity are considered reliable.

4.3 Small-animal MRI

In manuscript III, the MRI experiments are described in detail. We used a Bruker Biospec 7.0 MRI scanner (Bruker Biospin, Ettlingen, Germany) and a TurboRareT2-weighted protocol. We chose not to use gadolinium contrast as several MRI scans were performed, and we were afraid it would lead to toxicity in the xenografts. As it was difficult to differentiate between surrounding oedema and the true tumour margins, it is possibly that the MRI volume measurements were less accurate which potentially could influence our results. However, in contradiction to this reasoning, in response to anti-angiogenic treatment, a lack of correlation between decreased tumour growth and loss of contrast enhancement was recently demonstrated, which limits the interpretation of contrast enhancement as a predictor of tumour growth[119].

4.4 Bioluminescence

In study II and III, the neurosphere cells were transduced using a lentiviral construct. The stability of the LUC-expression was confirmed with repeated measurements of the BLI signal during a month in cell culture and 3 months *in vivo.* A limitation with BLI imaging, as a quantitative measure of viable cancer cells, is the use of potentially unstable LUC-transduced cell populations. Results from a study in leukaemia cell populations demonstrated unstable BLI signals in heterogeneous cell populations, and conclude that monoclonal cell lines are critical to develop robust and reproducible xenograft models[120]. However, as xenograft models with selected monoclonal cell lines have other drawbacks (e.g. loss of heterogeneity) we choose to use non-selected neurospheres; thus, the reliability of the BLI signal could be compromised in studies II and III in the present thesis.

4.5 Molecular analysis of tumour tissue

In the present thesis, the process of getting tissue samples was laborious, as the xenograft tumours were intracranial. In manuscript I, we used a surgical microscope and isolated the brain tumour from the brain, extracted RNA and performed qPCR (Figure 3). As a surgical microscope was needed, the brain tumour isolation procedure was rather complicated. Further, in manuscript I, we did not detect a treatment-induced difference in the gene expression of the proliferative marker Ki67, which made us question if changes in the protein expression was reflected at the mRNA level[121]. Therefore, in manuscript II, we chose to isolate the whole brain and performed immunohistochemistry (IHC). In manuscript III, we explored the possibility to divide the brain in the tumour injection site before PFA fixation. Thus, we used one half of the brain for IHC with the tumour *in situ,* and we isolated the brain tumour from the other half of the brain and performed qPCR. As we had some concern about how the technique would impact the tissue quality and IHC results, and if the small amount of isolated brain tumour were sufficient for qPCR, we only explored this method in a subset of the xenografts in manuscript III.

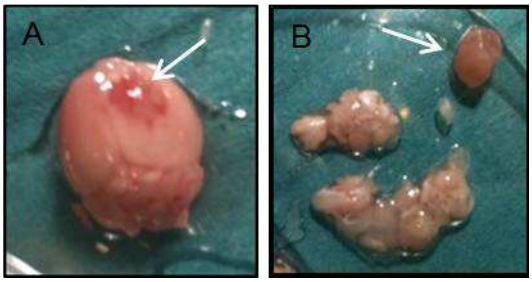

Figure 3: Isolation of the brain tumour. A) The picture shows an intact xenograft brain with the brain tumour *in situ* (white arrow). B) The picture shows the isolated brain tumour (white arrow).

4.5.1 Gene expression analysis

Several steps are involved in the process from tissue sample to gene expression data: Tissue handling, RNA extraction and RNA quality testing, reverse transcription of mRNA into cDNA, amplification of the target cDNA and finally, detection and quantification of the qPCR product. In the present thesis the Nanodrop 100 (Thermo Fischer Technologies, CA, US) was used to measure the quantity of mRNA, and RNA quality and RNA integrity numbers (RIN) were calculated using 2100 Bioanalyser (Agilent Techmologies, CA, US). In study I and III, a few patient samples with RIN ≤ 5 were excluded from gene expression analysis, as low quality mRNA could impact the qPCR results[122]. To create reliable qPCR results, qPCR assays must be optimized. In the present thesis, all assays were optimized to have an efficiency between 90 and 110%, melt-curve analysis were performed on each plate to confirm primer specificity, samples were in the linear range of the assays, and all samples were run in duplicates to assess and confirm reproducibility. In order to reduce operator variability and workload, all experiments were set up using the JANUS® automated workstation (Perkin Elmer, MA, US).

Quantification of the qPCR results is another fundamental step in gene expression analysis, and two strategies can be applied: absolute quantification usually using a calibration curve or relative quantification using normalization[123]. As we examined gene expression between different treatment groups, the relative quantification method was applied. When the concept of normalization was introduced, Cq values were converted into normalized relative quantities (NRQs) using the classical delta-delta-Cq method ($NRQ = 2^{-\Delta\Delta Cq}$), a single reference gene and a calibrator sample[123]. However, as considerable variation was observed in commonly used reference genes, the use of several reference genes are currently considered to be the most robust method for normalization[124,125]. In the present thesis, we used the geNorm algorithm integrated in the software qBase^{Plus} to determine the most stable reference genes from pre-fabricated panels of

common reference genes (TATA Biocenter, Sweden and the geNorm Kit, PrimerDesign, UK). In addition, the optimal number of reference genes was evaluated. Raw data from the qPCR analysis were imported into the qBase^{Plus} and the stability of the reference genes were re-evaluated and confirmed calculating the gene-stability measure (M) and the coefficient of variation (CV). In heterogeneous samples, reference genes with M ≤ 1 and CV ≤ 0.5 are acceptable to get reliable gene expression results using the qMase^{Plus} software[125]. I study I, M = 0.66 and CV = 0.23, and in study III, M = 0.82 and CV = 0.28 which confirms stable reference genes and hence, robust normalization in the studies.

To encourage better experimental practice and increase transparency and reproducibility in qPCR, the MIQE Guidelines (Minimum Information for Publication of Quantitative Real-Time PCR experiments) were recently defined[126]. The guidelines consider the important steps in qPCR among which some important steps have been discussed above.

4.5.2 Immunohistochemistry (IHC)

In IHC, antibodies linked to a dye are used for detection of specific antigens in a tissue sample. The technique consist of two main phases: 1) tissue and slide preparation (fixation, paraffin embedding and tissue sectioning) including stages required for the immune-staining (antigen retrieval, blocking of endogen peroxidase activity, non-specific blocking using serum, primary and secondary antibody incubation, antigen detection and counterstaining and 2) interpretation and quantification of the immunostains[127]. As the final quantification of antigen expression is influenced and possibly biased by differences in all the above-mentioned steps, IHC is only regarded as a semi-quantitative method to analyse antigen expression[127,128].

In this thesis, brains were fixed and processed uniformly and according to standard methods. We used standardized assays for detection of the nuclear antigen Ki67 and the endothelial cell marker CD31 and in addition, specimens from treatment and control tumours were stained in the same run reducing bias due to daily variation in staining assays. To standardize the quantification of the Ki67 labelling index, we used computer-assisted image analysis ImmunoRatio[129], which is easy to use and validated in breast cancer specimens. In the study described in manuscript II, we used the CAIMAN (Cancer Image Analysis: htpp://www.caiman.org.uk) online automatic algorithm to quantify MVD; however, in manuscript III, we used the Image J 1.47 software and counted the vessels manually, as the intensity of the DAB background in the slices was too high for digital image analysis. In summary, as all steps are optimized and performed uniformly, and as we make relative comparison of protein expression between tumour specimens from treated and untreated mice, the relative quantification of the antigen expression is regarded as rather robust [127].

4.6 Statistics

The ability to measure a statistically significant difference, between a control and a treatment group, depends on the variability in the groups and the magnitude of the difference between the groups[130]. The variability in the group is calculated as a coefficient of variation (CV), and it is the

ratio of the standard deviation (SD) to the mean: CV = SD/mean. In the present thesis, sample size calculations were performed to determine the appropriate sample size necessary to detect a treatment effect of 25-30% in mean T/B ratio with a CV of 20%. The type I error (or significance level) was set to 5%, and the risk of type II error was set to 20%, (equal to a power of 80%). Therefore, in study I and II the number of animals needed in each treatment group was 5-6[130,131]. In study III, we compared three treatment groups, and therefore, we needed a larger sample size, as we in the final analysis would correct for multiple comparisons. Sample size in study III was calculated to 9 mice[132]. Although we intended to include a specific number of mice in each treatment group, the ambition was impeded due to unexpected exclusion of xenografts in the experiments. However, if the CV in the treatment groups were smaller or/and if the difference between the treatment groups were larger than estimated, we still detected significant differences. However, when we failed to detect a significant difference between treatment groups, lack of power due to the small sample size could be an explanation.

5 RESULTS

5.1 Summary of the studies

5.1.1 Study I

"The use of longitudinal ^{18}F-FET MicroPET imaging to evaluate response to Irinotecan in orthotopic human glioblastoma multiforme xenografts"

Manuscript I is the first published report demonstrating the feasibility of using ^{18}F-FET MicroPET to follow tumour growth and to monitor a treatment response toward chemotherapy in an orthotopic murine model of human GBM. In addition, in study I we wanted to characterize the intracranial growth of the GBM048 neurosphere cells which has amplification of EGFR; the most common found genetic alteration in primary GBM. The main focus of the study was ^{18}F-FET as an imaging biomarker of treatment response. Hence, Irinotecan (CPT-11) and the GBM048 neurosphere cells were only used as examples of a chemotherapeutic agent and of an orthotopic GBM model, respectively. Figure 4 shows tumour development and longitudinal imaging of ^{18}F-FET uptake in an orthotopic human GBM xenograft.

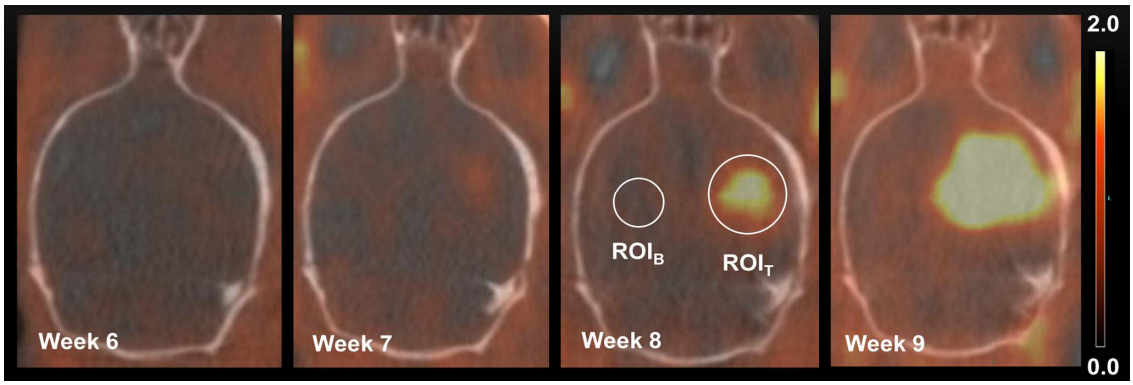

Figure 4: Fused ^{18}F-FET MicroPET/CT images showing tumour progression 6-9 weeks after tumour cell injection. Transverse views through the brain of the same mouse. Illustrated in the figure is a ROI$_T$ drawn round the tumour region with maximum tracer uptake and a 4mm^3 ROI$_B$ drawn in the contralateral hemisphere (background). Scale bar: 0.0-2.0 SUV$_{max}$.

The intracranial growth of GBM048 neurospheres was diverse in different xenografts and a wide range in time to TT (3-11 weeks) was observed, and therefore, several ^{18}F-PET scans were performed before TT was evident. A total of 16 mice were available for Irinotecan or control treatment, and tumour development was followed by ^{18}F-FET PET/CT after one and two weeks of treatment. ^{18}F-FET uptake was quantified using T/B ratio of SUV_{max} and SUV_{mean}. In figure 5, T/B ratios relative to baseline are plotted versus time after TT. A significant difference in ^{18}F-FET uptake in the Irinotecan group as compared to the control group is observed and only minor differences between the two different quantification methods (T/B ratio of SUV_{max} or SUV_{mean}).

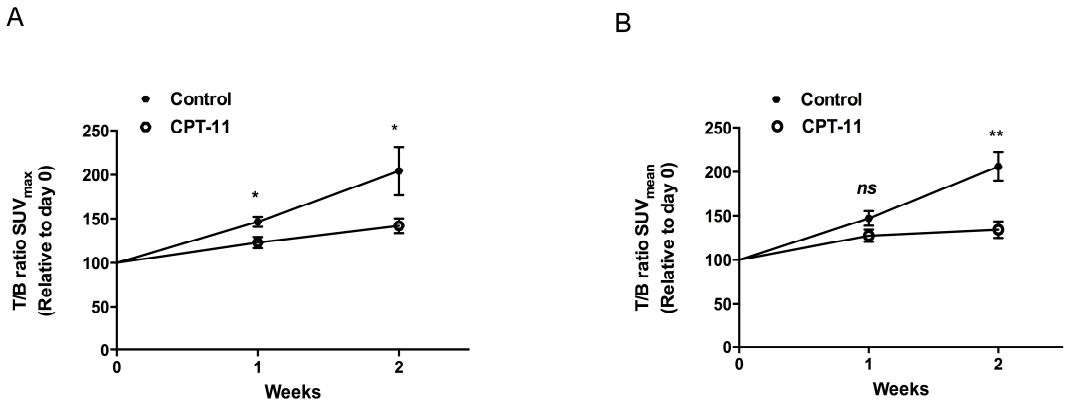

Figure 5: ^{18}F-FET uptake in xenografts. A) The relative T/B ratio of SUV_{max} versus time after tumour take. B) The relative T/B ratio of SUV_{mean} versus time after tumour take. Values are expressed as mean ± SEM in the CPT-11 (n=5-7) and in the control group (n=4-7), *p<0.05 and **p<0.01.

To confirm results from^{18}F-FET PET quantification, we wanted to investigate anti-cancer activity at the molecular level. Following two weeks of treatment, mice were sacrificed and brain tumours were isolated and used to quantify gene expression using qPCR. We failed to detect a significant difference in the Ki67 gene expression between the two treatment groups, and, as we did not perform survival analysis, it is difficult to determine if changes in the ^{18}F-FET uptake reflect "true" anti-cancer activity.

In study I, we further wanted to evaluate the gene expression of the amino acids transporters LAT1 and LAT2 as these transporters previously have been related to ^{18}F-FET uptake. In figure 6, the FET uptake is negatively correlated to the gene expression of LAT1 and LAT2, which was in contradiction to our expectations. However, we also found a much lower expression of especially LAT2 in xenograft tumours as compared to human tumours, which could indicate that LAT2 primarily are located in tumour vessels and as such not detected using human-specific primers. In manuscript I, we discuss the results in detail.

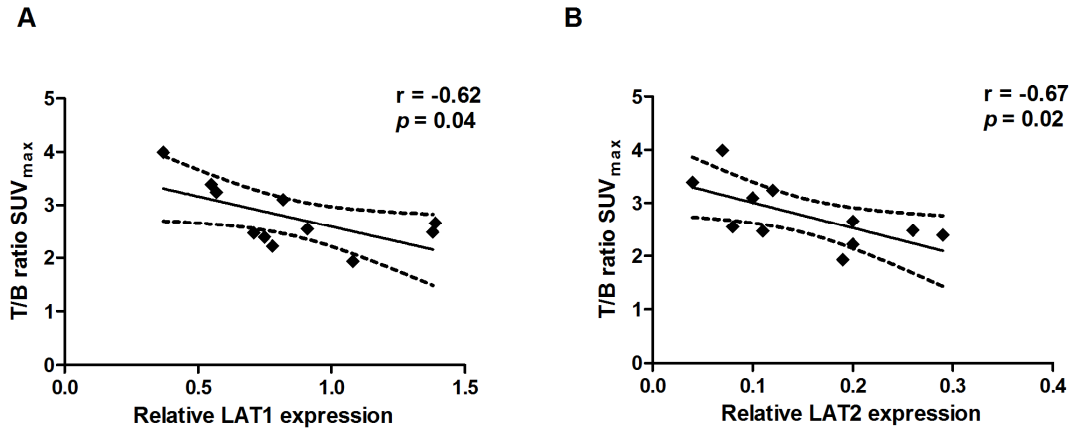

Figure 6: Univariate linear regression analysis of gene expression (n=11). A) LAT1 expression relative to T/B ratio of SUV_{max}. B) LAT2 expression relative to T/B ratio of SUV_{max}. The 95% CI is indicated by the broken lines.

5.1.2 Study II

"Comparison of ^{18}F-FET and ^{18}F-FLT MicroPET for the assessment of anti-VEGF efficacy in an orthotopic model of glioblastoma"

Based on results from study I, we wanted to evaluate if ^{18}F-FET PET additionally could be used to evaluate response towards anti-angiogenic treatment. Furthermore, as the experimental setup in study I was demanding and introduced unnecessary stress to xenografts (due to several ^{18}F-FET MicroPET scans before TT), we transduced the GBM048 neurosphere cells with luciferase to optimize the experimental setup. Thereby, BLI could be applied to monitor tumour development and to screen mice for possible TT before ^{18}F-FET MicroPET was performed. At TT, mice were treated with anti-VEGF or control, and, as we wanted to compare the potential of ^{18}F-FLT and ^{18}F-FET as biomarkers of treatment response, weekly ^{18}F-FLT in addition to weekly ^{18}F-FET were performed. In study II, we additionally investigated survival in the treatment groups, and mice were sacrificed when they had tumour-related symptoms. However, we only performed PET scans after one and two weeks of treatment even though some mice lived longer.

Representative MicroPET/CT images of an orthotopic GBM048_LUC tumour from a single mouse are shown in Figure 7 for visual comparison. A small increase in ^{18}F-FLT uptake and a larger increase in ^{18}F-FET uptake are observed every week. In the ^{18}F-FET PET images, the tumour ^{18}F-FET uptake is higher at week 7 and week 8 as compared to ^{18}F-FLT uptake images; however, the background activity is also higher leading to higher T/B ratios in the ^{18}F-FLT images compared to the ^{18}F-FET PET images.

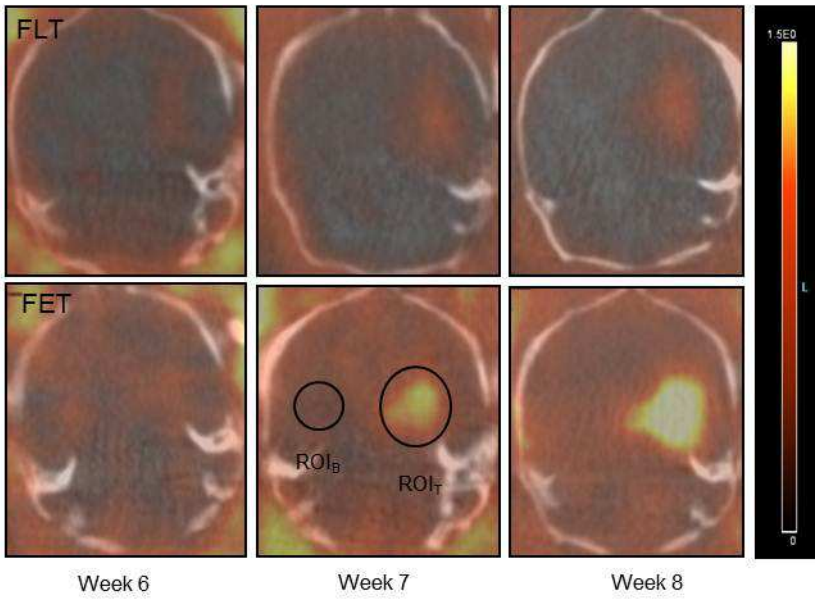

Figure 7: Fused ^{18}F-FLT (top) and ^{18}F-FET MicroPET/CT (bottom) images showing tumour progression in the same mice 6-8 weeks after tumour cell injection. ROI_T and ROI_B are illustrated. Scale bar: 0-1.5 SUV_{max}.

In figure 8, ^{18}F-FET and ^{18}F-FLT uptake quantified using T/B ratios are plotted versus time after tumour take showing a significant difference between the treatment groups using ^{18}F-FET T/B ratios, although there was no significant difference between treatment groups when ^{18}F-FLT T/B ratios were quantified.

To validate results from the ^{18}F-FET and ^{18}F-FLT quantifications in study II, we performed IHC and investigated the Ki67 proliferative index and MVD as molecular markers of anti-cancer activity. In line with results from study I, we failed to detect a significant difference in the Ki67 proliferative index and in addition; we did not demonstrate a survival benefit of anti-VEGF treatment. However, we found a significant lower MVD in the anti-VEGF treated group indicating that results from the ^{18}F-FET PET reflect changes in MVD. Results from study II are discussed in detail in manuscript II.

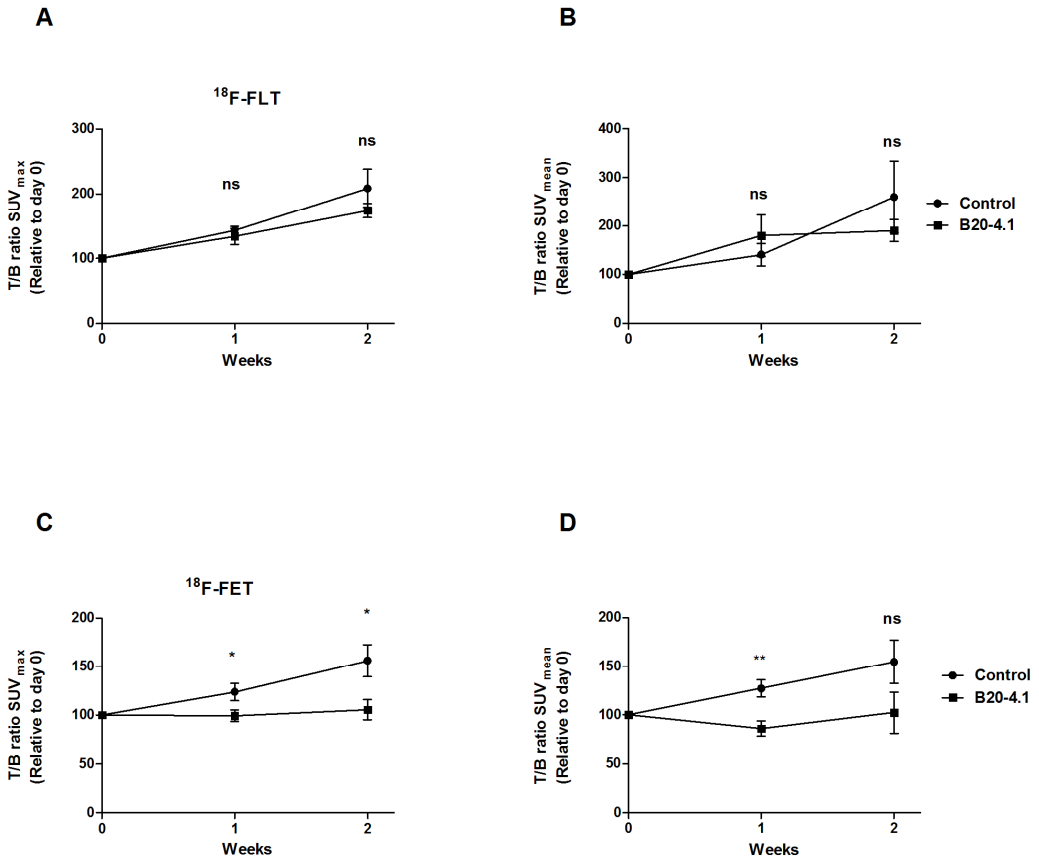

Figure 8: ^{18}F-FET and ^{18}F-FLT uptake in xenografts. A) FET SUV_{max} T/B ratio. B) FET SUV_{mean} T/B ratio. C) FLT SUV_{max} T/B ratio. D) FLT SUV_{mean} T/B ratio. Control group (n=4-5), B20-4.1 group (n=5-6). Values are expressed as mean ± SEM, *p<0.05, **p<0.01.

5.1.3 Study III

"^{18}F-FET MicroPET and MicroMRI for anti-VEGF and anti-PlGF response assessment in an orthotopic murine model of human glioblastoma"

In study III, we wanted to further explore the potential of ^{18}F-FET MicroPET as an early biomarker of treatment response in a different GBM models, and therefore, we used the luciferase-transduced neurosphere cell line GBM017_LUC that, as compared to the GBM048 neurospheres, formed tumours with a more similar and shorter time to TT (range 3-4 weeks). In study III, we combined anti-VEGF treatment with anti-PlGF treatment and included MRI to monitor treatment response. At TT, mice were followed with ^{18}F-FET MicroPET and MicroMRI for two weeks and sacrificed when they had tumour-related symptoms. Figure 9 shows representative MRI and ^{18}F-FET MicroPET/CT images. 34 mice were included in the study of which 13 mice were included in the control group, 11 mice in the anti-VEGF group and 10 mice in the anti-VEGF + anti-PlGF group.

In line with results from study I and II, ^{18}F-FET could be used to detect a treatment response after one and two weeks of treatment. In contrast, no measurable anatomical changes were observed using MicroMRI (Figure 10).

In study III, we further observed increased survival in the treatment groups, which was supportive of results from the ^{18}F-FET PET quantification indicating "true" anti-cancer activity. In line with results from study II, MVD was additionally decreased in response to anti-VEGF treatment, and also here the treatment effect was not reflected in a difference in the Ki67 proliferative index. Further, adding anti-PlGF to anti-VEGF monotherapy did not result in an additional effect on 18F-FET uptake, survival or MVD. In addition, and in line with study I, we demonstrated a much lower gene expression of PlGF and VEGFR-1 in xenografts as compared to a panel of GBM patients, which could indicate a stromal contribution of PlGF and VEGFR-1 in patients and in xenografts. In manuscript III, we discuss the results in detail.

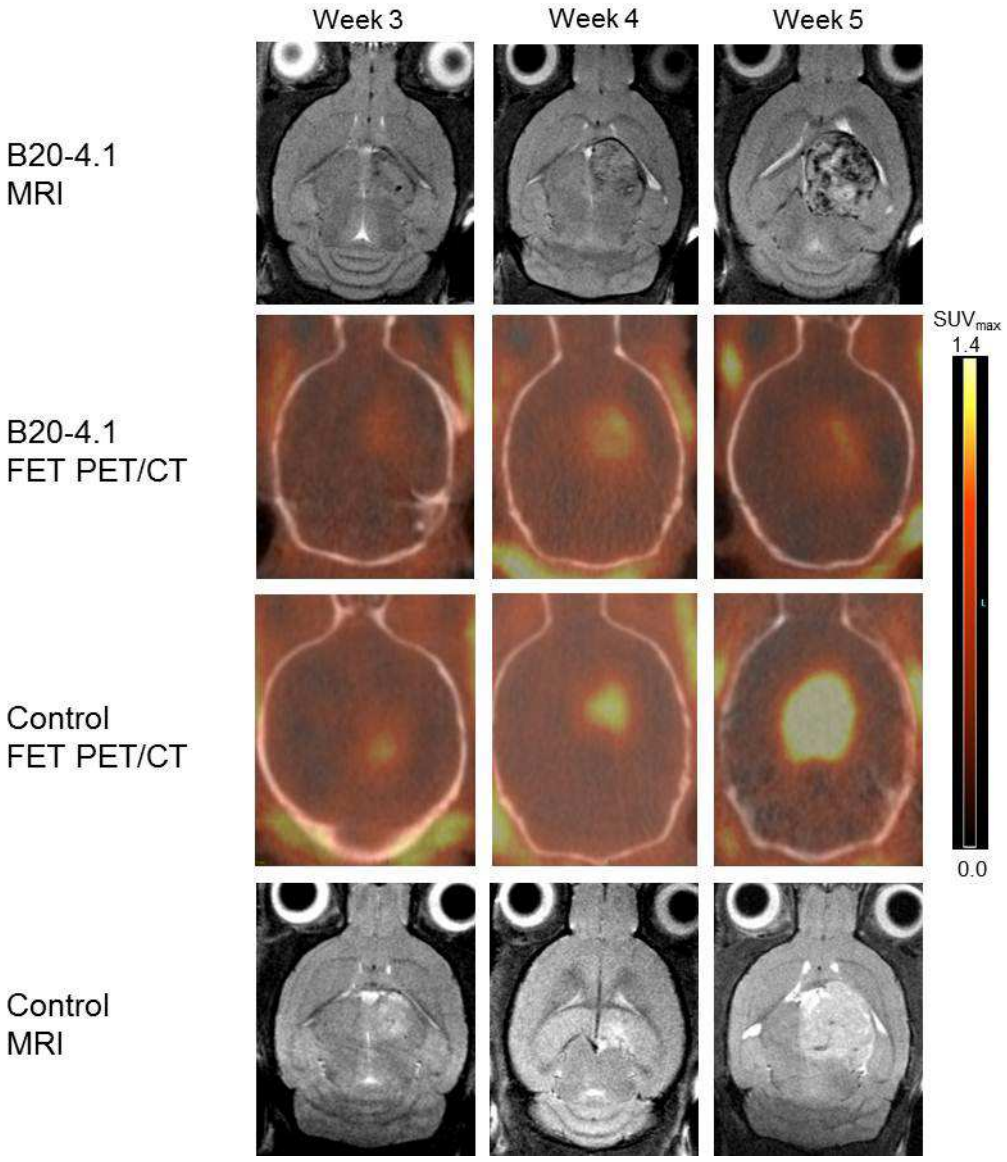

Figure 9: MRI and fused ^{18}F-FET MicroPET/CT images showing tumour progression 3-5 weeks after tumour cell injection. Transverse views through the brain of a mouse from the B20-4.1 group and a mouse from the control group. Scale bar: 0-1.4 SUVmax.

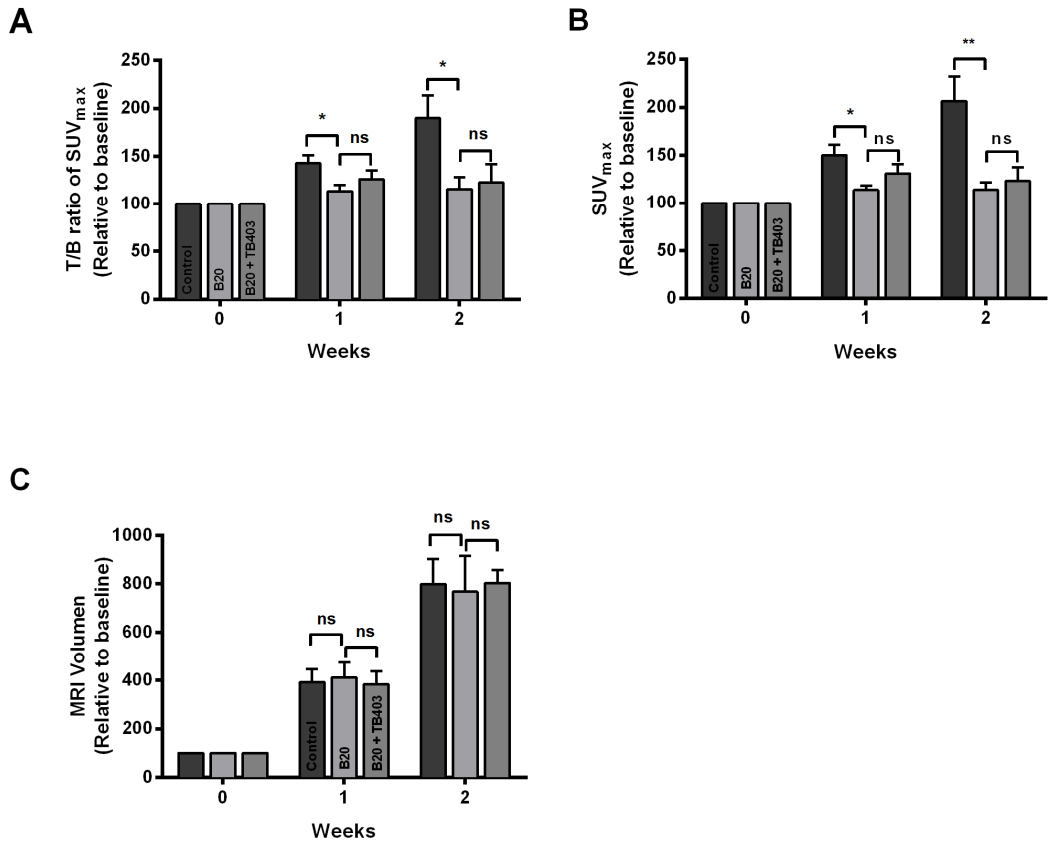

Figure 10: A) ^{18}F-FET uptake in the treatment groups expressed as T/B ratio and B) SUVmax C) MRI volume in the treatment groups. All values are expressed as mean ± SEM relative to baseline (week 0) after 1 week of treatment in the control (n=13), the B20 group (n=11) and in the B20+TB403 (n=9); and after 2 weeks of treatment in the control (n=5), the B20 group (n=8) and in the B20+TB403 group (n=6), *p<0.05, **p<0.01.

6 SUPPLEMENTARY DISCUSSION

6.1 How do we measure "true" anti-cancer activity?

The overall aim of the present thesis was to investigate if ^{18}F-FET PET could be used to monitor anti-cancer activity, which leads to an important question: what is "true" anti-cancer activity and how should we measure it? In the three experimental studies included in the present thesis, we have demonstrated that ^{18}F-FET PET can be used to monitor tumour development in an orthotopic xenograft model of GBM. Furthermore, ^{18}F-FET PET, in comparison to MRI and ^{18}F-FLT PET, ads additional information about tumour growth, which supports the findings in clinical studies[68-71,85]. In addition, we have demonstrated that ^{18}F-FET PET can be used to follow treatment-induced changes in MVD; however, we were unable to detect a significant decrease in the Ki67 level neither using IHC in study II or III, nor using qPCR in study I. In manuscript I, we speculated that the anti-proliferative activity of Irinotecan, and thus changes in the Ki67 protein level, were undetectable at the gene expression level, which we investigated. Hence, in study II and III, we investigated Ki67 at the protein level; however, we failed to detect significant changes using IHC to quantify the Ki67 labelling index. In study II and III, we performed survival analysis in addition to quantifying the Ki67 proliferative index, as overall survival (OS) in clinical phase 2 and 3 trials is the gold-standard endpoint for the measurement of treatment effectiveness. Therefore, regrowth of treatment-resistant cancer cells is possible, and hence, a plausible explanation for diminished anti-proliferative activity and no changes in the Ki67 proliferative index, when brain tumours were investigated at the end of the study-period. However, either no anti-proliferative effect or only a minor effect, which failed to reach statistical significance, is other explanations for the unchanged Ki67 gene expression and proliferative index.

Although OS is considered the most relevant end-point in clinical trials it is confounded by post-study treatments, and therefore, time to progression (TTP) or progression-free survival (PFS) using MRI based RANO criteria as imaging end points, are often used as surrogate markers of OS[133]. In the few clinical studies, investigating the ability of ^{18}F-FET PET to assess treatment response, the best threshold to differentiate responders (PFS ≥ 6 months) from non-responders (PFS ≤ 6 months) was a 45% reduction in the metabolically active tumour volume being defined as a T/B ratio of ≥ 1.6 at follow-up[69,113,134]. In addition, a 5% reduction or a 16% reduction in the mean T/B ratio was predictive values of treatment response[68,113,116]. In the studies presented in the present thesis, we evaluated mean ^{18}F-FET T/B ratios in the different treatment groups and demonstrated a tumour growth delay; although no decrease in mean ^{18}F-FET T/B ratios were observed. In addition, we demonstrated no response using non-contrast enhanced MRI in study III. However, in study III a significant survival benefit was observed, which confirmed "true" anti-cancer activity according to the clinical standards.

To summarize, as we demonstrated limited anti-cancer activity in study II (although a decreased ^{18}F-FET uptake was observed) it is impossible to draw any firm conclusions regarding ^{18}F-FET uptake as a measure of anti-cancer activity. However, the definition of response in clinical studies is not directly transferrable to the murine model as the brain tumour in xenografts initially is very

small (2-3 mm^3), and the resolution of the PET scanner is limited. Furthermore, rapid tumour growth prevents the inclusion of mice with larger tumours in preclinical treatment studies, as the treatment window in the control group often is narrow and only about 2 weeks. However, the narrow treatment window, due to rapid metabolism and tumour growth in mice, could compromise OS as the most valid measurement of "true" anti-cancer activity in preclinical trials. In order to establish the most accurate and reproducible threshold value to define an ^{18}F-FET response in orthotopic GBM models, further investigation of ^{18}F-FET uptake in response to different types of anti-cancer agents with different potency is necessary.

During the past decades we have realized that GBM (and primary cancers in general) is a heterogeneous disease and hence, respond differently to different anti-cancer agents. Therefore, different treatments presumable produce diverse molecular changes and feedback mechanisms in the individual patients; thus, it seems likely that accurate response assessment is unachievable with only one imaging method as the golden standard[64]. In study II, two different conclusions regarding anti-VEGF efficacy could be applied: either anti-cancer activity or no anti-cancer response depending on which PET tracer that were used. We speculated that ^{18}F-FET PET and ^{18}F-FLT PET demonstrated different aspect of the tumour and response to anti-VEGF treatment. Theoretically, multimodal imaging including PET with different tracers presumably permits the most accurate response assessment, although, it is not practical or economical achievable. However, it was recently demonstrated that MRI in conjunction with ^{18}F-FET PET could be cost-effective in GBM[135]. To establish how and/or when ^{18}F-FET and ^{18}F-FLT PET could aid in in the decision-making process, regarding response assessment and in the general management of GBM patients, further investigation of these two tracers are necessary in preclinical and clinical studies.

6.2 What are the mechanisms responsible for FET uptake in GBM?

In study I, we evaluated the gene expression of the amino acid transporters LAT1 and LAT2 and demonstrated strong negative correlations to ^{18}F-FET uptake, which were in contradiction to our expectations. However, the correlations were based on only 11 xenografts, which affect the reliability of the correlations as described in detail in manuscript I. In addition, we used human specific primers, and therefore, LATs located to the murine tumour vasculature were not measured. Although it is impossible to draw any firm conclusion regarding FET uptake in relation to the gene expression of LAT1 and LAT2, study I indicates that the expression of LAT1 is higher than the expression of LAT2 in tumour cells. However, in order to further elucidate the correlations between LATs and ^{18}F-FET uptake, and to fully establish the potential of ^{18}F-FET PET as an imaging biomarker in clinical and preclinical studies, further investigation is needed to elucidate the complex transport and retention mechanisms of ^{18}F-FET.

6.3 Dynamic ^{18}F-FET PET in glioma?

In manuscript I, we performed dynamic ^{18}F-FET PET in two mice with confirmed TT and we demonstrated accumulation and retention of ^{18}F-FET in both the normal brain and in the brain tumour. In figure 11, it is evident that although there are minor fluctuations in ^{18}F-FET uptake expressed as a T/B ratio, there is a clear trend and almost horizontal line demonstrating a stable T/B ratio 20-90 minutes after ^{18}F-FET injection. Several clinical studies have indicated that ^{18}F-FET kinetic analysis may provide additional diagnostic information about glioma grading[136-138]. High-grade gliomas are frequently characterized by an early peak of ^{18}F-FET followed by a decreasing pattern and an early wash out of ^{18}F-FET, while low-grade gliomas typically show a steadily increasing ^{18}F-FET uptake[136-138]. However, different kinetic patterns are observed in GBM patients, and the prognostic value of dynamic ^{18}F-FET PET needs to be further evaluated in clinical and preclinical studies[68,116,136]. In study I in the present thesis, we observed a constant ^{18}F-FET uptake; however, a decreasing kinetic pattern was observed when dynamic ^{18}F-FET was evaluated in the other preclinical study in orthotopic GBM[5]. The different kinetic patterns observed in the two preclinical studies in different GBM models are interesting, as it demonstrates some diversity in xenografts that may be partly similar to the heterogeneity in GBM patients. As such, the prognostic value and the molecular mechanism behind the different kinetic patterns could possibly be elucidated in future preclinical studies using dynamic ^{18}F-FET PET. However, our data do not indicate that much additional information is to be gained using kinetic analysis compared to static imaging.

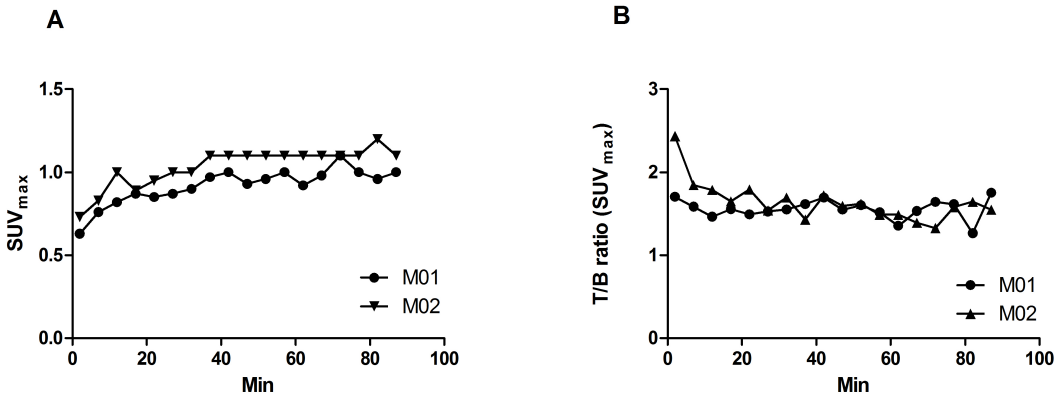

Figure 11: Time-activity curves of ^{18}F-FET in two different mice (M01, M02) presented as SUV_{max} in the tumour ROI (A) and tumour-to-brain (T/B) ratio (B).

6.4 Are murine models reliable to evaluate human cancer?

Having conducted three experimental studies of ^{18}F-FET PET in orthotopic murine models, it seems appropriate to ask a fundamental question: Is it possible to use murine models to study different molecular variations and to predict treatment efficacy in human patients, or is it a waste of mice, time and money? To answer this question some considerations must be explored: In study I and III, we compared the gene expression of several human genes (LAT1, LAT2, Ki67, PlGF and VEGFR-1) in patients and xenografts. Surprisingly, we demonstrated an extremely low expression of LAT2, PLGF and VEGFR-1 in xenografts as compared to human patients, although the expression of Ki67 and LAT1 were more comparable. We speculated that the proteins were located to the tumour vasculature or stroma cells, which hindered the detection using qPCR and human specific primers. In addition, we designed primers specific for murine VEGFR-1; however, this hindered the comparison of the gene expression between human and xenograft tumours. When performing the studies, we considered designing primers specific for both the human and the murine GOI; however, this process is complicated and not available in the Beacon primer designing software (Beacon Designer™, PREMIER Biosoft, US). As such, in xenograft murine models the cancer cells are human and the stroma cells are murine, which is an important concern when the xenograft model is used to answer scientific questions. Although we used an orthotopic GBM models to make the brain microenvironment more similar to the microenvironment in GBM patient, the model does not fully mimic the complex tumour-stroma interactions in human patients. As mentioned in paragraph 3.3, the missing immune response is probably the most important limitation using xenograft models; however, apart from the lack of immune-cells the complex molecular interactions in humans are not fully reflected in the xenograft model.

As such, anti-cancer activity of several upcoming anti-cancer agents in xenograft studies have failed to predict activity when tested in clinical trials[57], and only 5% of anti-cancer agents with activity in preclinical development get final FDA approval[139]. Therefore, in the light of the high attrition rate in the development of new anti-cancer compounds, the answer to the fundamental question would be that murine xenograft models are a waste of both mice and resources. However, only a limited number of patients are available for clinical evaluation of new anti-cancer agents, and therefore, accurately designed murine models that reflect the heterogeneity of the primary cancers under investigation, is probably a sufficient, feasibly and economical model for investigation of anti-cancer activity; although murine models are far from perfect[4,57]. Murine models can be used to help prioritize new anti-cancer agents and to investigate hypothesis regarding molecular mechanism or genetic alterations involved in resistance towards new anti-cancer agent. Murine models can additionally be used to evaluate and determine possible predictive imaging biomarkers like e.g. new PET tracers and further, to elucidate transport mechanism and molecular changes involved in the distribution and tumour uptake of new tracers.

7 CONCLUSION

In agreement with the overall hypothesis of the present thesis, our studies demonstrated that ^{18}F-FET MicroPET can be used to monitor tumour development and anti-VEGF induced changes in MVD in an intracranial GBM xenograft model. Furthermore, ^{18}F-FET can be used to evaluate anti-cancer activity of anti-VEGF and Irinotecan in some orthotopic GBM xenograft models; however, in order to establish the potential of ^{18}F-FET as an early biomarker of treatment response, further investigations are necessary to determine threshold values to accurately assess ^{18}F-FET PET treatment response in orthotopic GBM xenograft models. In addition, we found strong negative correlations between the ^{18}F-FET uptake and the gene expression of the amino acid transporters LAT1 and LAT2, which could be caused by an export transport function of LAT1 and LAT2. Further, we demonstrated a much lower expression of several human genes in xenograft tumours as compared to the original human tumour specimen, which could indicate that these genes mainly are expressed by murine stromal cells in the xenograft models. If this is not the case, difference in gene expression in xenografts as compared to the original patient tumour represents a limitation of the xenograft model. Lastly, and in contradiction to our hypothesis, the combination of anti-VEGF and anti-PlGF, as compared to anti-VEGF monotherapy, did not result in an additive effect on tumour growth or survival, in orthotopic GBM xenografts.

8 FUTURE PERSPECTIVES

The historical term "glioblastoma multiforme" was introduced in the initial grading of gliomas from 1926[140], and with the term "multiforme" the histopathological diversity of GBM was acknowledged. However, we are only now beginning to elucidate the complex heterogeneities that exist at the cellular and molecular level of GBM. Intra-patient heterogeneity was initially accepted; however, it has later been demonstrated that different subpopulations or clones of tumour cells exists within the same patient tumour, thus, in addition to intra-patient heterogeneity, there is heterogeneity at the intra-tumoural level[141]. The concept of "personalized medicine" has been described as "a form of medicine that uses information about a person's genes, proteins and environment to prevent, diagnose and treat disease"[142], although "molecular medicine" or "genomic medicine" may more accurately reflect the novelty of the concept[143]. Knowledge of intra-tumoural heterogeneity complicates the concept of personalized medicine, but it is crucial to acknowledge it when designing and evaluating new personalized treatment strategies[141]. In the present thesis we have used two different GBM models as initial models to explore ^{18}F-FET PET in orthotopic GBM xenografts. However, accurately designed animal models that reflect both the intra-patient and intra-tumour heterogeneity should be used in future preclinical studies of new anti-cancer compounds.

New concepts of mouse models have emerged as an attempt to integrate the mouse model in the concept of personalized medicine. "Mouse Avatars" or patient-derived tumour xenograft models (PDX) are created when tumour samples from a patient is transplanted to immunocompromised mice (using the biopsy method as described in section 3.3) and used for subsequent drug efficacy studies. Commercialization of PDX models could potentially eliminate time and resources required to generate xenograft models that reflect the heterogeneity of the original patient tumour and therefore, accelerate cancer research[4]. In the "Co-clinical Trials concept" GEM models are used to guide therapy in ongoing clinical trials in patients. Typically, a new anti-cancer agent is evaluated in GEM models simultaneous with a phase I/II trial in patients, allowing for comparison and integration of data regarding e.g. mutational background, responsiveness to the treatment and tumour imaging. In addition, PDX models can be established as a part of the Co-clinical Trial concept. It was recently concluded that the new models "have the potential to revolutionize the drug development and health care process"; however, several challenges remains to be solved and addressed[4,144]. Accurately response assessment is fundamental to make robust conclusions about anti-cancer activity of new compounds in more sophisticated GBM animal models. ^{18}F-FET PET in combination with MRI could be used to more accurately determine treatment response, and future evaluation of ^{18}F-FET PET in diverse murine models will further elucidate the value of ^{18}F-FET PET as a predictive imaging biomarker of treatment response.

9 REFERENCES

1. Cloughesy TF, Mischel PS. New strategies in the molecular targeting of glioblastoma: how do you hit a moving target? *Clinical cancer research : an official journal of the American Association for Cancer Research.* 2011; 17(1):6-11.

2. Chen L, Zhang Y, Yang J, Hagan JP, Li M. Vertebrate animal models of glioma: understanding the mechanisms and developing new therapies. *Biochimica et biophysica acta.* 2013; 1836(1):158-165.

3. Das Thakur M, Pryer NK, Singh M. Mouse tumour models to guide drug development and identify resistance mechanisms. *The Journal of pathology.* 2014; 232(2):103-111.

4. Malaney P, Nicosia SV, Dave V. One mouse, one patient paradigm: New avatars of personalized cancer therapy. *Cancer letters.* 2014; 344(1):1-12.

5. Sai KK, Huang C, Yuan L, et al. 18F-AFETP, 18F-FET, and 18F-FDG imaging of mouse DBT gliomas. *J.Nucl.Med.* 2013; 54(7):1120-1126.

6. Menichetti L, Petroni D, Panetta D, et al. A micro-PET/CT approach using O-(2-[18F]fluoroethyl)-L-tyrosine in an experimental animal model of F98 glioma for BNCT. *Appl.Radiat.Isot.* 2011; 69(12):1717-1720.

7. Wang HE, Wu SY, Chang CW, et al. Evaluation of F-18-labeled amino acid derivatives and [18F]FDG as PET probes in a brain tumor-bearing animal model. *Nucl.Med.Biol.* 2005; 32(4):367-375.

8. Ohgaki H, Kleihues P. Population-based studies on incidence, survival rates, and genetic alterations in astrocytic and oligodendroglial gliomas. *Journal of neuropathology and experimental neurology.* 2005; 64(6):479-489.

9. Louis DN, Ohgaki H, Wiestler OD, et al. The 2007 WHO classification of tumours of the central nervous system. *Acta neuropathologica.* 2007; 114(2):97-109.

10. Retningslinier for behandling af intrakranielle gliomer hos voksne. *www.dnog.dk.* 2012.

11. Gan HK, Kaye AH, Luwor RB. The EGFRvIII variant in glioblastoma multiforme. *Journal of clinical neuroscience : official journal of the Neurosurgical Society of Australasia.* 2009; 16(6):748-754.

12. Karpel-Massler G, Schmidt U, Unterberg A, Halatsch ME. Therapeutic inhibition of the epidermal growth factor receptor in high-grade gliomas: where do we stand? *Molecular cancer research : MCR.* 2009; 7(7):1000-1012.

13. Phillips HS, Kharbanda S, Chen R, et al. Molecular subclasses of high-grade glioma predict prognosis, delineate a pattern of disease progression, and resemble stages in neurogenesis. *Cancer cell.* 2006; 9(3):157-173.

14. Ohgaki H, Kleihues P. The definition of primary and secondary glioblastoma. *Clinical cancer research : an official journal of the American Association for Cancer Research.* 2013; 19(4):764-772.

15. Norden AD, Drappatz J, Wen PY. Antiangiogenic therapies for high-grade glioma. *Nature reviews. Neurology.* 2009; 5(11):610-620.

16. de Groot J, Milano V. Improving the prognosis for patients with glioblastoma: the rationale for targeting Src. *Journal of neuro-oncology.* 2009; 95(2):151-163.

17. Stupp R, Hegi ME, Mason WP, et al. Effects of radiotherapy with concomitant and adjuvant temozolomide versus radiotherapy alone on survival in glioblastoma in a randomised phase III study: 5-year analysis of the EORTC-NCIC trial. *The lancet oncology.* 2009; 10(5):459-466.

18. Rinne ML, Lee EQ, Nayak L, et al. Update on bevacizumab and other angiogenesis inhibitors for brain cancer. *Expert.Opin.Emerg.Drugs.* 2013; 18(2):137-153.

19. Park DM, Sathornsumetee S, Rich JN. Medical oncology: treatment and management of malignant gliomas. *Nat.Rev.Clin.Oncol.* 2010; 7(2):75-77.

20. Sathornsumetee S, Rich JN. Antiangiogenic therapy in malignant glioma: promise and challenge. *Current pharmaceutical design.* 2007; 13(35):3545-3558.

21. Rogers MS, Novak K, Zurakowski D, et al. Spontaneous reversion of the angiogenic phenotype to a nonangiogenic and dormant state in human tumors. *Molecular cancer research : MCR.* 2014; 12(5):754-764.

22. Takano S, Yoshii Y, Kondo S, et al. Concentration of vascular endothelial growth factor in the serum and tumor tissue of brain tumor patients. *Cancer research.* 1996; 56(9):2185-2190.

23. Knizetova P, Ehrmann J, Hlobilkova A, et al. Autocrine regulation of glioblastoma cell cycle progression, viability and radioresistance through the VEGF-VEGFR2 (KDR) interplay. *Cell cycle.* 2008; 7(16):2553-2561.

24. Chi AS, Sorensen AG, Jain RK, Batchelor TT. Angiogenesis as a therapeutic target in malignant gliomas. *Oncologist.* 2009; 14(6):621-636.

25. Steiner HH, Karcher S, Mueller MM, Nalbantis E, Kunze S, Herold-Mende C. Autocrine pathways of the vascular endothelial growth factor (VEGF) in glioblastoma multiforme: clinical relevance of radiation-induced increase of VEGF levels. *Journal of neuro-oncology.* 2004; 66(1-2):129-138.

26. Miletic H, Niclou SP, Johansson M, Bjerkvig R. Anti-VEGF therapies for malignant glioma: treatment effects and escape mechanisms. *Expert opinion on therapeutic targets.* 2009; 13(4):455-468.

27. Ferrara N, Gerber HP, LeCouter J. The biology of VEGF and its receptors. *Nature medicine.* 2003; 9(6):669-676.

28. Bogler O, Mikkelsen T. Angiogenesis in glioma: molecular mechanisms and roadblocks to translation. *Cancer journal.* 2003; 9(3):205-213.

29. Chi AS, Sorensen AG, Jain RK, Batchelor TT. Angiogenesis as a therapeutic target in malignant gliomas. *The oncologist.* 2009; 14(6):621-636.

30. Jain RK, di Tomaso E, Duda DG, Loeffler JS, Sorensen AG, Batchelor TT. Angiogenesis in brain tumours. *Nature reviews. Neuroscience.* 2007; 8(8):610-622.

31. Hamerlik P, Lathia JD, Rasmussen R, et al. Autocrine VEGF-VEGFR2-Neuropilin-1 signaling promotes glioma stem-like cell viability and tumor growth. *The Journal of experimental medicine.* 2012; 209(3):507-520.

32. Bais C, Wu X, Yao J, et al. PlGF blockade does not inhibit angiogenesis during primary tumor growth. *Cell.* 2010; 141(1):166-177.

33. Olsson AK, Dimberg A, Kreuger J, Claesson-Welsh L. VEGF receptor signalling - in control of vascular function. *Nature reviews. Molecular cell biology.* 2006; 7(5):359-371.

34. Autiero M, Waltenberger J, Communi D, et al. Role of PlGF in the intra- and intermolecular cross talk between the VEGF receptors Flt1 and Flk1. *Nature medicine.* 2003; 9(7):936-943.

35. Wu FT, Stefanini MO, Mac Gabhann F, Kontos CD, Annex BH, Popel AS. A systems biology perspective on sVEGFR1: its biological function, pathogenic role and therapeutic use. *Journal of cellular and molecular medicine.* 2010; 14(3):528-552.

36. Carmeliet P, Moons L, Luttun A, et al. Synergism between vascular endothelial growth factor and placental growth factor contributes to angiogenesis and plasma extravasation in pathological conditions. *Nature medicine.* 2001; 7(5):575-583.

37. Fischer C, Jonckx B, Mazzone M, et al. Anti-PlGF inhibits growth of VEGF(R)-inhibitor-resistant tumors without affecting healthy vessels. *Cell.* 2007; 131(3):463-475.

38. Bagley RG, Ren Y, Weber W, et al. Placental growth factor upregulation is a host response to antiangiogenic therapy. *Clinical cancer research : an official journal of the American Association for Cancer Research.* 2011; 17(5):976-988.

39. Loges S, Schmidt T, Carmeliet P. "Antimyeloangiogenic" therapy for cancer by inhibiting PlGF. *Clinical cancer research : an official journal of the American Association for Cancer Research.* 2009; 15(11):3648-3653.

40. (EMA) EMA. Avastin, Summary of Product Characteristics (SPC).

41. Santos ES, Gomez JE, Raez LE. Targeting angiogenesis from multiple pathways simultaneously: BIBF 1120, an investigational novel triple angiokinase inhibitor. *Investigational new drugs.* 2012; 30(3):1261-1269.

42. Wick W, Weller M, van den Bent M, Stupp R. Bevacizumab and recurrent malignant gliomas: a European perspective. *Journal of clinical oncology : official journal of the American Society of Clinical Oncology.* 2010; 28(12):e188-189; author reply e190-182.

43. Chinot OL, Wick W, Mason W, et al. Bevacizumab plus radiotherapy-temozolomide for newly diagnosed glioblastoma. *The New England journal of medicine.* 2014; 370(8):709-722.

44. Gilbert MR, Dignam JJ, Armstrong TS, et al. A randomized trial of bevacizumab for newly diagnosed glioblastoma. *The New England journal of medicine.* 2014; 370(8):699-708.

45. Fine HA. Bevacizumab in glioblastoma--still much to learn. *The New England journal of medicine.* 2014; 370(8):764-765.

46. Maru D, Venook AP, Ellis LM. Predictive biomarkers for bevacizumab: are we there yet? *Clinical cancer research : an official journal of the American Association for Cancer Research.* 2013; 19(11):2824-2827.

47. Van de Veire S, Stalmans I, Heindryckx F, et al. Further pharmacological and genetic evidence for the efficacy of PlGF inhibition in cancer and eye disease. *Cell.* 2010; 141(1):178-190.

48. Xu L, Cochran DM, Tong RT, et al. Placenta growth factor overexpression inhibits tumor growth, angiogenesis, and metastasis by depleting vascular endothelial growth factor homodimers in orthotopic mouse models. *Cancer research.* 2006; 66(8):3971-3977.

49. Hedlund EM, Yang X, Zhang Y, et al. Tumor cell-derived placental growth factor sensitizes antiangiogenic and antitumor effects of anti-VEGF drugs. *Proceedings of the National Academy of Sciences of the United States of America.* 2013; 110(2):654-659.

50. Eriksson A, Cao R, Pawliuk R, et al. Placenta growth factor-1 antagonizes VEGF-induced angiogenesis and tumor growth by the formation of functionally inactive PlGF-1/VEGF heterodimers. *Cancer cell.* 2002; 1(1):99-108.

51. Yao J, Wu X, Zhuang G, et al. Expression of a functional VEGFR-1 in tumor cells is a major determinant of anti-PlGF antibodies efficacy. *Proceedings of the National Academy of Sciences of the United States of America.* 2011; 108(28):11590-11595.

52. Barth RF, Kaur B. Rat brain tumor models in experimental neuro-oncology: the C6, 9L, T9, RG2, F98, BT4C, RT-2 and CNS-1 gliomas. *Journal of neuro-oncology.* 2009; 94(3):299-312.

53. Jacobs VL, Valdes PA, Hickey WF, De Leo JA. Current review of in vivo GBM rodent models: emphasis on the CNS-1 tumour model. *ASN neuro.* 2011; 3(3):e00063.

54. Huszthy PC, Daphu I, Niclou SP, et al. In vivo models of primary brain tumors: pitfalls and perspectives. *Neuro-oncology.* 2012; 14(8):979-993.

55. Kawamata M, Ochiya T. Gene-manipulated embryonic stem cells for rat transgenesis. *Cellular and molecular life sciences : CMLS.* 2011; 68(11):1911-1915.

56. Lee J, Kotliarova S, Kotliarov Y, et al. Tumor stem cells derived from glioblastomas cultured in bFGF and EGF more closely mirror the phenotype and genotype of primary tumors than do serum-cultured cell lines. *Cancer cell.* 2006; 9(5):391-403.

57. Sharpless NE, Depinho RA. The mighty mouse: genetically engineered mouse models in cancer drug development. *Nat.Rev.Drug Discov.* 2006; 5(9):741-754.

58. Chaichana K, Zamora-Berridi G, Camara-Quintana J, Quinones-Hinojosa A. Neurosphere assays: growth factors and hormone differences in tumor and nontumor studies. *Stem cells.* 2006; 24(12):2851-2857.

59. Singh SK, Clarke ID, Terasaki M, et al. Identification of a cancer stem cell in human brain tumors. *Cancer research.* 2003; 63(18):5821-5828.

60. Azvolinsky A. Cancer stem cells: getting to the root of cancer. *Journal of the National Cancer Institute.* 2012; 104(12):893-895.

61. Rankin SL, Zhu G, Baker SJ. Review: insights gained from modelling high-grade glioma in the mouse. *Neuropathology and applied neurobiology.* 2012; 38(3):254-270.

62. James ML, Gambhir SS. A molecular imaging primer: modalities, imaging agents, and applications. *Physiological reviews.* 2012; 92(2):897-965.

63. Phelps M. PET: Molecular Imaging and Its Biological Applications. *1st ed. Springer.* 2004.

64. Gulyas B, Halldin C. New PET radiopharmaceuticals beyond FDG for brain tumor imaging. *Q.J.Nucl.Med.Mol.Imaging.* 2012; 56(2):173-190.

65. la Fougere C, Suchorska B, Bartenstein P, Kreth FW, Tonn JC. Molecular imaging of gliomas with PET: opportunities and limitations. *Neuro-oncology.* 2011; 13(8):806-819.

66. Nihashi T, Dahabreh IJ, Terasawa T. PET in the clinical management of glioma: evidence map. *AJR Am.J.Roentgenol.* 2013; 200(6):W654-W660.

67. Demetriades AK, Almeida AC, Bhangoo RS, Barrington SF. Applications of positron emission tomography in neuro-oncology: A clinical approach. *The surgeon : journal of the Royal Colleges of Surgeons of Edinburgh and Ireland.* 2014; 12(3):148-157.

68. Galldiks N, Rapp M, Stoffels G, et al. Response assessment of bevacizumab in patients with recurrent malignant glioma using [18F]Fluoroethyl-L-tyrosine PET in comparison to MRI. *European journal of nuclear medicine and molecular imaging.* 2013; 40(1):22-33.

69. Hutterer M, Nowosielski M, Putzer D, et al. O-(2-18F-fluoroethyl)-L-tyrosine PET predicts failure of antiangiogenic treatment in patients with recurrent high-grade glioma. *Journal of nuclear medicine : official publication, Society of Nuclear Medicine.* 2011; 52(6):856-864.

70. Popperl G, Goldbrunner R, Gildehaus FJ, et al. O-(2-[18F]fluoroethyl)-L-tyrosine PET for monitoring the effects of convection-enhanced delivery of paclitaxel in patients with recurrent glioblastoma. *European journal of nuclear medicine and molecular imaging.* 2005; 32(9):1018-1025.

71. Popperl G, Gotz C, Rachinger W, et al. Serial O-(2-[(18)F]fluoroethyl)-L: -tyrosine PET for monitoring the effects of intracavitary radioimmunotherapy in patients with malignant glioma. *European journal of nuclear medicine and molecular imaging.* 2006; 33(7):792-800.

72. Heiss P, Mayer S, Herz M, Wester HJ, Schwaiger M, Senekowitsch-Schmidtke R. Investigation of transport mechanism and uptake kinetics of O-(2-[18F]fluoroethyl)-L-tyrosine in vitro and in vivo. *J.Nucl.Med.* 1999; 40(8):1367-1373.

73. Langen KJ, Jarosch M, Muhlensiepen H, et al. Comparison of fluorotyrosines and methionine uptake in F98 rat gliomas. *Nucl.Med.Biol.* 2003; 30(5):501-508.

74. Kim DK, Kim IJ, Hwang S, et al. System L-amino acid transporters are differently expressed in rat astrocyte and C6 glioma cells. *Neurosci.Res.* 2004; 50(4):437-446.

75. Chalkidou A, Landau DB, Odell EW, Cornelius VR, O'Doherty MJ, Marsden PK. Correlation between Ki-67 immunohistochemistry and 18F-fluorothymidine uptake in patients with cancer: A systematic review and meta-analysis. *European journal of cancer.* 2012; 48(18):3499-3513.

76. Jensen MM, Erichsen KD, Bjorkling F, et al. Early detection of response to experimental chemotherapeutic Top216 with [18F]FLT and [18F]FDG PET in human ovary cancer xenografts in mice. *PloS one.* 2010; 5(9):e12965.

77. Munk JM, Erichsen KD, Bjorkling F, et al. [18F]FLT PET for non-invasive assessment of tumor sensitivity to chemotherapy: studies with experimental chemotherapy TP202377 in human cancer xenografts in mice. *PLoS.One.* 2012; 7(11):e50618.

78. McKinley ET, Ayers GD, Smith RA, et al. Limits of [18F]-FLT PET as a biomarker of proliferation in oncology. *PloS one.* 2013; 8(3):e58938.

79. Paproski RJ, Ng AM, Yao SY, Graham K, Young JD, Cass CE. The role of human nucleoside transporters in uptake of 3'-deoxy-3'-fluorothymidine. *Molecular pharmacology.* 2008; 74(5):1372-1380.

80. Spence AM, Muzi M, Link JM, et al. NCI-sponsored trial for the evaluation of safety and preliminary efficacy of 3'-deoxy-3'-[18F]fluorothymidine (FLT) as a marker of proliferation in patients with recurrent gliomas: preliminary efficacy studies. *Molecular imaging and biology : MIB : the official publication of the Academy of Molecular Imaging.* 2009; 11(5):343-355.

81. Choi SJ, Kim JS, Kim JH, et al. [18F]3'-deoxy-3'-fluorothymidine PET for the diagnosis and grading of brain tumors. *European journal of nuclear medicine and molecular imaging.* 2005; 32(6):653-659.

82. Jacobs AH, Thomas A, Kracht LW, et al. 18F-fluoro-L-thymidine and 11C-methylmethionine as markers of increased transport and proliferation in brain tumors. *Journal of nuclear medicine : official publication, Society of Nuclear Medicine.* 2005; 46(12):1948-1958.

83. Schwarzenberg J, Czernin J, Cloughesy TF, et al. 3'-deoxy-3'-18F-fluorothymidine PET and MRI for early survival predictions in patients with recurrent malignant glioma treated with bevacizumab. *J.Nucl.Med.* 2012; 53(1):29-36.

84. Harris RJ, Cloughesy TF, Pope WB, et al. 18F-FDOPA and 18F-FLT positron emission tomography parametric response maps predict response in recurrent malignant gliomas treated with bevacizumab. *Neuro-oncology.* 2012; 14(8):1079-1089.

85. Chen W, Delaloye S, Silverman DH, et al. Predicting treatment response of malignant gliomas to bevacizumab and irinotecan by imaging proliferation with [18F] fluorothymidine positron emission tomography: a pilot study. *Journal of clinical oncology : official journal of the American Society of Clinical Oncology.* 2007; 25(30):4714-4721.

86. Schiepers C, Dahlbom M, Chen W, et al. Kinetics of 3'-deoxy-3'-18F-fluorothymidine during treatment monitoring of recurrent high-grade glioma. *Journal of nuclear medicine : official publication, Society of Nuclear Medicine.* 2010; 51(5):720-727.

87. Moonshi SS, Bejot R, Atcha Z, Vijayaragavan V, Bhakoo KK, Goggi JL. A comparison of PET imaging agents for the assessment of therapy efficacy in a rodent model of glioma. *Am.J.Nucl.Med.Mol.Imaging.* 2013; 3(5):397-407.

88. Mittra ES, Fan-Minogue H, Lin FI, et al. Preclinical efficacy of the anti-hepatocyte growth factor antibody ficlatuzumab in a mouse brain orthotopic glioma model evaluated by bioluminescence, PET, and MRI. *Clinical cancer research : an official journal of the American Association for Cancer Research.* 2013; 19(20):5711-5721.

89. Viel T, Boehm-Sturm P, Rapic S, et al. Non-invasive imaging of glioma vessel size and densities in correlation with tumour cell proliferation by small animal PET and MRI. *European journal of nuclear medicine and molecular imaging.* 2013; 40(10):1595-1606.

90. Viel T, Schelhaas S, Wagner S, et al. Early assessment of the efficacy of temozolomide chemotherapy in experimental glioblastoma using [18F]FLT-PET imaging. *PloS one.* 2013; 8(7):e67911.

91. Corroyer-Dulmont A, Peres EA, Petit E, et al. Detection of glioblastoma response to temozolomide combined with bevacizumab based on muMRI and muPET imaging reveals [18F]-fluoro-L-thymidine as an early and robust predictive marker for treatment efficacy. *Neuro.Oncol.* 2013; 15(1):41-56.

92. Nowosielski M, Difranco MD, Putzer D, et al. An Intra-Individual Comparison of MRI, [18F]-FET and [18F]-FLT PET in Patients with High-Grade Gliomas. *PloS one.* 2014; 9(4):e95830.

93. Wen PY, Macdonald DR, Reardon DA, et al. Updated response assessment criteria for high-grade gliomas: response assessment in neuro-oncology working group. *Journal of clinical oncology : official journal of the American Society of Clinical Oncology.* 2010; 28(11):1963-1972.

94. Pope WB, Young JR, Ellingson BM. Advances in MRI assessment of gliomas and response to anti-VEGF therapy. *Current neurology and neuroscience reports.* 2011; 11(3):336-344.

95. Wen PY, Macdonald DR, Reardon DA, et al. Updated response assessment criteria for high-grade gliomas: response assessment in neuro-oncology working group. *J.Clin.Oncol.* 2010; 28(11):1963-1972.

96. Durst CR, Raghavan P, Shaffrey ME, et al. Multimodal MR imaging model to predict tumor infiltration in patients with gliomas. *Neuroradiology.* 2014; 56(2):107-115.

97. Morse DL, Galons JP, Payne CM, et al. MRI-measured water mobility increases in response to chemotherapy via multiple cell-death mechanisms. *NMR in biomedicine.* 2007; 20(6):602-614.

98. Chung C, Jalali S, Foltz W, et al. Imaging biomarker dynamics in an intracranial murine glioma study of radiation and antiangiogenic therapy. *International journal of radiation oncology, biology, physics.* 2013; 85(3):805-812.

99. Hu LS, Eschbacher JM, Heiserman JE, et al. Reevaluating the imaging definition of tumor progression: perfusion MRI quantifies recurrent glioblastoma tumor fraction, pseudoprogression, and radiation necrosis to predict survival. *Neuro-oncology.* 2012; 14(7):919-930.

100. Prescher JA, Contag CH. Guided by the light: visualizing biomolecular processes in living animals with bioluminescence. *Current opinion in chemical biology.* 2010; 14(1):80-89.

101. Hochgrafe K, Mandelkow EM. Making the brain glow: in vivo bioluminescence imaging to study neurodegeneration. *Molecular neurobiology.* 2013; 47(3):868-882.

102. Contag CH, Jenkins D, Contag PR, Negrin RS. Use of reporter genes for optical measurements of neoplastic disease in vivo. *Neoplasia.* 2000; 2(1-2):41-52.

103. Stockhausen MT, Broholm H, Villingshoj M, et al. Maintenance of EGFR and EGFRvIII expressions in an in vivo and in vitro model of human glioblastoma multiforme. *Experimental cell research.* 2011; 317(11):1513-1526.

104. Kuroda J, Kuratsu J, Yasunaga M, et al. Antitumor effect of NK012, a 7-ethyl-10-hydroxycamptothecin-incorporating polymeric micelle, on U87MG orthotopic glioblastoma in mice compared with irinotecan hydrochloride in combination with bevacizumab. *Clin.Cancer Res.* 2010; 16(2):521-529.

105. Verreault M, Strutt D, Masin D, et al. Irinophore C, a lipid-based nanoparticulate formulation of irinotecan, is more effective than free irinotecan when used to treat an orthotopic glioblastoma model. *J.Control Release.* 2012; 158(1):34-43.

106. Sasine JP, Savaraj N, Feun LG. Topoisomerase I inhibitors in the treatment of primary CNS malignancies: an update on recent trends. *Anti-cancer agents in medicinal chemistry.* 2010; 10(9):683-696.

107. Leppard JB, Champoux JJ. Human DNA topoisomerase I: relaxation, roles, and damage control. *Chromosoma.* 2005; 114(2):75-85.

108. Liang WC, Wu X, Peale FV, et al. Cross-species vascular endothelial growth factor (VEGF)-blocking antibodies completely inhibit the growth of human tumor xenografts and measure the contribution of stromal VEGF. *J.Biol.Chem.* 2006; 281(2):951-961.

109. Kienast Y, Klein C, Scheuer W, et al. Ang-2-VEGF-A CrossMab, a novel bispecific human IgG1 antibody blocking VEGF-A and Ang-2 functions simultaneously, mediates potent antitumor, antiangiogenic, and antimetastatic efficacy. *Clinical cancer research : an official journal of the American Association for Cancer Research.* 2013; 19(24):6730-6740.

110. Oude Munnink TH, Tamas KR, Lub-de Hooge MN, et al. Placental growth factor (PlGF)-specific uptake in tumor microenvironment of 89Zr-labeled PlGF antibody RO5323441. *Journal of nuclear medicine : official publication, Society of Nuclear Medicine.* 2013; 54(6):929-935.

111. Thiele F, Ehmer J, Piroth MD, et al. The quantification of dynamic FET PET imaging and correlation with the clinical outcome in patients with glioblastoma. *Physics in medicine and biology.* 2009; 54(18):5525-5539.

112. Piroth MD, Holy R, Pinkawa M, et al. Prognostic impact of postoperative, pre-irradiation (18)F-fluoroethyl-l-tyrosine uptake in glioblastoma patients treated with radiochemotherapy. *Radiother.Oncol.* 2011; 99(2):218-224.

113. Galldiks N, Langen KJ, Holy R, et al. Assessment of treatment response in patients with glioblastoma using O-(2-18F-fluoroethyl)-L-tyrosine PET in comparison to MRI. *J.Nucl.Med.* 2012; 53(7):1048-1057.

114. Dunet V, Rossier C, Buck A, Stupp R, Prior JO. Performance of 18F-fluoro-ethyl-tyrosine (18F-FET) PET for the differential diagnosis of primary brain tumor: a systematic review and Metaanalysis. *Journal of nuclear medicine : official publication, Society of Nuclear Medicine.* 2012; 53(2):207-214.

115. Sweeney R, Polat B, Samnick S, Reiners C, Flentje M, Verburg FA. O-(2-[(18)F]fluoroethyl)-L-tyrosine uptake is an independent prognostic determinant in patients with glioma referred for radiation therapy. *Annals of nuclear medicine.* 2014; 28(2):154-162.

116. Piroth MD, Liebenstund S, Galldiks N, et al. Monitoring of Radiochemotherapy in Patients with Glioblastoma Using O-(2-[18F]fluoroethyl)-L-Tyrosine Positron Emission Tomography: Is Dynamic Imaging Helpful? *Molecular imaging.* 2013; 12(0):1-8.

117. Pauleit D, Floeth F, Hamacher K, et al. O-(2-[18F]fluoroethyl)-L-tyrosine PET combined with MRI improves the diagnostic assessment of cerebral gliomas. *Brain : a journal of neurology.* 2005; 128(Pt 3):678-687.

118. Soret M, Bacharach SL, Buvat I. Partial-volume effect in PET tumor imaging. *Journal of nuclear medicine : official publication, Society of Nuclear Medicine.* 2007; 48(6):932-945.

119. Jalali S, Chung C, Foltz W, et al. MRI biomarkers identify the differential response of glioblastoma multiforme to anti-angiogenic therapy. *Neuro-oncology.* 2014; 16(6):868-879.

120. Christoph S, Schlegel J, Alvarez-Calderon F, et al. Bioluminescence imaging of leukemia cell lines in vitro and in mouse xenografts: effects of monoclonal and polyclonal cell populations on intensity and kinetics of photon emission. *Journal of hematology & oncology.* 2013; 6:10.

121. Vogel C, Marcotte EM. Insights into the regulation of protein abundance from proteomic and transcriptomic analyses. *Nat.Rev.Genet.* 2012; 13(4):227-232.

122. Fleige S, Pfaffl MW. RNA integrity and the effect on the real-time qRT-PCR performance. *Molecular aspects of medicine.* 2006; 27(2-3):126-139.

123. Livak KJ, Schmittgen TD. Analysis of relative gene expression data using real-time quantitative PCR and the 2(-Delta Delta C(T)) Method. *Methods.* 2001; 25(4):402-408.

124. Vandesompele J, De Preter K, Pattyn F, et al. Accurate normalization of real-time quantitative RT-PCR data by geometric averaging of multiple internal control genes. *Genome biology.* 2002; 3(7):RESEARCH0034.

125. Hellemans J, Mortier G, De PA, Speleman F, Vandesompele J. qBase relative quantification framework and software for management and automated analysis of real-time quantitative PCR data. *Genome Biol.* 2007; 8(2):R19.

126. Bustin SA, Benes V, Garson JA, et al. The MIQE guidelines: minimum information for publication of quantitative real-time PCR experiments. *Clinical chemistry.* 2009; 55(4):611-622.

127. Matos LL, Trufelli DC, de Matos MG, da Silva Pinhal MA. Immunohistochemistry as an important tool in biomarkers detection and clinical practice. *Biomarker insights.* 2010; 5:9-20.

128. Seidal T, Balaton AJ, Battifora H. Interpretation and quantification of immunostains. *The American journal of surgical pathology.* 2001; 25(9):1204-1207.

129. Tuominen VJ, Ruotoistenmaki S, Viitanen A, Jumppanen M, Isola J. ImmunoRatio: a publicly available web application for quantitative image analysis of estrogen receptor (ER), progesterone receptor (PR), and Ki-67. *Breast cancer research : BCR.* 2010; 12(4):R56.

130. Eckelman WC, Kilbourn MR, Joyal JL, Labiris R, Valliant JF. Justifying the number of animals for each experiment. *Nuclear medicine and biology.* 2007; 34(3):229-232.

131. Eckelman WC. Further discussions on choosing the number of animals for an experiment. *Nuclear medicine and biology.* 2008; 35(1):1-2.

132. Aide N, Visser EP, Lheureux S, Heutte N, Szanda I, Hicks RJ. The motivations and methodology for high-throughput PET imaging of small animals in cancer research. *European journal of nuclear medicine and molecular imaging.* 2012; 39(9):1497-1509.

133. Hickey R, Vouche M, Sze DY, et al. Cancer concepts and principles: primer for the interventional oncologist-part I. *Journal of vascular and interventional radiology : JVIR.* 2013; 24(8):1157-1164.

134. Galldiks N, Rapp M, Stoffels G, et al. Response assessment of bevacizumab in patients with recurrent malignant glioma using [18F]Fluoroethyl-L-tyrosine PET in comparison to MRI. *Eur.J.Nucl.Med.Mol.Imaging.* 2013; 40(1):22-33.

135. Heinzel A, Muller D, Langen KJ, et al. The Use of O-(2-18F-Fluoroethyl)-L-Tyrosine PET for Treatment Management of Bevacizumab and Irinotecan in Patients with Recurrent High-Grade Glioma: A Cost-Effectiveness Analysis. *J.Nucl.Med.* 2013; 54(8):1217-1222.

136. Popperl G, Kreth FW, Mehrkens JH, et al. FET PET for the evaluation of untreated gliomas: correlation of FET uptake and uptake kinetics with tumour grading. *Eur.J.Nucl.Med.Mol.Imaging.* 2007; 34(12):1933-1942.

137. Weckesser M, Langen KJ, Rickert CH, et al. O-(2-[18F]fluorethyl)-L-tyrosine PET in the clinical evaluation of primary brain tumours. *European journal of nuclear medicine and molecular imaging.* 2005; 32(4):422-429.

138. Popperl G, Kreth FW, Herms J, et al. Analysis of 18F-FET PET for grading of recurrent gliomas: is evaluation of uptake kinetics superior to standard methods? *Journal of nuclear medicine : official publication, Society of Nuclear Medicine.* 2006; 47(3):393-403.

139. Hutchinson L, Kirk R. High drug attrition rates--where are we going wrong? *Nature reviews. Clinical oncology.* 2011; 8(4):189-190.

140. Bailey P, Cushing H. A Classification of Tumors of the Glioma Group on a Histogenetic Basis. *Lippincott, Philadelphia.* 1926:146-167.

141. Stieber D, Golebiewska A, Evers L, et al. Glioblastomas are composed of genetically divergent clones with distinct tumourigenic potential and variable stem cell-associated phenotypes. *Acta neuropathologica.* 2014; 127(2):203-219.

142. Institute NC. http://www.cancer.gov/dictionary/?CdrID=561717. *Accessed 22 Jun 2014.*

143. Steele FR. Personalized Medicine: something old, something new. *Personalized Medicine.* 2009; 6(1):1-5.

144. Kopetz S, Lemos R, Powis G. The promise of patient-derived xenografts: the best laid plans of mice and men. *Clinical cancer research : an official journal of the American Association for Cancer Research.* 2012; 18(19):5160-5162.

APPENDICES I-III

Appendix I

Manuscript I

Nedergaard MK, Kristoffersen K, Michaelsen SR, Madsen J, Poulsen HS, Stockhausen MT, Ulrik Lassen U and Kjaer A. The Use of Longitudinal ^{18}F-FET MicroPET Imaging to Evaluate Response to Irinotecan in Orthotopic human Glioblastoma Multiforme Xenografts.

PLoS One. 2014;9(2):e100009.

OPEN ACCESS Freely available online

PLOS ONE

The Use of Longitudinal ^{18}F-FET MicroPET Imaging to Evaluate Response to Irinotecan in Orthotopic Human Glioblastoma Multiforme Xenografts

Mette K. Nedergaard[1]*, Karina Kristoffersen[2], Signe R. Michaelsen[2], Jacob Madsen[1], Hans S. Poulsen[2], Marie-Thérése Stockhausen[2], Ulrik Lassen[3☯], Andreas Kjaer[1☯]

1 Department of Clinical Physiology, Nuclear Medicine & PET and Cluster for Molecular Imaging, Rigshospitalet and University of Copenhagen, Copenhagen, Denmark, **2** Department of Radiation Biology, The Finsen Center, Rigshospitalet, Copenhagen, Denmark, **3** Phase 1 Unit, Department of Oncology, The Finsen Center, Rigshospitalet, Copenhagen, Denmark

Abstract

Objectives: Brain tumor imaging is challenging. Although ^{18}F-FET PET is widely used in the clinic, the value of ^{18}F-FET MicroPET to evaluate brain tumors in xenograft has not been assessed to date. The aim of this study therefore was to evaluate the performance of *in vivo* ^{18}F-FET MicroPET in detecting a treatment response in xenografts. In addition, the correlations between the ^{18}F-FET tumor accumulation and the gene expression of Ki67 and the amino acid transporters LAT1 and LAT2 were investigated. Furthermore, Ki67, LAT1 and LAT2 gene expression in xenograft and archival patient tumors was compared.

Methods: Human GBM cells were injected orthotopically in nude mice and ^{18}F-FET uptake was followed by weekly MicroPET/CT. When tumor take was observed, mice were treated with CPT-11 or saline weekly. After two weeks of treatment the brain tumors were isolated and quantitative polymerase chain reaction were performed on the xenograft tumors and in parallel on archival patient tumor specimens.

Results: The relative tumor-to-brain (T/B) ratio of SUV_{max} was significantly lower after one week (123±6%, n = 7 vs. 147±6%, n = 7; p = 0.018) and after two weeks (142±8%, n = 5 vs. 204±27%, n = 4; p = 0.047) in the CPT-11 group compared with the control group. Strong negative correlations between SUV_{max} T/B ratio and LAT1 ($r = -0.62$, p = 0.04) and LAT2 ($r = -0.67$, p = 0.02) were observed. In addition, a strong positive correlation between LAT1 and Ki67 was detected in xenografts. Furthermore, a 1.6 fold higher expression of LAT1 and a 23 fold higher expression of LAT2 were observed in patient specimens compared to xenografts.

Conclusions: ^{18}F-FET MicroPET can be used to detect a treatment response to CPT-11 in GBM xenografts. The strong negative correlation between SUV_{max} T/B ratio and LAT1/LAT2 indicates an export transport function. We suggest that ^{18}F-FET PET may be used for detection of early treatment response in patients.

Citation: Nedergaard MK, Kristoffersen K, Michaelsen SR, Madsen J, Poulsen HS, et al. (2014) The Use of Longitudinal ^{18}F-FET MicroPET Imaging to Evaluate Response to Irinotecan in Orthotopic Human Glioblastoma Multiforme Xenografts. PLoS ONE 9(6): e100009. doi:10.1371/journal.pone.0100009

Editor: Waldemar Debinski, Wake Forest University, School of Medicine, United States of America

Received March 4, 2014; **Accepted** May 21, 2014; **Published** June 11, 2014

Funding: Funding from The Danish Cancer Society; Danish National Advanced Technology Foundation, AP Møller Foundation, The Lundbeck Foundation, Novo Nordisk Foundation, Svend Andersen Foundation, The John and Birthe Meyer Foundation. The funders had no role in study design, data collection and analysis, decision to publish, or preparation of the manuscript.

Competing Interests: The authors have declared that no competing interests exist.

* E-mail: Mette.kjoelhede.nedergaard@regionh.dk

☯ These authors contributed equally to this work.

Introduction

The majority of primary brain tumors are gliomas and glioblastoma multiforme (GBM) is the most common and aggressive type of glioma in adults. The prognosis for patients diagnosed with GBM remains mainly palliative despite multimodal therapies, including aggressive surgery and radiotherapy combined with chemotherapy. The new Response Assesment in Neuro-Oncology (RANO) criteria was recently published [1]; however, there are still difficulties in assessing true tumor response on magnetic resonance imaging (MRI). Contrast enhancing and non-enhancing regions are non-tumor-specific and are influenced by different processes, such as subacute radiation effects, postoperative changes, changes in glucocorticoid dosage as well as anti-angiogenic treatments that affect the permeability of the tumor vasculature [1,2]. One further challenge to the traditional, morphological imaging techniques is the wish to differentiate between responders and non-responders in the early phases of a treatment course.

Functional tumor imaging with positron emission tomography (PET) plays an increasingly important role in the diagnosis of cancer and monitoring of cancer therapy. Accordingly, PET with 2′-deoxy-2′-^{18}F-fluoro-D-glucose (^{18}F-FDG) have become a key

imaging modality in the clinical management of a majority of cancer patients [3]. Due to the high rate of glucose metabolism in normal brain tissue and increased glucose uptake in inflammatory cells, ^{18}F-FDG PET has shown diagnostic limitations when used for brain tumor imaging [4]. By contrast, radiolabeled amino acids have a relatively low uptake in normal brain tissue and usually accumulate intensely in tumor cells. The high tumor-to-brain (T/B) ratio makes radiolabeled amino acids particularly applicable in neuro-oncology *(5)*. A number of studies have demonstrated that O-(2-^{18}F-fluoroethyl)-L-tyrosine (^{18}F-FET) PET compared to MRI alone adds additional information about brain tumor growth [5–7]. Accumulation of ^{18}F-FET in brain tumor cells is presumable linked to high expression of the L-type amino acid transporters (LATs), which are the major transport system for large neutral amino acid [8,9]. Four subtypes of LATs have been identified of which subtype 1 (LAT1) and subtype 2 (LAT2) have been related to the cellular uptake of ^{18}F-FET in cancer cells [10], although it has been speculated that ^{18}F-FET accumulation primarily is mediated by LAT2 [11]. Despite that ^{18}F-FET PET is widely used in the clinic, only a few animal studies have evaluated the performance of ^{18}F-FET MicroPET in GBM xenografts [12–14]. Furthermore, the transport mechanisms of ^{18}F-FET have not been thoroughly investigated [9,15].

The primary objective of this preclinical study was therefore to evaluate the performance of ^{18}F-FET MicroPET in monitoring brain tumor growth and in assessing a treatment response in an orthotopic xenograft model of human GBM. In addition, we wanted to test the hypothesis that ^{18}F-FET accumulation was correlated to the gene expression of LAT1 and/or LAT2 in the tumor. Finally, we wanted to investigate the gene expression of Ki67, LAT1 and LAT2 in tumor specimens from GBM patients and compare it with the results from the xenograft tumors.

Materials and Methods

Ethics Statement

This study was performed according to the Declaration of Helsinki and Danish legislation. The use of patient tissue was approved by the Scientific Ethical Committee for Copenhagen and Frederiksberg (KF-01-327718) and permissions were given from the Danish Data Protection Agency (2006-41-6979). Written informed consent was obtained from the patients. Animal care and all experimental procedures were performed under the approval of the Danish Animal Welfare Council (2013-15-2934-00064).

Establishment of the Human Orthotopic GBM Model

Establishment, maintenance and characterization of the neurosphere cell culture (NGBM_CPH048p6) used in this study has previously been described [16,17]. Ten to 12 weeks old NMRI (Naval Medical Research Institute) nude female mice acquired from Taconic Europe (Lille Skensved, Denmark) were anaesthetized with Hypnorm/Midazolam (1 ml/100 g body weight) and the head was fixed in a stereotactic frame (KOPF model 963, 926-B and 922: Better Hospital Equipment Corp). A longitudinal incision was made in the scalp exposing the *calvarium*. Using a micro-drill, a burr-hole was drilled in the skull 1.5 mm right of the *sutura saggitalis* and 0.5 mm posterior to the *bregma*. Ten µl cell suspension (100,000 cells) of NGBM_CHP048p6 neurosphere cells was injected at a depth of 2–2.5 mm at a rate of 60 nl/sec using a 100 µl syringe with a 25-gauge needle (SGE100RN: World Precision Instruments, UK) placed in a micro infusion pump (Micro 4 pump and MicroSyringePump Controller: World Precision Instruments and KOPF model 1770-C: Better Hospital Equipment Corp). When injection was finished the needle was withdrawn after 1 min. Bupivacain (0.2 mg/100 g body weight) and Lidocain (1 mg/100 g body weight) were administrated in the incision site for local anesthetic before the skin was closed with an Ethicon 5-0 prolene suture.

Experimental Design

Mice were injected with NGBM_CPH048p6 neurosphere cells at week 0 and the *in vivo* uptake of ^{18}F-FET was monitored by weekly MicroPET and computed tomography (CT) scans to follow tumor growth. At confirmed tumor take, mice were divided in two groups and treated weekly with irinotecan hydroclorid (CPT-11) intraperitoneally (i.p.) (66.7 mg/kg) or 0.9% NaCl solution i.p. (control). Anti-cancer activity of CPT-11 in orthotopic glioma xenografts has been reported previously and the treatment regimen was based on these studies [18,19]. At tumor take the treatment response was monitored by MicroPET/CT for two weeks and treatments were given the day after the scans were performed. In order to obtain similar tumor growth characteristic in the treatment and the control group, only mice with tumor take before 12 weeks were included in the study. In addition, the treatment and the control groups were matched according to standardized uptake values (SUV_{max}) and time to tumor take. Mice were humanly euthanized after two weeks of treatment, or if they showed tumor related symptoms such as neurological signs and/or considerable weight loss. Subsequently, the brains were removed and the tumor was isolated for RNA analysis. Two separate mice with confirmed tumor take were used to perform a dynamic ^{18}F-FET MicroPET/CT and they were not included in the treatment part of the study.

Synthesis of ^{18}F-FET

^{18}F-FET was synthesized using (2S)-O-(2-Tosyloxyethyl)-N-trityl-L-tyrosine-*tert*-butyl ester as precursor and synthesized on a GE TracerLab MX Synthesizer. All reagents and FET cassettes were purchased from ABX (Radeberg, Germany). The radiochemical purity was determined after measuring the content of fluoride-18 and other radioactive impurities in the ^{18}F-FET solution measured with TLC and HPLC, respectively. The content of ethanol and acetonitrile was determined by GC analysis. The pH was measured with a pH-meter. In separate preparations the stability of the preparations was examined after 8 hours. HPLC was performed on a Dionex HPLC system (Dionex A/S, Denmark) equipped with an in-line radioactivity detector. The HPLC column was a Kinetx 2.6 µ, C18, 100A, 50×4.6 mm (Phenomenex, Denmark). The eluent was 98% 25 nM acetate buffer/2% acetonitrile pH 4.75 and a flow rate of 1.5 ml/min with UV detection at 275 nm. TLC plates were obtained from Merck and acetonitrile/acetate buffer pH 3.8 (70/30) was used as eluent. Residual solvents were determined on a Shimatzu GC 2014 (Holm & Halby, A/S, Denmark) equipped with a Chromosorb 101, 100–120 Mesh, 1/8″×10′ column, FID detector and helium carrier gas. The radiochemical purity of ^{18}F-FET was >98% with a specific radioactivity ranging from 150–300 GBq/µmol at end of synthesis (EOS). The ethanol content was in the range 2.5–3.5% and the amount of acetonitrile was below the detection limit. The pH was 7.0–7.8. The radiochemical purity, ethanol content and pH did not change after 8 hours of storage at room temperature.

MicroPET/CT Imaging

Mice were anaesthetized with Hypnorm/Midazolam (1 ml/100 g) and injected intravenously (i.v.) on average with 10.5±0.09 MBq ^{18}F-FET. Mice were kept on a heat-pad to prevent hypothermia while anaesthetized and a 10 min static PET image was obtained at 20–30 minutes after tracer injection using a

MicroPET Focus 120 (Siemens Medical Solutions, Malvern, PA, USA). The dynamic PET image was obtained two min before tracer injection and for 90 minutes. The energy window for the emission scan was set to 350–650 keV with a time resolution of 6 ns. PET data were post-processed into sinograms and subsequently reconstructed with the maximum a posteriori (MAP) reconstruction algorithm. Evaluation of the dynamic acquisition involved 18 time frames (18×5 min). The quantification unit was provided in Bq/ml. The intrinsic PET resolution was 1.2 mm full-width at half-maximum and the voxel size was $0.3\times0.3\times0.8$ mm^3. Scatter and attenuation correction were not applied [20]. A 4 minutes MicroCT scan was acquired in order to get anatomical information for brain delineation (MicroCAT II system, Siemens Medical Solutions). MicroPET and MicroCT images were manually fused using the Inveon software (Siemens Medical Solutions). A 3D spheric region of interest (ROI) was placed at the location of maximum tracer uptake in the tumor (ROI_T). In the contralateral normal hemisphere a 4 mm^3 spheric ROI was drawn (ROI_B). To quantify the ^{18}F-FET uptake, the standardized uptake values (SUVs) were calculated from the equation: $SUV = C_T/(D_{inj}\times W)$, where C_T is the radioactivity in tissue with the unit Bq/ml, D_{inj} is the injected dose and W is the weight of the mouse in grams. SUV_{max} was calculated from the voxel with the highest tracer concentration in the ROI. SUV_{mean} was calculated as the mean radioactivity in the ROI. Tracer uptake was expressed as T/B ratio of SUV_{max} (SUV_{max} ROI_T/SUV_{max} ROI_B) and SUV_{mean} (SUV_{max} ROI_T/SUV_{mean} ROI_B). We chose to express tracer uptake as a T/B ratio instead of absolute SUVs as there is a high unexplained inter-subject variability of SUV in the tumor model and also in GBM patients it is common to use the T/B ratio. Tumor take was predefined as a T/B ratio of $SUV_{max}\geq1.3$.

Patient Specimens

Tumor specimens from 19 GBM patients obtained at primary surgery were randomly chosen and used for the gene expression analysis. The patient tumor (GBM_CPH048) used for establishment of the neurosphere cell culture NGBM_CPH048p6 utilized in the xenograft model was included. Isolated RNA from archival human jejunum was used as a positive control in the gene expression analysis as a high expression of LAT2 has been detected in the intestine [21].

RNA Extraction and Reverse Transcription

After resection, tumor specimens from patients were snap-frozen and stored in liquid nitrogen. Total RNA was isolated using Trizol reagens (Gibco BRL 15596-018) and Qiagen TissueLyser before RNA purification with the RNeasy Miniki (Qiagen, Denmark). Resected xenograft tumors were immediately placed in tubes containing RNAlater (Sigma-Aldrich A/S, Denmark) and stored at 4°C for 2–3 days. Subsequently, the supernatant was removed and samples were stored at −80°C until further processing. The xenograft brain tumors were lyzed and homogenized in PrecellysR-24 (Bertin Techmologies, France). Total RNA from xenograft tumors was isolated with RNAzolRT in accordance with the protocol of the manufacturer (Molecular Research Center Inc., USA). The Agilent 2100 Bioanalyzer in conjunction with the Agilent RNA 6000 Nano Kits (Angilent Technologies Denmark A/S, Denmark) was used to measure the quality of the isolated RNA. RNA concentration was measured using the NanoDrop 1000 (Therme Fischer Scientific, USA). Total RNA (0.3 ug) was reversed transcribed (RT) using the Affinity-ScriptTM QPCR cDNA Synthesis Kit (Stratagene, USA) in accordance with the protocol of the manufacturer. RT reactions were performed using the Eppendorf Mastercycler Gradient (Eppendorf AG, Germany) and the protocol: incubation at 25°C for 5 minutes (primer annealing), 42°C for 15 minutes (cDNA synthesis) and 95°C for 5 minutes (termination of cDNA synthesis). Immediately after RT, samples were cooled and stored at −20°C.

Quantitative Real–time PCR

The optimal housekeeping genes were selected from two panels of common endogenous control genes (TATA Biocenter, Sweden and the geNorm Kit, PrimerDesign, UK). The geNorm software was used to analyze gene expression stability and ubiquitin C (UBC) and actin beta (ACTB) were found to be the best candidate reference genes. Primers were designed using Beacon Designer^{TM} (PREMIER Biosoft, USA). A BLAST search for sequence homology and a secondary structure search were included in the designs, and primers were optimized to be human specific and to distinguish between LAT1 and LAT2. Primer sequences were UBC-FP: 5′ctggaagatggtcgtacc-3′, UBC-RP: 5′gtcagggtcttcac-gaag-3′, ACTB-FP: 5′-tggcatccacgaaactac-3′, ACTB-RP: 5′ggcagtgatctccttctg-3′, LAT1-FP: 5′-ggctgagttctggttcat-3′, LAT1-RP: 5′-tgtgtctgccttttcttgt-3′, LAT2-FP: 5′-ttgtcaggcagtgg-tagg3′, LAT2-RP: 5′-tggttctttgggtatgaatgtc-3′, Ki67-FP: 5′-tcccgcctgttttctttctgac-3′, Ki67-RP: 5′-ctctccaaggatgatgatgctttac-3′. All primers were purchased from Sigma-Aldrich (Sigma-Aldrich, USA).

The Brilliant SYBRGreen QPCR Master Mix (Stratagene) was used and gene expression was quantified on the Mx300P real-time PCR system (Stratagene). The following thermal profile was used: denaturation for 10 minutes at 95°C followed by 45 cycles of 30 seconds denaturation at 95°C, primer annealing for 1 minute at 60°C and 1 minute extension at 72°C. Subsequently, the PCR product was denatured for 1 minute at 95°C followed by a ramp down to 55°C and a dissociation curve was acquired by a stepwise increase in temperature from 55°C to 95°C with steps of 0.5°C/cycle. All samples were run in duplicates using 1 µl of cDNA and to each sample a no-template control (NTC) was included. No reverse transcription control (NoRT) for all samples was tested using the housekeeping genes and LAT1. All xenograft and patient samples were included in a single run for every gene and assays were optimized to have efficiencies between 90% and 110%. Quantification of results was based on the computation of target quantification cycle (Cq) values and housekeeping gene Cq values in the qbase^{PLUS} software (Biogazelle NV, Belgium) [22]. Genes of interest (GOI) were normalized to the arithmetic mean expression of the two housekeeping genes with a reference target stability of 0.66 (M-value) and 0.23 (CV-value). A default amplification efficacy of 100% was used. Results were reported as normalized relative quantities (NRQs). For relative comparison of the NRQs between murine and human samples a cDNA sample from human jejunum was included in all runs and GOI are expressed relative to the expression of GOI in the jejunum sample.

Immunohistochemistry (IHC)

One brain from each treatment group was fixed for 24 hours in 4% paraformaldehyde (PFA), which subsequently was exchanged for EtOH 70%. After fixation the brains were divided in two by coronal cutting in the incision site and two pieces of each brain were embedded in the same paraffin block. From the brain anterior and posterior to the incision site, 4 µm histological sections were prepared for IHC. The sections were manually stained with hematoxylin and eosin (HE) for normal histological evaluation.

Statistical Analysis

All statistical analysis was performed using GraphPad Prism version 5.01 for Windows (GraphPad Software Inc., USA). All data are presented as mean ± SEM (standard error of mean) if not stated otherwise. $P<0.05$ was considered statistically significant. In xenografts comparison between the treatment and the control group was performed using unpaired Student's t-test. Univariate linear regression was performed in the gene expression analysis and the SUV_{max} T/B ratio was used. Comparison of the relative gene expression between patient and xenograft tumors was performed on log transformed data in order to obtain consistency with the Gaussian distribution. Student's t-test with Welsh's correction was used for the comparison between patient and xenograft tumors. All data were evaluated by the D'Agostino-Pearson normality test.

Results

Tumor Model Characteristics

In order to establish GBM xenografts for the characterization of ^{18}F-FET uptake, 20 mice were intracranially injected with NGBM_CPH048p6 neurosphere cells. Four mice were excluded from the study: Two mice due to absence of tumor take before the predefined limit of 12 weeks. One mouse was euthanized due to considerable weight loss, which was caused by intraventricular tumor growth, which was not visible on ^{18}F-FET PET. The last mouse was excluded because of rapid tumor growth and weight loss within one week which hindered an evaluation MicroPET/CT. The tumor take rate (before 12 weeks) was 85% (17/20). Median time to tumor take was 6 weeks (range 3–11 weeks). A total of 16 mice were included in the treatment study: CPT-11 group (n = 8) and control group (n = 8). Figure 1 shows a HE stained section of a formalin-fixed paraffin-embedded mouse brain from the CPT-11 group 7 weeks after tumor cell injection. Marked cellularity and pleomorphism is evident in the section which are histopathological features typical for GBM.

^{18}F-FET PET Imaging of Orthotopic GBM Xenografts

Representative ^{18}F-FET MicroPET/CT images of an orthotopic NGBM_CPH048p6 tumor from a single mouse are shown in Figure 2, with ROI_T and ROI_B illustrated. The ^{18}F-PET images show a high ^{18}F-FET uptake in the tumor and a very low background uptake in the brain. The size of the tumor and the intensity of the signal increased every week, indicating that ^{18}F-FET MicroPET/CT can be used to monitor *in vivo* tumor growth. ^{18}F-FET dynamics in the brain tumor and the contralateral normal hemisphere was evaluated in 2 separate mice not included in the treatment study. ^{18}F-FET accumulation in the brain tumor was constantly increasing or stable (Figure 3A) and the T/B ratio was stable for the evaluation time (Figure 3B). In order to investigate whether the ^{18}F-FET MicroPET/CT could be used to detect response to treatment, in this case CPT-11, the relative ^{18}F-FET uptake in the two groups (the mean T/B ratio of SUV_{max} and $SUV_{mean,}$ respectively) was plotted versus time after tumor engraftment (Figure 4A and 4B). The relative T/B ratio of SUV_{max} was significantly lower after one week (123±6%, n = 7 vs. 146±6%, n = 7; p = 0.018) and after two weeks (142±8, n = 5 vs. 204±27, n = 4; p = 0.047) in the CPT-11 group as compared with the control group. In addition, the relative T/B ratio of SUV_{mean} was significantly lower after two weeks (134±10%, n = 5 vs. 206±16%, n = 4; p = 0.0049) in the CPT-11 group, although after one week there was only a trend towards significance between the treatment and the control group (127±7%, n = 7 and 147±8%, n = 7; p = 0.09).

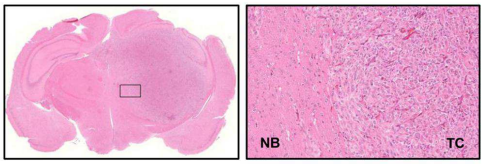

Figure 1. HE of xenograft tumor. A) HE section across a formalin-fixed paraffin-embedded mouse brain showing the GBM tumor 7 weeks after tumor cell injection. B) HE, magnification×20.
doi:10.1371/journal.pone.0100009.g001

Quantitative mRNA Expression of Ki-67, LAT1 and LAT2 in Xenografts

As we were able to detect a tumor response to CPT-11 using ^{18}F-FET MicroPET/CT we wanted to evaluate the effect of CPT-11 on tumor cell proliferation. For this, we compared the gene expression of Ki67 in the treatment group to the control group after two weeks of treatment. Surprisingly, we found no difference in the relative Ki67 expression in the treatment group as compared to the control group (1.14±0.1 vs. 1±0.08; $p = 0.35$), (Figure 5). To examine the relationship between the relative gene expression of the amino acid transporters LAT1 and LAT2 compared to the ^{18}F-FET uptake, we performed qPCR against both transcripts and a univariate linear regression analysis. We found a strong negative correlation between the gene expression of LAT1 and the relative T/B ratio (r = −0.62, p = 0.04) as well as between the gene expression of LAT2 and the relative T/B ratio (r = −0.67, p = 0.02), (Figure 6A and 6B). Furthermore, we found a positive correlation between the gene expression of Ki67 and LAT1 (r = 0.63, p = 0.04), (Figure 6C). However, we did not find a correlation between the gene expression of Ki67 and LAT2 or between the T/B ratio and the gene expression of Ki67 (Figure 6D and 6E).

Quantitative mRNA Expression in Xenografts Compared to Patient Specimens

In order to investigate if the expression of Ki67, LAT1 and LAT2 were similar between the xenografts, the patient tumor (GBM_CHP048) used for the establishment of the xenografts and tumor specimens from a panel of 19 GBM patients, we performed qPCR and compared the NRQs relative to the gene expression in human jejunum, which was adjusted to 100. The relative gene expression of Ki67, LAT1 and LAT2 are illustrated in Figure 7. As expected, we found a larger variation in the human samples as compared to the xenograft tumors. The relative Ki67 expression was not significantly different between xenografts and patients (152; 95% CI: 131–176 vs. 231; 95% CI: 154–347; p = 0.053). However, the difference of the relative LAT1 expression was borderline significant with 1.6 fold higher LAT1 expression in GBM patients compared to the xenografts (744; 95% CI: 503–1099 vs. 467; 95% CI: 358–610; p = 0.045). In addition, we found a low LAT2 expression in the patients as compared to the expression of LAT2 in jejunum (16; 95% CI: 10–25 vs. 100). Surprisingly, the expression in xenografts was even lower as compared to the patients with an approximately 23 fold changes in relative expression of LAT2 (0.7; 95% CI: 0.5–1 vs. 16; 95% CI 10–25; $p<0.0001$). In general, the relative gene expression of Ki67, LAT1 and LAT2 in xenograft tumors were significantly different from the original patient tumor GBM_CPH048

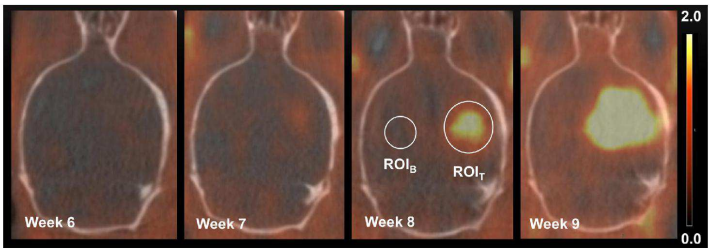

Figure 2. Fused ^{18}F-FET PET/CT images. Fused ^{18}F-FET MicroPET/CT images showing tumor progression 6–9 weeks after tumor cell injection. Transverse views through the brain of the same mouse. Illustrated in the figure is a ROI$_T$ drawn round the region with maximum tracer uptake and a 4 mm^3 ROI$_B$ drawn in the contralateral hemisphere. Scale bar: 0.0–2.0 SUV$_{max}$.
doi:10.1371/journal.pone.0100009.g002

(Figure 7). We did not find any correlations between Ki67 and LAT1 or LAT2 in the patient specimens (Figure 8).

Discussion

In this study we demonstrated the feasibility of *in vivo* imaging of orthotopic human GBM in mice using ^{18}F-FET MicroPET/CT. To our knowledge there are no other published reports evaluating the use of *longitudinal* ^{18}F-FET imaging for treatment response evaluation in orthotopic glioma models. At present the most widely used amino acid tracers are L-methyl-^{11}C-methionine (^{11}C-MET) and ^{18}F-FET [23]. Multiple clinical and preclinical studies have evaluated ^{11}C-MET PET for the visualization of brain tumors, and it has been successfully used in neuro-oncology [9,24]. However, in clinical practice, ^{18}F-FET has logistic and economic advantages over ^{11}C-MET due to the longer physical half-life of ^{18}F (109.8 min vs. 20.4 min). ^{18}F-FET is synthesized with a relatively high radiochemical yield (up to 40%), which is in contrast to other ^{18}F labeled amino acids like ^{18}F-fluro-L-tyrosine (^{18}F-TYR) and ^{18}F-fluro-L-methyl-tyrosine (^{18}F-FMT) [25]. Only a few studies have evaluated the bio-distribution and tumor accumulation of ^{18}F-FET in glioma models and these studies were, except from one study [12], all performed in rats [8,13,14]. The various advantages and disadvantages of the different glioma models are beyond the scope of this article. However, orthotopic tumor models are considered better predictive models of drug efficacy than traditional subcutaneous models [26]. With the use of orthotopic GBM models more advanced imaging techniques like MRI and PET are necessary. In the present study we have demonstrated the feasibility of using ^{18}F-FET PET to monitor tumor growth non-invasive in a murine GBM model which makes is possible, in addition to MRI, to obtain complementary information about tumor growth. As such, the preclinical setting corresponds to the clinical setup were both imaging modalities frequently are used.

In addition to validation of ^{18}F-FET as a feasible imaging tracer, it was possible to detect a treatment response with ^{18}F-FET. Using the T/B ratio of SUV$_{max}$ and SUV$_{mean}$ we were able to distinguish between the treatment and the control group after 2 weeks of treatment. Furthermore, using the T/B ratio of SUV$_{max}$ we detected a treatment response already after one week of treatment and results for the T/B ratio of SUV$_{mean}$ were similar, although borderline significant. These results are in line with recently published results from the clinic, where it was possible to identify responders to bevacizumab and CPT-11 with ^{18}F-FET PET at an early follow-up (median 4.9 weeks) [6]. In another clinical study, it was similarly concluded that changes in the ^{18}F-FET PET signal might be a useful measure to predict treatment response at an early stage of GBM [7]. Our findings suggest that responders and non-responders may have been differentiated by ^{18}F-FET PET at an even earlier time point.

In order to interpret ^{18}F-FET, it is essential to understand the transport mechanisms and the major factors that influence the transport and tumor uptake of ^{18}F-FET. The tumor uptake of ^{18}F-FET is related to the higher transport rate of amino acids rather than to proliferation. In addition, a disruption of the blood-brain

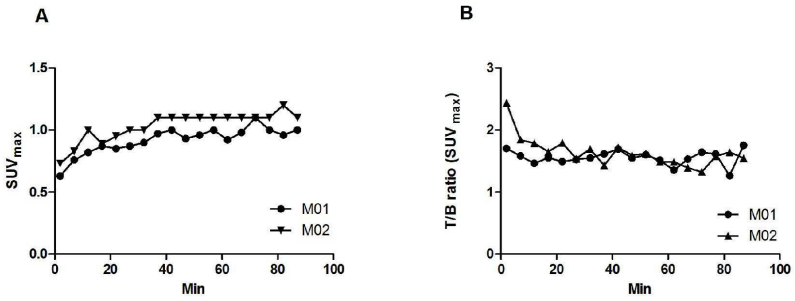

Figure 3. Time-activity curves of ^{18}F-FET in xenografts. Time-activity curves of ^{18}F-FET in two different mice (M01, M02) presented as SUV$_{max}$ in the tumor ROI (A) and tumor-to-brain (T/B) ratio (B).
doi:10.1371/journal.pone.0100009.g003

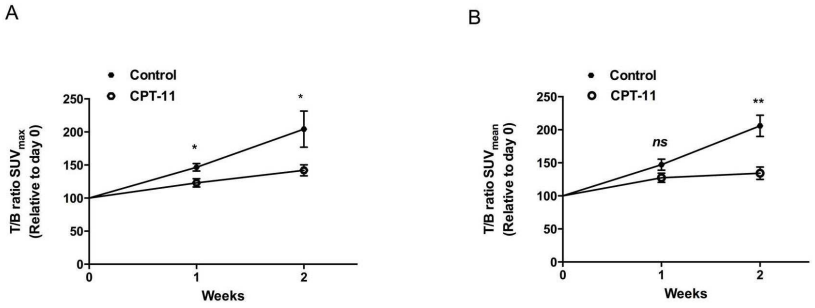

Figure 4. ^{18}F-FET uptake in xenografts. A) The relative T/B ratio of SUV_{max} versus time after tumor engraftment. B) The relative T/B ratio of SUV_{mean} versus time after tumor engraftment. Values expressed as mean ± SEM in the CPT-11 (n = 5–7) and in the control group (n = 4–7), *$p<0.05$ and **$p<0.01$.
doi:10.1371/journal.pone.0100009.g004

barrier (BBB) is not mandatory for ^{18}F-FET uptake in gliomas [27]. As such, ^{18}F-FET is different from the proliferation tracer 3′-deoxy-3′-^{18}F-fluorothymidine (^{18}F-FLT) which is a marker of DNA synthesis. ^{18}F-FLT is not transported across the intact BBB which affects the sensitivity of ^{18}F-FLT in gliomas [28]. The major transport systems for neutral amino acids like L-tyrosine are: System A (alanine preferring), system ASC (alanine-serine-cystine preferring) and system L (leucine preferring) [29]. A few *in vitro* studies have determined the Na^+-independent system L as the main transport system of L-tyrosine and its analog ^{18}F-FET [8,9]. Among the four subtypes of system L, especially LAT1 expression has attracted much attention and it has been investigated in several cancer types, although only a few reports exist regarding LAT1 expression in gliomas [30]. In a clinical study the LAT1 IHC staining was located to the vascular endothelium as well as the tumor cell membrane and cytoplasm in tumor specimens from patients with glioma [30]. In a rat C6 glioma cell line, LAT1, but not LAT2, was expressed, and in normal astrocytes LAT2, but not LAT1, was expressed, indicating LAT1 as a possible target for anti-cancer therapy [15]. In the present study, we found LAT1 as well as LAT2 to be expressed in GBM tissue from patients and from xenografts. We also observed a positive correlation between LAT1 and Ki67 in the xenograft tumors which is in line with another study where LAT1 correlated with the glioma pathological grading, and the IHC staining of Ki67 [30]. However, and in contrary to this study [30], we failed to detect this LAT1/Ki67 correlation in our patient samples. Other reports have confirmed the expression of LAT1 at the blood-brain barrier (BBB) [21], however, expression of LAT2 in the BBB is controversial and limited information exists regarding LAT2 expression in gliomas [21]. In our study, we found a much lower expression of LAT2 in xenografts compared to patient specimens. As we did not perform IHC, we are unable to conclude if LAT1 and LAT2 were located primarily at the BBB, in the tumor cells or if the location is overlapping. If LAT2 primarily is located at the BBB, this could be a possible explanation for the low expression of LAT2 in xenografts as the LAT2 primers were specifically designed for human LAT2 and tumor vessels in the xenograft tumor are primarily murine. Different expression of LAT2 between species is another possible explanation for this difference in LAT2 expression. However, this needs further investigation.

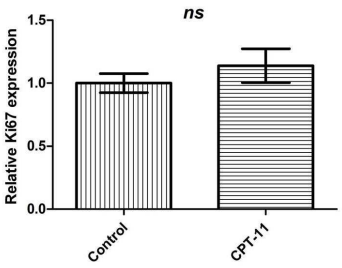

Figure 5. Ki67 expression in xenografts. The gene expression of Ki67 the CPT-11 (n = 7) relative to the control group (n = 4). Values expressed as mean ± SEM, $p = 0.35$.
doi:10.1371/journal.pone.0100009.g005

As described above, the transport of ^{18}F-FET is mainly facilitated by system L and presumably linked to the expression of LAT1 and/or LAT2 [10,11,31]. The dynamic ^{18}F-FET PET performed in this study demonstrated accumulation and retention of ^{18}F-FET in the normal brain and in the brain tumor. A similar pattern is seen in some GBM patients, while other GBM patients show a decreasing pattern with an early wash out of ^{18}F-FET [32]. In the present study, we observed a strong negative correlation between the relative ^{18}F-FET T/B ratio and the gene expression of LAT1 and LAT2, which could indicate an export transport function. The LATs are amino acid exchangers with 1:1 stoichiometry and the net direction of ^{18}F-FET depends on the extra- and intracellular concentrations of ^{18}F-FET [21]. The retention mechanisms of ^{18}F-FET have not been clarified and one could speculate that a saturation of the retention mechanism is possible in the xenograft model where ^{18}F-FET is given in much higher concentrations compared to human patients. As such, ^{18}F-FET would, to a small extent, be transported out of the cell as the retention system is saturated and the blood concentration is decreasing. This transport out of the cell could be dependent on the amount of LATs present in the cell membrane. As a result there would be a negative correlation between the T/B ratio and LAT1 and LAT2, although most of ^{18}F-FET is still retained in the tumor cells as demonstrated in the dynamic ^{18}F-FET PET (Figure 3). However, the small sample size of this study makes the observed correlations less reliable and it needs to be verified in larger studies.

In the present study, the relative difference in T/B ratio between the treatment and the control group was not reflected in a

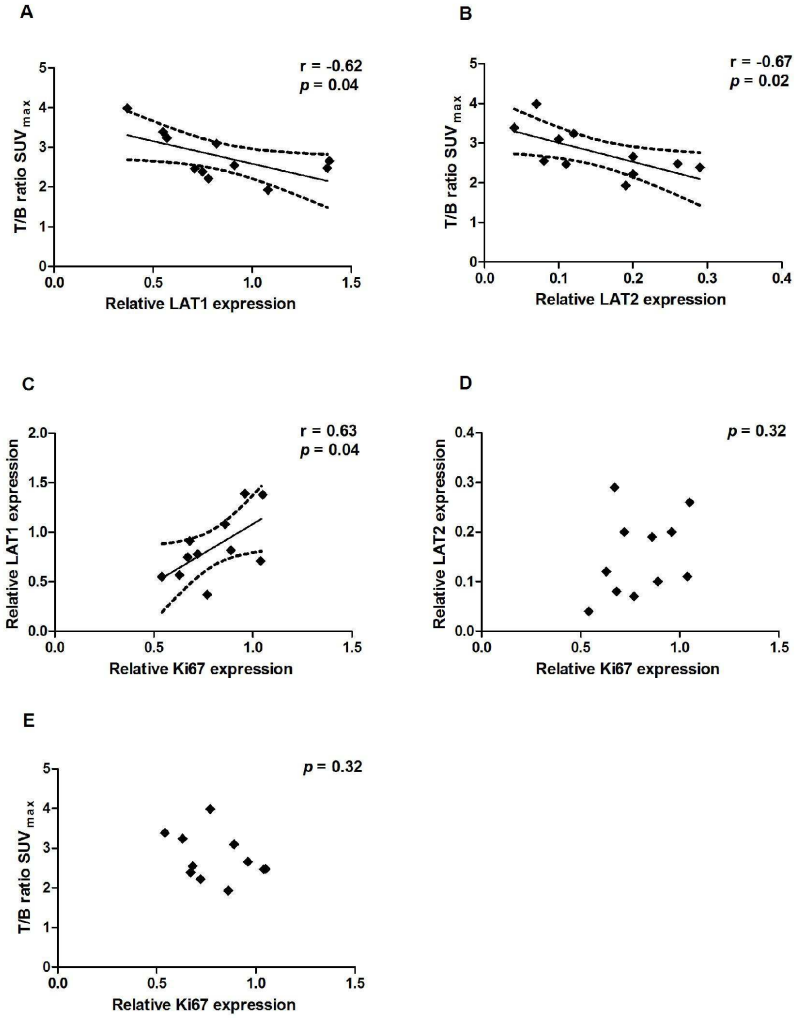

Figure 6. Gene expression and ^{18}F-FET uptake in xenografts. Univariate linear regression analysis of gene expression (n = 11). A) LAT1 expression relative to T/B ratio of SUV_{max}. B) LAT2 expression relative to T/B ratio of SUV_{max}. C) Ki67 expression relative to LAT1. D) Ki67 expression relative to LAT2. E) Ki67 expression relative to T/B ratio of SUV_{max}. The 95% CI is indicated by the broken lines.
doi:10.1371/journal.pone.0100009.g006

decrease in the Ki67 gene expression level in the treatment group. Although other studies have demonstrated anti-cancer activity of CPT-11 in GBM murine models [18,19], we did not perform a survival analysis in this study and further studies are thus needed to explore if the changes in the ^{18}F-FET uptake reflect true anti-cancer activity. The controversial topic about protein expression and mRNA level is another possible explanation for the observed unchanged Ki67 gene expression level in the present study. In general, expression of proteins correlate with their corresponding mRNAs, but the correlation is not very strong [33]. It remains questionable if small changes at the protein level are reflected in the gene expression level. The correlation between mRNA expression and protein level of Ki67 in this tumor model thus needs further investigation.

The optimal imaging strategy for evaluating patients with GBM has not been elucidated and comparative evidence whether PET has superior properties compared to modern MRI techniques or whether a specific PET tracer outperforms another is limited. Several clinical studies have documented the diagnostic performance of ^{18}F-FET PET in primary brain tumors, and in

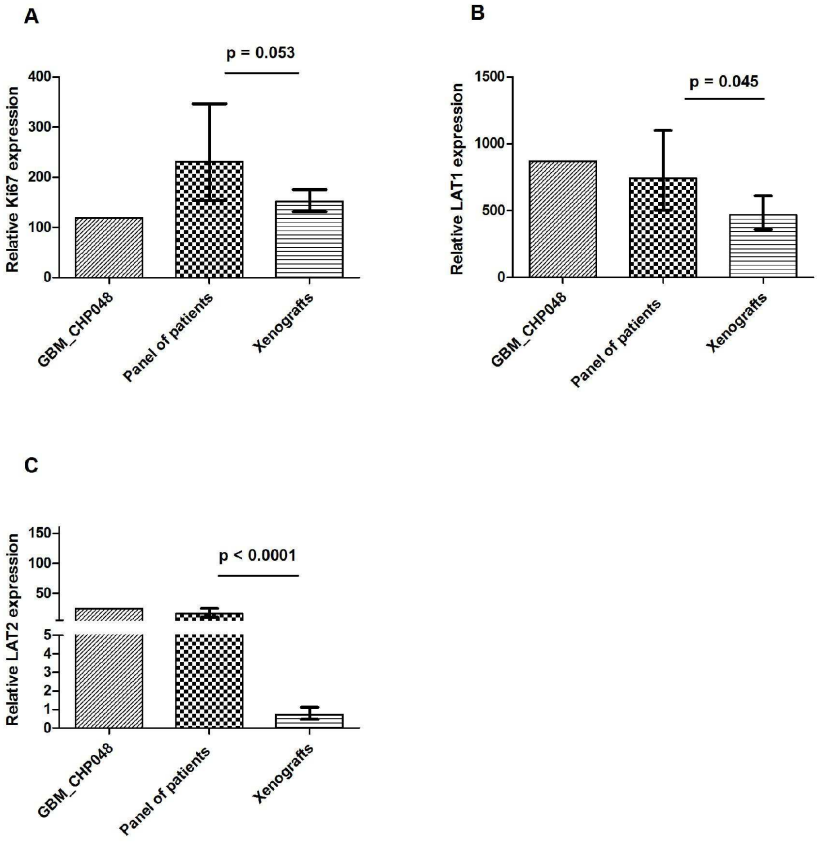

Figure 7. Gene expression in patients compared to xenografts. Relative gene expression in patient GBM_CPH048, the GBM patient panel (n = 19) and xenografts (n = 11). A) Ki67. B) LAT1. C) LAT2. All genes are normalized to housekeeping genes and are relative to human jejunum (jejunum = 100). Values are displayed as geometric mean±95% CI.
doi:10.1371/journal.pone.0100009.g007

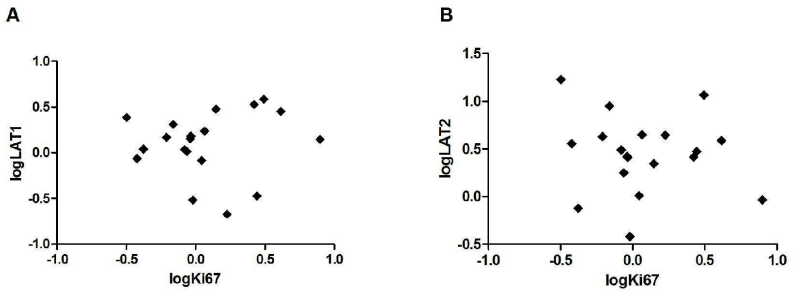

Figure 8. A) Person's correlation between logki67 and logLAT1 in patient specimens. B) Pearson's correlation between logki67 and logLAT2 in patient specimens (n = 19).
doi:10.1371/journal.pone.0100009.g008

conjugation with MRI, ^{18}F-FET PET has revealed supplementary information on tumor growth and metabolism [6,34]. Furthermore, a good correlation between ^{18}F-FET uptake and treatment response has also been demonstrated in clinical studies [5–7,35]. In the present study, we used a patient derived GBM cell line in a murine model and demonstrated the feasibility of monitoring a treatment response with ^{18}F-FET PET. The development and implementation of new anti-GBM therapies require valid tumor models and a translational method for drug testing and response assessment. ^{18}F-FET PET (in conjunction with MRI and/or bioluminescence) can possibly be used to evaluate new treatment regimens and novel therapeutic agents in several human xenograft GBM models with different molecular characteristic. With more accurate animal models and imaging techniques we will likely create better results that translate into satisfactory treatment outcomes in the clinic.

Conclusion

In conclusion, we have demonstrated the feasibility of *in vivo* imaging of orthotopic human GBM in a murine model with ^{18}F-FET PET. In addition, we found that with ^{18}F-FET uptake we were able to detect a CPT-11 treatment response after one and two weeks of treatment, suggesting that ^{18}F-FET uptake may be an early and non-invasive biomarker for detection of anti-tumor activity or treatment failure in preclinical and in clinical studies. As such, this study supports the additional use of ^{18}F-FET PET in the evaluation of patients with GBM and in preclinical trials. We found a strong positive correlation between the gene expression of Ki67 and LAT1 in xenografts, however there was no correlation in patient specimens. Furthermore, we found a much higher expression of LAT2 in patient specimens compared to xenografts, which could be caused by human specific LAT primers or indicate a difference between species. Interestingly, we found a strong negative correlation between the T/B ratio and the gene expression of LAT1 and LAT2 in xenografts, which may be explained by the ^{18}F-FET kinetics and tumor cell retention mechanisms. However, further studies are needed to clarify the ^{18}F-FET dynamics and exact transport mechanisms in humans and in xenografts.

Acknowledgments

We thank Mette Villingshøj for maintaining the cell line and preparing tumor cells and Babloo Lukram for performing the IHC.

Author Contributions

Conceived and designed the experiments: MKN KK SRM JM HSP MTS UL AK. Performed the experiments: MKN KK SRM. Analyzed the data: MKN MTS UL AK. Contributed reagents/materials/analysis tools: MKN SRM JM. Wrote the paper: MKN MTS.

References

1. Wen PY, Macdonald DR, Reardon DA, Cloughesy TF, Sorensen AG, et al. (2010) Updated response assessment criteria for high-grade gliomas: response assessment in neuro-oncology working group. J Clin Oncol 28: 1963–1972.
2. Pope WB, Young JR, Ellingson BM (2011) Advances in MRI assessment of gliomas and response to anti-VEGF therapy. Curr Neurol Neurosci Rep 11: 336–344.
3. Fletcher JW, Djulbegovic B, Soares HP, Siegel BA, Lowe VJ, et al. (2008) Recommendations on the use of 18F-FDG PET in oncology. J Nucl Med 49: 480–508.
4. Olivero WC, Dulebohn SC, Lister JR (1995) The use of PET in evaluating patients with primary brain tumours: is it useful? J Neurol Neurosurg Psychiatry 58: 250–252.
5. Hutterer M, Nowosielski M, Putzer D, Waitz D, Tinkhauser G, et al. (2011) O-(2-18F-fluoroethyl)-L-tyrosine PET predicts failure of antiangiogenic treatment in patients with recurrent high-grade glioma. J Nucl Med 52: 856–864.
6. Galldiks N, Rapp M, Stoffels G, Fink GR, Shah NJ, et al. (2013) Response assessment of bevacizumab in patients with recurrent malignant glioma using [18F]Fluoroethyl-L-tyrosine PET in comparison to MRI. Eur J Nucl Med Mol Imaging 40: 22–33.
7. Galldiks N, Langen KJ, Holy R, Pinkawa M, Stoffels G, et al. (2012) Assessment of treatment response in patients with glioblastoma using O-(2-18F-fluoroethyl)-L-tyrosine PET in comparison to MRI. J Nucl Med 53: 1048–1057.
8. Heiss P, Mayer S, Herz M, Wester HJ, Schwaiger M, et al. (1999) Investigation of transport mechanism and uptake kinetics of O-(2-[18F]fluoroethyl)-L-tyrosine in vitro and in vivo. J Nucl Med 40: 1367–1373.
9. Langen KJ, Jarosch M, Muhlensiepen H, Hamacher K, Broer S, et al. (2003) Comparison of fluorotyrosines and methionine uptake in F98 rat gliomas. Nucl Med Biol 30: 501–508.
10. Wiriyasermkul P, Nagamori S, Tominaga H, Oriuchi N, Kaira K, et al. (2012) Transport of 3-fluoro-L-alpha-methyl-tyrosine by tumor-upregulated L-type amino acid transporter 1: a cause of the tumor uptake in PET. J Nucl Med 53: 1253–1261.
11. Langen KJ, Hamacher K, Weckesser M, Floeth F, Stoffels G, et al. (2006) O-(2-[18F]fluoroethyl)-L-tyrosine: uptake mechanisms and clinical applications. Nucl Med Biol 33: 287–294.
12. Sai KK, Huang C, Yuan L, Zhou D, Piwnica-Worms D, et al. (2013) 18F-AFETP, 18F-FET, and 18F-FDG imaging of mouse DBT gliomas. J Nucl Med 54: 1120–1126.
13. Menichetti L, Petroni D, Panetta D, Burchielli S, Bortolussi S, et al. (2011) A micro-PET/CT approach using O-(2-[18F]fluoroethyl)-L-tyrosine in an experimental animal model of F98 glioma for BNCT. Appl Radiat Isot 69: 1717–1720.
14. Wang HE, Wu SY, Chang CW, Liu RS, Hwang LC, et al. (2005) Evaluation of F-18-labeled amino acid derivatives and [18F]FDG as PET probes in a brain tumor-bearing animal model. Nucl Med Biol 32: 367–375.
15. Kim DK, Kim IJ, Hwang S, Kook JH, Lee MC, et al. (2004) System L-amino acid transporters are differently expressed in rat astrocyte and C6 glioma cells. Neurosci Res 50: 437–446.
16. Kristoffersen K, Villingshoj M, Poulsen HS, Stockhausen MT (2013) Level of Notch activation determines the effect on growth and stem cell-like features in glioblastoma multiforme neurosphere cultures. Cancer Biol Ther 14: 625–637. 24595.
17. Stockhausen MT, Broholm H, Villingshoj M, Kirchhoff M, Gerdes T, et al. (2011) Maintenance of EGFR and EGFRvIII expressions in an in vivo and in vitro model of human glioblastoma multiforme. Exp Cell Res 317: 1513–1526.
18. Verreault M, Strutt D, Masin D, Anantha M, Waterhouse D, et al. (2012) Irinophore C, a lipid-based nanoparticulate formulation of irinotecan, is more effective than free irinotecan when used to treat an orthotopic glioblastoma model. J Control Release 158: 34–43.
19. Kuroda J, Kuratsu J, Yasunaga M, Koga Y, Kenmotsu H, et al. (2010) Antitumor effect of NK012, a 7-ethyl-10-hydroxycamptothecin-incorporating polymeric micelle, on U87MG orthotopic glioblastoma in mice compared with irinotecan hydrochloride in combination with bevacizumab. Clin Cancer Res 16: 521–529.
20. El Ali HH, Bodholdt RP, Jørgensen JT, Myschetzky R, Kjaer A (2012) Importance of Attenuation Correction (AC) for Small Animal PET Imaging. Diagnostics 2: 42–51.
21. del Amo EM, Urtti A, Yliperttula M (2008) Pharmacokinetic role of L-type amino acid transporters LAT1 and LAT2. Eur J Pharm Sci 35: 161–174.
22. Hellemans J, Mortier G, De PA, Speleman F, Vandesompele J (2007) qBase relative quantification framework and software for management and automated analysis of real-time quantitative PCR data. Genome Biol 8: R19.
23. Gulyas B, Halldin C (2012) New PET radiopharmaceuticals beyond FDG for brain tumor imaging. Q J Nucl Med Mol Imaging 56: 173–190.
24. Nihashi T, Dahabreh IJ, Terasawa T (2013) PET in the clinical management of glioma: evidence map. AJR Am J Roentgenol 200: W654–W660.
25. Wester HJ, Herz M, Weber W, Heiss P, Senekowitsch-Schmidtke R, et al. (1999) Synthesis and radiopharmacology of O-(2-[18F]fluoroethyl)-L-tyrosine for tumor imaging. J Nucl Med 40: 205–212.
26. Fomchenko EI, Holland EC (2006) Mouse models of brain tumors and their applications in preclinical trials. Clin Cancer Res 12: 5288–5297.
27. Popperl G, Gotz C, Rachinger W, Gildehaus FJ, Tonn JC, Tatsch K (2004) Value of O-(2-[18F]fluoroethyl)- L-tyrosine PET for the diagnosis of recurrent glioma. Eur J Nucl Med Mol Imaging 31: 1464–1470.
28. Jeong SY, Lim SM (2012) Comparison of 3′-deoxy-3′-[18F]fluorothymidine PET and O-(2-[18F]fluoroethyl)-L-tyrosine PET in patients with newly diagnosed glioma. Nucl Med Biol 39: 977–981.
29. Wang L, Qu W, Lieberman BP, Plossl K, Kung HF (2011) Synthesis, uptake mechanism characterization and biological evaluation of (18)F labeled fluoroalkyl phenylalanine analogs as potential PET imaging agents. Nucl Med Biol 38: 53–62.

30. Haining Z, Kawai N, Miyake K, Okada M, Okubo S, et al. (2012) Relation of LAT1/4F2hc expression with pathological grade, proliferation and angiogenesis in human gliomas. BMC Clin Pathol 12: 4.
31. Lahoutte T, Caveliers V, Camargo SM, Franca R, Ramadan T, et al. (2004) SPECT and PET amino acid tracer influx via system L (h4F2hc-hLAT1) and its transstimulation. J Nucl Med 45: 1591–1596.
32. Popperl G, Kreth FW, Mehrkens JH, Herms J, Seelos K, et al. (2007) FET PET for the evaluation of untreated gliomas: correlation of FET uptake and uptake kinetics with tumour grading. Eur J Nucl Med Mol Imaging 34: 1933–1942.
33. Vogel C, Marcotte EM (2012) Insights into the regulation of protein abundance from proteomic and transcriptomic analyses. Nat Rev Genet 13: 227–232.
34. Galldiks N, Filss CP, Goldbrunner R, Langen KJ (2012) Discrepant MR and [(18)F]Fluoroethyl-L-Tyrosine PET Imaging Findings in a Patient with Bevacizumab Failure. Case Rep Oncol 5: 490–494.
35. Heinzel A, Muller D, Langen KJ, Blaum M, Verburg FA, et al. (2013) The Use of O-(2-18F-Fluoroethyl)-L-Tyrosine PET for Treatment Management of Bevacizumab and Irinotecan in Patients with Recurrent High-Grade Glioma: A Cost-Effectiveness Analysis. J Nucl Med 54: 1217–1222.

Appendix II

Manuscript II

Nedergaard MK, Michaelsen SR, Perryman L, Erler, Poulsen HS, Lassen U, Stockhausen MT and Kjaer A. Comparison of ^{18}F-FET and ^{18}F-FLT MicroPET for the assessment of anti-VEGF efficacy in an orthotopic model of glioblastoma.

Submitted to *The Journal of Nuclear Medicine* June 02, 2014

Comparison of ^{18}F-FET and ^{18}F-FLT MicroPET for the assessment of anti-VEGF efficacy in an orthotopic model of glioblastoma

By:

Mette K. Nedergaard[1#], Signe R. Michaelsen[2], Lara Perryman[3], Janine Erler[3], Hans S. Poulsen[2], Ulrik Lassen[4], Marie-Thérése Stockhausen[2] and Andreas Kjaer[1]

[1]Department of Clinical Physiology, Nuclear Medicine & PET and Cluster for Molecular Imaging, Rigshospitalet and University of Copenhagen, Copenhagen, Denmark

[2]Department of Radiation Biology, The Finsen Center, Rigshospitalet, Copenhagen, Denmark

[3]Biotech Research and Innovation Center (BRIC), University of Copenhagen, Copenhagen, Denmark

[4]Phase 1 Unit, Department of Oncology, The Finsen Center, Rigshospitalet, Copenhagen, Denmark

ABSTRACT

^{18}F-FLT and ^{18}F-FET PET are widely used for brain tumor imaging, however, comparative studies are scarce. Due to the limited transport of FLT across the intact blood-brain barrier (BBB) we hypothesize that FLT PET compared to FET PET are more affected by anti-VEGF induced changes in the tumor vasculature. The aim of this study therefore was, to evaluate and compare the value of FLT and FET PET for assessment of anti-VEGF response in orthotopic human glioma xenografts.

Methods: Cells of human glioblastoma multiforme (GBM) neurosphere culture (NGBM_CHP048p6_LUC) were injected orthotopically in NMRI nude mice. At confirmed tumor take, mice were treated with anti-VEGF therapy (B20-4.1) or saline as control. Weekly bioluminescence, ^{18}F-FLT and ^{18}F-FET MicroPET/CT were used to follow treatment response. The end-point was survival and brains from sacrificed mice were used for immunohistochemistry and subsequent quantification of the Ki67 proliferation index and micro-vessel density (MVD).

Results: The relative ^{18}F-FET tumor-to-brain (T/B) ratio of SUV_{max} was significantly decreased after one week (99±6%, n=6 vs. 124±9%, n=5; p=0.04) and after two weeks (106±10%, n=5 vs. 156±17%, n=4; p=0.03) in the B20-4.1 group as compared with the control group. In contrast, using ^{18}F-FLT MicroPET there was no significant difference in the T/B ratio of SUV_{max} neither after one week of treatment (134±12%, n=6 vs. 144±6%, n=6; p=0.49) nor after two weeks of treatment (174±11%, n=5 vs. 208±30%, n=5; p=0.34). We found a significant lower MVD in the B20-4.1 group as compared to the control group (66±8%, n=8 vs. 100±10% n=7; p=0.02). However, we found no difference in the Ki67 proliferation index in the treatment group as compared to the control group (18.9±1, n=7 vs. 19.8±2; n=6; p=0.7). In addition, the mean survival was not prolonged in the treatment group compared to the control group (19 vs. 21 days; p=0.34).

Conclusion: In orthotopic GBM xenografts anti-VEGF treatment reduced MVD and ^{18}F-FET uptake but had no effect on ^{18}F-FLT uptake, the Ki67 proliferation index or survival. We suggest that ^{18}F-FET PET may be used to monitor the anti-VEGF treatment effect on MVD.

Key words: Glioma, ^{18}F-FET, ^{18}F-FLT, MicroPET

INTRODUCTION

Imaging of gliomas is a challenge and there are difficulties in assessing true tumor response by conventional magnetic resonance imaging (MRI) (*1*). Accordingly, new functional imaging techniques are increasingly used to obtain additional information about glioma growth and response to therapy. Positron emission tomography (PET) plays an important role in the management of cancer patients and the majority of PET scans are performed with the glucose analogue 2'-deoxy-2'-^{18}F-fluoro-D-glucose (^{18}F-FDG) (*2*). In cancer cells, the increased ^{18}F-FDG uptake is caused by increased metabolism and a higher expression of the glucose transporters as compared to normal cells (*3*). However, in normal brain tissue a high rate of glucose metabolism is observed. As such, a low tumor-to-background (T/B) uptake decreases the sensitivity of FDG, and uptake of glucose in inflammatory cells compromises the specificity of FDG in the brain (*4*). PET with radiolabeled amino acids like O-(2-^{18}F-fluoroethyl)-L-tyrosine (^{18}F-FET) and the radiolabeled thymidine analog 3'-deoxy-3'-^{18}F-fluorothimidine (^{18}F-FLT) overcome some of these limitations of FDG PET (*5, 6*). A low uptake in normal brain tissue in combination with intense accumulation in tumor cells is usually observed with both FLT and FET. Recently, the value of FLT compared to FET for non-invasive grading (*7*) and for analysis of tumor volume (*8*) in glioma patients were evaluate. Due to the limited transport of FLT across the intact blood-brain barrier (BBB) the sensitivity of FET PET was higher as compared to FLT PET. However, to our knowledge other comparative studies between FLT PET and FET PET have not been performed in clinical or preclinical studies.

Bevacizumab is a humanized monoclonal anti-VEGF antibody, which is used increasingly in patients with recurrent glioma (*9*). Bevacizumab treatment causes normalization of the tumor vasculature, a restored BBB and anti-tumor effect (*10*). We hypothesize that Bevacizumab response assessment with FLT PET primarily reflect changes in the BBB, whereas FET PET is less affected by the tumor vasculature. As such, FET PET may be a better imaging biomarker for anti-angiogenic response assessment in gliomas. The purpose of this study was therefore to evaluate the value of FET PET for anti-angiogenic response assessment in an orthotopic xenograft model of human glioblastoma and compare it with the value of FLT PET.

MATERIALS AND METHODS

Establishment of the orthotopic GBM model

The neurosphere GBM cell culture NGBM_CPH048p6 (*11*) was stably transfected with a lentiviral vector for expression of Fluc-mCherry. Briefly, HEK293T cells were grown to 60% confluence and 3ug of lentiviral constructs with Lipofectamine 2000 were used to generate viral supernatants (in accordance with manufacturer's instructions). The lentiviral supernatant and 4ug/ml polybrene (Millipore, Watford, UK) were used to infect NGBM_CPH048p6. Stability of the expression was confirmed with repeated measurements of the bioluminescent signal over a month in culture and 3 months *in vivo*.

Animal care and all experimental procedures were performed under the approval from the Danish Animal Welfare Council (2013-15-2934-00064). Six weeks old NMRI (Naval Medical Research Institute) nude female mice were acquired from Taconic Europe (Lille Skensved, Denmark). Following one to two week of acclimation ten µl cell suspension (100,000 cells) of NGBM_CHP048p6_LUC neurosphere cells were injected intracranially, as we have described previously (12).

Experimental design

Figure 1 shows a schematic view of the experimental design. Mice were injected with NGBM_CPH048p6_LUC neurosphere cells at week 0 and tumor growth was monitored by weekly bioluminescence (BLI). ^{18}F-FET and ^{18}F-FLT MicroPET in combination with computed tomography (CT) scanning were performed when the BLI signal reached a total flux of 500,000 p/s/cm^2/sr. Tumor take (TT) was considered as a FET SUV_{max} T/B ratio above 1.2. The ^{18}F-FET PET at TT was defined as the baseline FET PET. The BLI scan performed two days before and the FLT PET performed one day before the baseline FET PET were also regarded as baseline scans. Mice were subsequently divided in two groups, matched according to FET T/B ratio and time to TT and included in the treatment study. B20-4.1 intraperitoneally (i.p.), (5mg/kg) or 0.9% NaCl solution i.p. (control) was administered twice weekly. Treatment was initiated one day after the baseline ^{18}F-FET PET. B20-4.1 is an antibody against vascular endothelial growth factor A (VEGF-A). Unlike Bevacizumab, B20-4.1 has affinity for both the human and the murine VEGF-A (*13*). Anti-cancer activity of B20-4.1 in several xenograft tumors has previously been reported and the treatment regimen (5mg/kg twice weekly) was based on these studies (*14, 15*). B20-4.1 was kindly provided by Roche (pRED oncology). The treatment response was monitored by BLI, FLT and FET MicroPET/CT performed on three consecutive days one and two weeks after treatment initiation. Mice were sacrificed if they showed tumor related symptoms and/or weight loss above 20%. Subsequently, the brains were used for immunohistochemistry (IHC).

Bioluminescence imaging

Groups of three mice were injected i.p. with 150mg/kg D-luciferin in phosphate-buffered saline (Perkin Elmer, USA). Subsequently, mice were anesthetized using 2% isoflurane and placed in the IVIS Lumina XR optical imaging system (Caliper Life Sciences, Perkin Elmer, USA), approximately 5 minutes after D-luciferin injection. Imaging parameters, like field of view and F-stop, were kept constant and acquisition time was adjusted to optimize the signal without saturating the image. Scanning was continued until the peak signal was captured for each mouse. The *Living Image 4.3.2* software on the IVIS system was used for image analysis. A two-dimensional region of interest (ROI) at a fixed size was manually drawn covering the skull of the mouse and total photon flux was measured.

MicroPET/CT imaging

^{18}F-FET and ^{18}F-FLT was synthesized as previously described (*12, 16*). Mice were anaesthetized with Hypnorm/Midazolam (1ml/100g bodyweight) and kept on a heat-pad to prevent hypothermia. 8.1±0.18 MBq ^{18}F-FET or 7.8±0.13 MBq ^{18}F-FLT were injected intravenously (i.v) in the tail vein of the mice. A 10 min static PET image was obtained 20-30 minutes after ^{18}F-FET injection and 60-70 minutes after ^{18}F-FLT injection using a MicroPET Focus 120 (Siemens Medical Solutions, Malvern, PA, USA). PET acquisition and image analysis were performed as previously described (*12*). In brief, the Inveon software (Siemens Medical Solutions) was used for co-registration of MicroPET and MicroCT images. At the location of maximum tracer uptake in the tumor a 3D spherical region of interest (ROI) was placed (ROI_T). In the contralateral normal hemisphere a 4 mm^3 spherical ROI was drawn (ROI_B). SUV_{max} was calculated from the voxel with the highest tracer concentration in the ROI. SUV_{mean} was calculated as the mean radioactivity in the ROI_B. Tracer uptake was expressed as a T/B ratio of SUV_{max} ((SUV_{max} in ROI_T)/(SUV_{max} in ROI_B)) and SUV_{mean} ((SUV_{max} in ROI_T)/(SUV_{mean} in ROI_B)). Treatment response was calculated as the difference in T/B ratio of SUV_{max} and T/B ratio of SUV_{mean} after one and two weeks of treatment relative to base-line scans.

Immunohistochemistry

Intact brains were removed from sacrificed mice and fixed in 4% paraformaldehyde for 24-48 hours at 4°C followed by incubation in 70% ethanol. After fixation brains were divided in two by coronal cutting in the incision site. IHC was performed on formalin-fixed, paraffin-embedded tissue and histological sections (4μM) were stained with hematoxylin and eosin (HE) for normal histological evaluation and with antibodies detecting Ki67 and CD31. All IHC stainings were performed manually and according to manufacturer's instruction. Primary antibodies used: CD31 (detecting both human and murine CD31, diluted 1:50, Abcam, UK) and Ki67 (diluted 1:100, Abcam, UK). The Pannoramic MIDI Slide scanner and the software Pannoramic Viewer 1.15.3 (3DHistech, Hungary) were used for IHC analysis.

The micro-vessel density (MVD) was quantified using the CAIMAN (Cancer Image Analysis: htpp://www.caiman.org.uk) online automatic algorithm for endothelial cell segmentation (*17*). Images with a known size (approximately 2mm^2) were captured at a magnification of ×10 from three to four regions of interest from each mouse. The majority of the tumor from each slide was covered in the images. Images were uploaded and the returned analyzed image file with the segmentation overlaid was inspected and approved. MVD (micro-vessels/mm^2) of the specimen was estimated as a mean of MVD in the tree to four analyzed regions.

The online available image analysis software ImmunoRatio (*18*) was used for quantification of the Ki67 proliferation index (percent of DAB-staining area out of the total area). Depending on the tumor size three to ten images were captured at the magnification of ×20 covering the regions in which Ki67 staining was particularly prevalent (hot spots). Camera settings and staining intensity was evaluated according to the web-application. The hematoxylin and DAB thresholds were manually adjusted and results were interpreted with the pseudo-colored images and the original image. The Ki67 proliferation index was estimated as a mean of the Ki67 proliferation index in the three regions with the highest Ki67 proliferation index.

Statistical analysis

All statistical analysis was performed using GraphPad Prism version 5.01 for Windows (GraphPad Software Inc., USA). All data are presented as mean±SEM (standard error of mean) if not stated otherwise. $P < 0.05$ was considered statistically significant. Comparisons between the treatment and the control group were performed using unpaired Student's t-test assuming Gaussian distribution. Pearson correlation analysis was used for comparison of FET and FLT T/B ratios and SUV_{max}. Survival analysis was performed using the Kaplan-Meier method and the log-rank test.

RESULTS

Tumor model characteristics

Nine mice were included in the B20-4.1 group and eight mice were included in the control group. The mean time to TT was 7±0.3 weeks in the control group and 6.8±0.4 weeks in the B20-4.1 group. The T/B ratio of SUV_{max} was 1.93±0.1 in the control group and 2.1±0.3 in the B20-4.1 group. Mice were included in the analysis if there was a base-line MicroPET and at least one evaluation MicroPET of ^{18}F-FLT and ^{18}F-FET, respectively. As such, some of the mice did not have two evaluation MicroPET scans primarily due to tumor-related symptoms and euthanasia of the mice before the second scanning week.

^{18}F-FET and ^{18}F-FLT MicroPET imaging of GBM xenografts

Representative MicroPET/CT images of an orthotopic NGBM_CPH048p6_LUC tumor from a single mouse are shown in Figure 2 for visual comparison. ROI_T and ROI_B are illustrated in the figure. The ^{18}F-FLT PET images show FLT uptake in the tumor and a very low background uptake. A small increase in FLT uptake is observed every week. In the ^{18}F-FET PET images the FET uptake in the tumor is higher at week 7 and week 8 as compared to FLT uptake in the ^{18}F-FLT PET images, however, the background activity is also higher leading to higher T/B ratios in the FLT images compared to the FET MicroPET images. In order to compare the SUV_{max} and T/B ratios of FLT and FET we performed Pearson correlation analysis and included all baseline scans in the analysis. Strong positive correlations of SUV_{max} (r=0.72, p=0.001, n=14) and T/B ratios (r=0.73, p=0.003, n=14) were observed (Figure 3A, 3B). In addition, we compared the mean of SUV_{max} and T/B ratio in the FLT images with that of the FET images (Figure 3C, 3D). FLT SUV_{max} values were significantly lower than the FET SUV_{max} values (1±0.1 vs. 1.4±0.1, n=14; p=0.002). However, we found a significantly higher mean FLT T/B ratio as compared to mean FET T/B ratio (3±0.2 vs. 2±0.1, n=14; p=0.002).

In order to investigate if ^{18}F-FLT and ^{18}F-FET MicroPET/CT could be used to detect response to B20-4.1, the T/B ratio of SUV_{max} or SUV_{mean} for the ^{18}F-FET and ^{18}F-FLT uptake (relative to baseline) in the two groups was plotted versus time after TT (Figure 4). In the ^{18}F-FET images we found a significant decrease in the relative T/B ratio of SUV_{max} after one week (99±6%, n=6 vs. 124±9%, n=5; p=0.04) and after two weeks (106±10%, n=5 vs. 156±17%, n=4; p=0.03) in the B20-4.2 group as compared with the control group (Figure 4A). In line with this, the T/B ratio of SUV_{mean} for ^{18}F-FET was significantly decreased after one week (86±8%, n=6 vs. 127±9%, n=5; p=0.007), while the difference was not significant after two weeks (102±21%, n=4 vs. 155±22%, n=5; p=0.14), (Figure 4B). In contrast, ^{18}F-FLT images showed no significant difference in the T/B ratio of SUV_{max} between the treatment and the control group neither after one week of treatment (134±12%, n=6 vs. 144±6%, n=6; p=0.49) nor after two weeks of treatment (174±11%, n=5 vs. 208±30%, n=5; p=0.34), (Figure 4C). The T/B ratio of SUV_{mean} confirmed these results by showing no significantly difference between the groups after one week (180±43%, n=6 vs. 141±23%, n=6; p=0.44) and after two weeks of treatment (190±23%, n=6 vs. 260±43%, n=6; p=0.41), (Figure 4D).

Bioluminescence imaging of GBM xenografts

As we detected a difference in the ^{18}F-FET uptake between the treatment and the control group, we wanted to evaluate if there was a similar response in the BLI images, where total flux is a measure of viable tumor cell. Figure 5A shows BLI images of a representative xenograft mouse from the B20-4.1 and from the control group for visual comparison. The relative total flux was similar in the two xenografts. In Figure 5B the mean relative total flux between the treatment and the control group is compared. In line with results from the ^{18}F-FLT MicroPET we did not find a significant difference in the relative total flux between the treatment and the control group neither after one week of treatment (350±27%, n=9 vs. 280±55%, n=8; p=0.24) nor after two weeks of treatment (1275±350%, n=9 vs. 775±184%, n=7; p=0.27), (Figure 5B).

Ki67 labeling index and Micro-Vessel Density

To evaluate if the changes in the ^{18}F-FET tumor uptake following B20-4.1 treatment correlated with effects on tumor cell proliferation and MVD, we performed IHC on brains removed at the end of treatment. Figure 6A shows representative IHC pictures from HE, Ki67 and CD31 stained tissue sections and results from quantification of Ki67 and MVD are shown in figure 6B and 6C. In contrast to our expectations, we found no difference in the Ki67 labeling index in the treatment group as compared to the control group (18.9±1, n=7 vs. 19.8±2; n=6; p=0.7), (Figure 6B). In order to investigate if the therapy resulted in changes in the tumor vasculature, we compared the MVD in the treatment and the control groups. We found a significant lower MVD in the B20-4.1 group as compared to the control group (66±8%, n=8 vs. 100±10% n=7; p=0.02), (Figure 6C).

Effect of B20-4.1 on survival

Figure 7 shows Kaplan-Meier survival curves. We did not observe any difference in median survival in the B20-4.1 as compared to the control group (19 vs. 21 days; p=0.34; Hazard Ratio=1.9, 95% CI: 0.5-6.7).

DISCUSSION

The purpose of the present study was to make a direct comparison of ^{18}F-FLT and ^{18}F-FET MicroPET and to evaluate the performance of the individual tracers for detection of anti-VEGF anti-tumor activity. Several studies have evaluated the performance of the individual tracers for response assessment (*5, 6, 19, 20*), but to our knowledge there is no published data from direct comparison between the tracers for response assessment in glioma patients or xenografts. In the present study we report for the first time data from a comparative study between FLT and FET in orthotopic GBM xenografts.

In line with the two comparative FLT/FET studies performed in glioma patients (where the tracers potential for non-invasive grading (*7*) and volume assessment were evaluated (*8*)), we found a very low background uptake of FLT and a higher T/B ratio of FLT as compared to FET in xenografts. This indicates that the FLT/FET uptake kinetics in the GBM tumor model used in the present study is comparable to the FLT/FET kinetics in glioma patients. However, in contrast to the comparative studies in patients, we found a strong correlation of T/B ratio and SUV_{max} between the tracers (Figure 3). This difference between patients and xenografts could possibly be explained by the difference in time from FLT injection to acquisition in the patient studies (30-37 minutes) as compared to the present study in xenogafts (60 minutes). However, we also found highly significant differences between the SUV_{max} and T/B ratios of the tracers, which emphasizes that there are major differences between the tracers in the xenograft model. Therefore, the tracers will presumably have different potentials as imaging biomarkers.

In the present study, we performed FET MicroPET and found a difference in FET uptake in response to anti-VEGF treatment after one and two weeks of treatment. However, we did not find a difference in FLT uptake or in total photon flux when we performed BLI; neither did we find any effect of treatment on survival. In addition, we observed a decrease in MVD in the anti-VEGF group as compared to the control group, but not a detectable decrease in the Ki67 proliferation index. It is most likely, that the observed changes in the FET PET uptake in part reflect changes in the tumor vasculature and/or tumor blood-pool and not tumor cell regression due to B20-4.1 treatment. This theory is supported by recently published data where a highly significant correlation between regional cerebral blood flow and FET T/B ratio was demonstrated in glioma patients 20-40 minutes after FET injection (*21*). Apparently, in the present study the FLT PET uptake is less influenced by changes in the tumor vasculature. Another possible explanation for the divergent FLT and FET uptake is the different time from tracer injection to acquisition. Based on previous studies, FET MicroPET images were acquired 20-30 minutes after FET injection (*22, 23*), whereas FLT MicroPET images were acquired 60-70 minutes after FLT injection (*16*). However, the correlation between FET uptake and regional blood flow in the tumor is strongest early after tracer injection (0-5 minutes) and the FET contribution from the blood-pool is presumably constant at later time-points (*21*). This indicates that the results would most likely have been the same if MicroPET had been performed 60-70 minutes after FET injection.

Other studies have demonstrated anti-cancer activity and a survival benefit of Bevacizumab in glioma xenografts (*10, 24*). In the present study, we used a different GBM tumor model and initiated

B20-4.1 treatment at later time points or in another treatment schedule as compared to previous studies, which could explain the lack of impact on the Ki67 labeling index or survival (Figure 6C and 7). We evaluated the Ki67 labeling index at the end of the experiment (median survival of 20 days), although changes in the FET uptake were observed already after one and two weeks of treatment. As such, it could be speculated that we could have detected a difference in the Ki67 labeling index between the treatment groups if we had analyzed the tumors at an earlier time point, before the tumors grew very large. This reasoning is in contradiction to our BLI results, where we failed to detect any difference between the treatment groups during the course of the experiment. However, spontaneous regression of the BLI signal during tumor growth has been reported from previous studies (*25*), which could compromise the reliability of the optical signal as a measure of tumor cell viability.

We hypothesized that FLT compared to FET uptake would be more affected by changes in the permeability of the BBB; however, in the present study we could not confirm this hypothesis. Others have demonstrated that Bevacizumab treatment reduces the MVD in addition to a decrease in vessel permeability (*10*). Therefore, we evaluated the reduction in MVD as a surrogate marker for the BBB permeability changes. Surprisingly, only FET and not FLT were influenced by the changes in the MVD; nonetheless, further investigations are necessary in order to confirm our results and reject the hypothesis.

FLT is a thymidine analogue that reflects DNA synthesis, thus serving as a surrogate marker of proliferation. Tumor accumulation of FLT in tumor cells is influenced by several factors among which, the thymidine kinase 1(TK1) activity is thought to be a key regulator. However, the FLT uptake mechanisms are apparently not as simple as earlier predicted (*26*). FET is an amino acid analogue and accumulation of ^{18}F-FET in tumor cells is presumable linked to increased expression of the L-type amino acid transporters (LATs) in cancer cells (*21, 27*), although this has not been thoroughly investigated (*12*). The present study leaves many unanswered questions, nevertheless, in order to be able to fully interpret the discrepancy between the FLT and FET MicroPET data observed in this study and in future studies, a more comprehensive understanding and investigation of the transport and retention mechanisms of FLT and FET tracers is required.

CONCLUSION

In orthotopic GBM xenografts anti-VEGF treatment reduced MVD and ^{18}F-FET uptake but had no effect on ^{18}F-FLT uptake, the Ki67 proliferation index or survival. We suggest that ^{18}F-FET PET may be used to monitor anti-VEGF treatment effect on MVD in future studies.

REFERENCES

1. Pope WB, Young JR, Ellingson BM. Advances in MRI assessment of gliomas and response to anti-VEGF therapy. *Curr Neurol Neurosci Rep.* 2011;11(3):336-344.

2. Fletcher JW, Djulbegovic B, Soares HP, et al. Recommendations on the use of 18F-FDG PET in oncology. J Nucl Med. 2008;49(3):480-508.

3. Dierckx RA, Van de Wiele C. FDG uptake, a surrogate of tumour hypoxia? *Eur J Nucl Med Mol Imaging.* 2008;35(8):1544-1549.

4. Gulyas B, Halldin C. New PET radiopharmaceuticals beyond FDG for brain tumor imaging. *Q J Nucl Med Mol Imaging.* 2012;56(2):173-190.

5. Hutterer M, Nowosielski M, Putzer D, et al. O-(2-18F-fluoroethyl)-L-tyrosine PET predicts failure of antiangiogenic treatment in patients with recurrent high-grade glioma. *J Nucl Med.* 2011;52(6):856-864.

6. Schwarzenberg J, Czernin J, Cloughesy TF, et al. 3'-deoxy-3'-18F-fluorothymidine PET and MRI for early survival predictions in patients with recurrent malignant glioma treated with bevacizumab. *J Nucl Med.* 2012;53(1):29-36.

7. Jeong SY, Lim SM. Comparison of 3'-deoxy-3'-[18F]fluorothymidine PET and O-(2-[18F]fluoroethyl)-L-tyrosine PET in patients with newly diagnosed glioma. *Nucl Med Biol.* 2012;39(7):977-981.

8. Nowosielski M, Difranco MD, Putzer D, et al. An Intra-Individual Comparison of MRI, [18F]-FET and [18F]-FLT PET in Patients with High-Grade Gliomas. *PloS One.* 2014;9(4):e95830.

9. Rinne ML, Lee EQ, Nayak L, et al. Update on bevacizumab and other angiogenesis inhibitors for brain cancer. *Expert Opin Emerg Drugs.* 2013;18(2):137-153.

10. von BL, Brucker D, Tirniceru A, et al. Bevacizumab has differential and dose-dependent effects on glioma blood vessels and tumor cells. *Clin Cancer Res.* 2011;17(19):6192-6205.

11. Stockhausen MT, Broholm H, Villingshoj M, et al. Maintenance of EGFR and EGFRvIII expressions in an in vivo and in vitro model of human glioblastoma multiforme. *Exp Cell Res.* 2011;317(11):1513-1526.

12. Nedergaard MK, Kristoffersen K, Michaelsen SR, et al. The use of longitudinal 18F-FET MicroPET imaging to evaluate response to irinotecan in orthotopic human glioblastoma multiforme xenografts. *PLoS One.* 2014;9(2):e100009.

13. Liang WC, Wu X, Peale FV, et al. Cross-species vascular endothelial growth factor (VEGF)-blocking antibodies completely inhibit the growth of human tumor xenografts and measure the contribution of stromal VEGF. *J Biol Chem.* 2006;281(2):951-961.

14. Kienast Y, Klein C, Scheuer W, et al. Ang-2-VEGF-A CrossMab, a novel bispecific human IgG1 antibody blocking VEGF-A and Ang-2 functions simultaneously, mediates potent antitumor, antiangiogenic, and antimetastatic efficacy. *Clinical cancer research.* 2013;19(24):6730-6740.

15. Bais C, Wu X, Yao J, et al. PlGF blockade does not inhibit angiogenesis during primary tumor growth. *Cell.* 2010;141(1):166-177.

16. Jensen MM, Erichsen KD, Bjorkling F, et al. Early detection of response to experimental chemotherapeutic Top216 with [18F]FLT and [18F]FDG PET in human ovary cancer xenografts in mice. *PLoS One.* 2010;5(9):e12965.

17. Reyes-Aldasoro CC, Williams LJ, Akerman S, Tozer GM. An automatic algorithm for the segmentation and morphological analysis of microvessels in immunostained histological tumour sections. *J Microsc.* 2011;242(3):262-278.

18. Tuominen VJ, Ruotoistenmaki S, Viitanen A, Jumppanen M, Isola J. ImmunoRatio: a publicly available web application for quantitative image analysis of estrogen receptor (ER), progesterone receptor (PR), and Ki-67. *Breast Cancer Res.* 2010;12(4):R56.

19. Chen W, Delaloye S, Silverman DH, et al. Predicting treatment response of malignant gliomas to bevacizumab and irinotecan by imaging proliferation with [18F] fluorothymidine positron emission tomography: a pilot study. *J Clin Oncol.* 2007;25(30):4714-4721.

20. Galldiks N, Rapp M, Stoffels G, et al. Response assessment of bevacizumab in patients with recurrent malignant glioma using [18F]Fluoroethyl-L-tyrosine PET in comparison to MRI. *Eur J Nucl Med Mol Imaging.* 2013;40(1):22-33.

21. Zhang K, Langen KJ, Neuner I, et al. Relationship of regional cerebral blood flow and kinetic behaviour of O-(2-18F-fluoroethyl)-L-tyrosine uptake in cerebral gliomas. *Nucl Med Commun.* 2014;35(3):245-251.

22. Popperl G, Kreth FW, Mehrkens JH, et al. FET PET for the evaluation of untreated gliomas: correlation of FET uptake and uptake kinetics with tumour grading. *Eur J Nucl Med Mol Imaging.* 2007;34(12):1933-1942.

23. Rapp M, Heinzel A, Galldiks N, et al. Diagnostic performance of 18F-FET PET in newly diagnosed cerebral lesions suggestive of glioma. *J Nucl Med.* 2013;54(2):229-235.

24. Kuroda J, Kuratsu J, Yasunaga M, et al. Antitumor effect of NK012, a 7-ethyl-10-hydroxycamptothecin-incorporating polymeric micelle, on U87MG orthotopic glioblastoma in mice compared with irinotecan hydrochloride in combination with bevacizumab. *Clin Cancer Res.* 2010;16(2):521-529.

25. Jost SC, Collins L, Travers S, Piwnica-Worms D, Garbow JR. Measuring brain tumor growth: combined bioluminescence imaging-magnetic resonance imaging strategy. *Mol Imaging.* 2009;8(5):245-253.

26. Lee SJ, Yeo JS, Lee HJ, et al. Thymidine phosphorylase influences [F]fluorothymidine uptake in cancer cells and patients with non-small cell lung cancer. *Eur J Nucl Med Mol Imaging.* 2014.

27. Heiss P, Mayer S, Herz M, Wester HJ, Senekowitsch-Schmidtke R. Investigation of transport mechanism and uptake kinetics of O-(2-[18F]fluoroethyl)-L-tyrosine in vitro and in vivo. *J Nucl Med.* 1999;40(8):1367-1373.

FIGURE LEGENDS

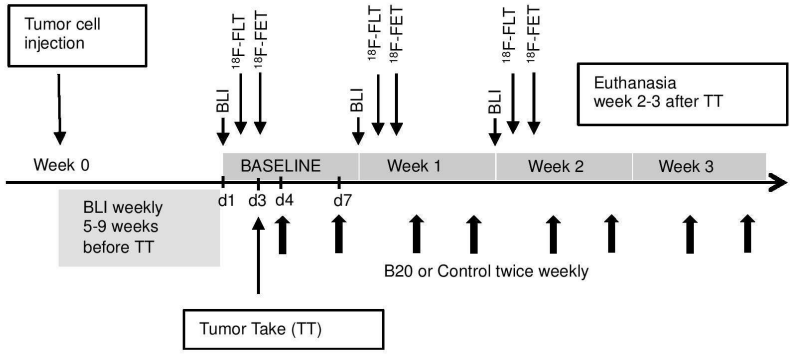

Figure 1: Schematic view of the experimental design. Days illustrated as d1, d3, d4 and d7.

BLI: Bioluminescence.

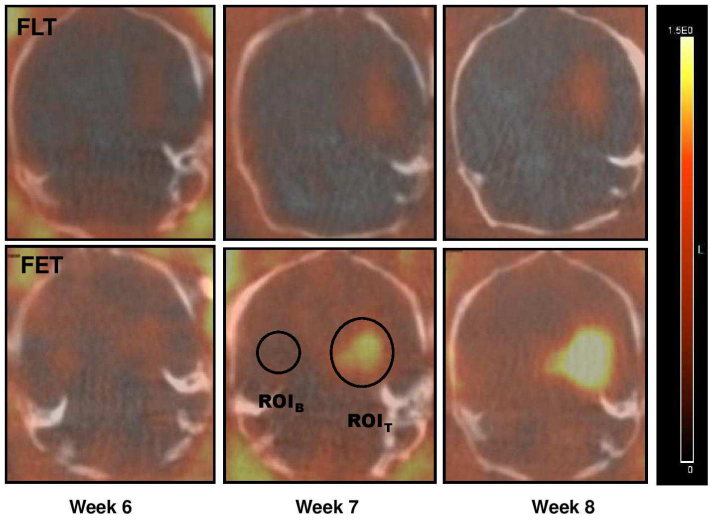

Figure 2: Fused ^{18}F-FLT (top) and ^{18}F-FET MicroPET/CT (bottom) images showing tumor progression in the same mice 6-8 weeks after tumor cell injection. ROI_T and ROI_B are illustrated. Scale bar: 0-1.5 SUV_{max}.

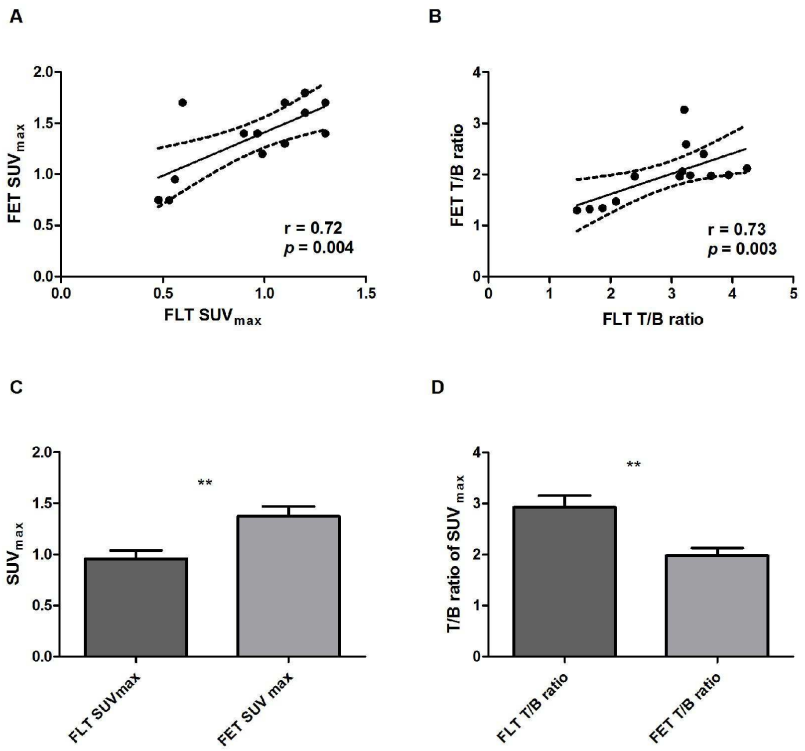

Figure 3: ^{18}F-FLT and ^{18}F-FET MicroPET correlations between A) SUV_{max} and B) SUV_{max} T/B ratio (n=14). C) SUV_{max} of FLT and FET. D) T/B ratio of FLT and FET. Mean±SEM, **p<0.01.

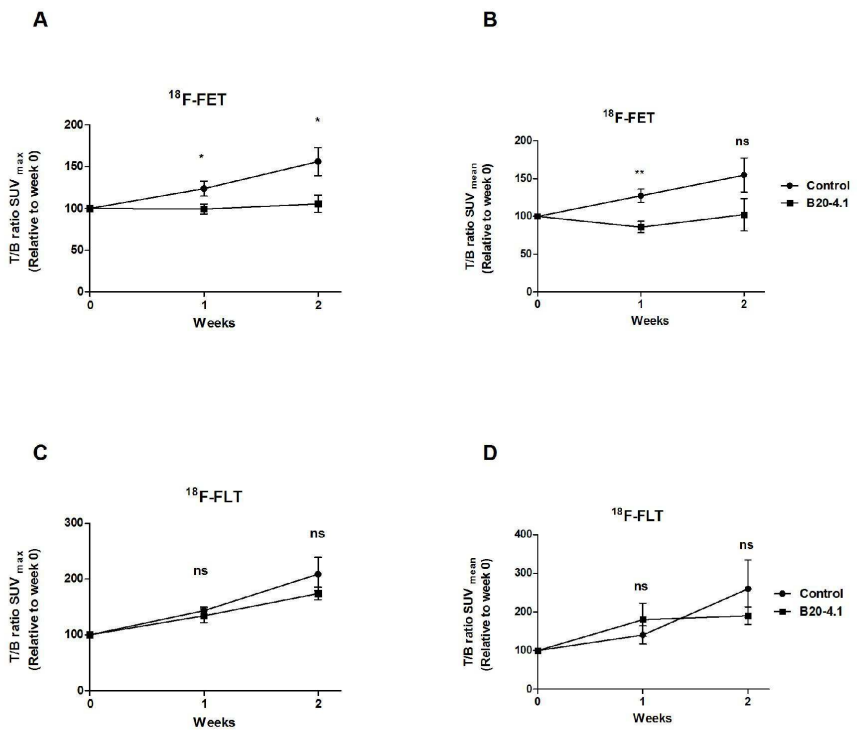

Figure 4: ^{18}F-FET and ^{18}F-FLT uptake in xenografts**.** A) FET SUV_{max} T/B ratio. B) FET SUV_{mean} T/B ratio. C) FLT SUV_{max} T/B ratio. D) FLT SUV_{mean} T/B ratio. Control group (n=4-5), B20-4.1 group (n=5-6). Mean±SEM. *p<0.05, **p<0.01.

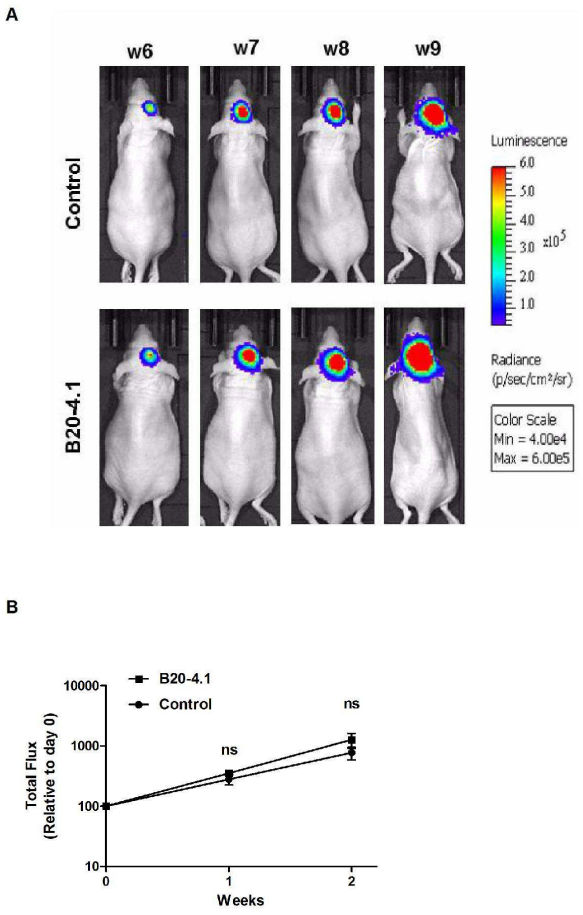

Figure 5: A) Representative images of bioluminescence 6-9 weeks after tumor cell injection showing similar tumor progression between a B20-4.1 mouse and a control mouse.

B) Quantification of total flux relative to week 0 versus time after tumor take. Mean±SEM in the B20-4.1 group (n=9) and in the control group (n=7-8).

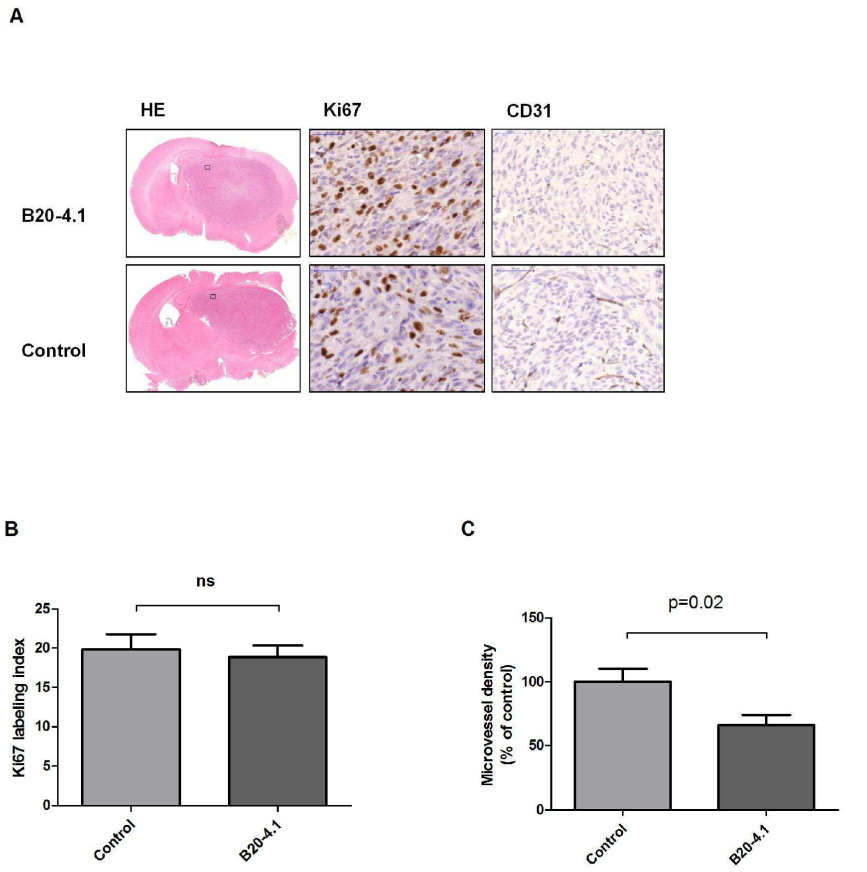

Figure 6: A) Representative IHC fields of HE and high magnification of Ki67 (×20) and CD31 (×10). B) Ki67 proliferation index in the control group (n=7) and in the B20-4.1 group (n=6; p=0.69). C) MVD in the B20-4.1 group (n=8) relative to the control group (n=7). Mean±SEM.

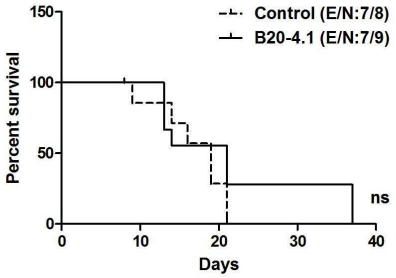

Figure 7: Kaplan Meier survival curves begin at tumor take. P=0.34 (determined by log-rank test). E: events; N: number of animals.

DISCLOSURE

No potential conflict of interest.

ACKNOWLEDGEMENTS

We thank Mette Villingshøj for maintaining the cell line used for orthotopic transplantation, Babloo Lukram for performing the IHC and radiochemists at The Department of Clinical Physiology, Nuclear Medicine & PET for providing ^{18}F-FLT and ^{18}F-FET.

We thank the following organizations for funding the project: Danish Cancer Research Foundation; The Danish Cancer Society; Danish National Advanced Technology Foundation; AP Møller Foundation; The Lundbeck Foundation; Novo Nordisk Foundation; Svend Andersen Foundation; Danish Research Council; Rigshospitalets Research Foundation.

Appendix III

Manuscript III

Nedergaard MK, Michaelsen SR, Urup T, Broholm H, El Ali H, Poulsen HS, Stockhausen MT, Kjaer A and Lassen U. ^{18}F-FET MicroPET and MicroMRI for anti-VEGF and anti-PlGF response assessment in an orthotopic murine model of human glioblastoma.

Submitted to *Neuro-Oncology* July 18, 2014

^{18}F-FET MicroPET and MicroMRI for anti-VEGF and anti-PlGF response assessment in an orthotopic murine model of human glioblastoma

By:

Mette K. Nedergaard[1], Signe R. Michaelsen[2], Thomas Urup[2], Helle Broholm[3], Henrik El Ali[1], Hans S. Poulsen[2], Marie-Thérése Stockhausen[2], Andreas Kjaer[1*] and Ulrik Lassen[4*]

[1]Department of Clinical Physiology, Nuclear Medicine & PET and Cluster for Molecular Imaging, Rigshospitalet and University of Copenhagen, Copenhagen, Denmark

[2]Department of Radiation Biology, The Finsen Center, Rigshospitalet, Copenhagen, Denmark

[3]Department of Neuropathology, Center of Diagnostic Investigation, Rigshospitalet, Copenhagen, Denmark.

[4]Phase 1 Unit, Department of Oncology, The Finsen Center, Rigshospitalet, Copenhagen, Denmark

*) Shared senior-authorship.

ABSTRACT

Background: Conflicting data exist for anti-cancer effects of anti-PlGF in combination with anti-VEGF. Still, this treatment combination has not been evaluated in intracranial glioblastoma (GBM) xenografts. In clinical studies, ^{18}F-FET PET and MRI add complementary but distinct information about glioma growth; however, the value of ^{18}F-FET MicroPET combined with MicroMRI has not been investigated preclinically. Here we examined the use of ^{18}F-FET MicroPET and MicroMRI for evaluation of anti-VEGF and anti-PlGF treatment response in GBM xenografts.

Methods: Mice with intracranial GBM were treated with anti-VEGF, anti-PlGF + anti-VEGF or saline. Bioluminescence, ^{18}F-FET MicroPET and MRI were used to follow tumour development. Primary end-point was survival, and tumours were subsequently analysed for Ki67 proliferation index and micro-vessel density (MVD). Further, PlGF and VEGFR-1 expression were examined in a subset of the xenograft tumours and in 13 GBM patient tumours.

Results: Anti-VEGF monotherapy increased survival and decreased ^{18}F-FET uptake, bioluminescence and MVD, while no additive effect of anti-PlGF was observed. ^{18}F-FET tumour-to-brain ratio was significantly decreased after one week (114±6%, n=11 vs. 143±8%, n=13; p=0.02) and two weeks of treatment (116±12%, n=8 vs. 190±24%, n=5; p=0.02) in the anti-VEGF group as compared with the control group. In contrast, MRI volume was unaffected by anti-VEGF. Gene expression of PlGF and VEGFR-1 in xenografts was significantly lower than in patient tumours.

Conclusion: No additive effect of anti-PlGF and anti-VEGF was observed, but ^{18}F-FET PET was superior to MRI for anti-angiogenic response evaluation. Thus, this study supports use of ^{18}F-FET PET in future studies.

Keywords: Glioma, PET, MRI, FET, PlGF, VEGF

INTRODUCTION

It is widely accepted that angiogenesis is a fundamental process for tumour progression and metastasis. Vascular endothelial growth factor A (VEGF) is considered a major pro-angiogenic mediator in glioblastoma multiforme (GBM), the most common and aggressive type of primary brain tumours in adults.[1] VEGF signalling is primarily mediated through the receptors VEGFR-1 and VEGFR-2; although VEGFR-2 is the major receptor involved in angiogenesis.[2] Placental growth factor (PlGF) is a member of the VEGF family of growth factors. PlGF binds selectively to VEGFR-1 and its soluble isoform, termed sVEGFR-1.[3] Under pathological conditions, such as cancer, the expression of PlGF is up-regulated and binding of PlGF to VEGFR-1 is in general considered as pro-angiogenic; however, the precise function of PlGF and VEGFR-1 in angiogenesis and tumour growth is still under debate.[3-5] PlGF is one of several growth factors that have been implicated in resistance to anti-angiogenic therapies.[6] Still, conflicting opinions exist on the value of neutralizing PlGF as a therapeutic target in oncology. Fischer *et al.* reported that anti-VEGF and anti-PlGF had an additive anti-tumour activity in several subcutaneous xenograft tumour models[6] and these results were later supported by others.[7] Conversely, other groups have found either no anti-tumour activity of anti-PlGF [4] or even a suppressive effect of PlGF on tumour growth and angiogenesis.[8-11] However, none of these studies have evaluated the anti-cancer activity of anti-PLGF in an intracranial GBM model. Furthermore, it has been demonstrated that the expression of VEGFR-1 in cancer cells could determine the efficacy of anti-PlGF treatment, a hypothesis that was suggested as a possible explanation for the conflicting data in the literature.[12]

Imaging and response assessment of gliomas by conventional magnetic resonance imaging (MRI) is complicated.[13,14] As we have demonstrated previously, positron emission tomography (PET) with the radiolabeled amino acid O-(2-^{18}F-fluoroethyl)-L-tyrosine (^{18}F-FET) is feasible for assessment of treatment response in an orthotopic xenograft model of GBM.[15] In patients with glioma, ^{18}F-FET PET (compared to MRI alone) adds additional information about tumour growth;[16-19] however, these two modalities have not been combined and evaluated in an orthotopic xenograft model of GBM.

In the present study, we hypothesized that by combining anti-VEGF and anti-PlGF therapies it would be possible to obtain an additive anti-tumour effect in an orthotopic xenograft model of GBM. In addition, we hypothesized that the combination of MRI and ^{18}F-FET MicroPET would give additional information about tumour growth and response to therapy.

MATERIALS AND METHODS

Ethics Statement

This study was performed according to the Declaration of Helsinki and Danish legislation. The Scientific Ethical Committee for Copenhagen and Frederiksberg (KF-01-327718) approved the use of patient tissue, and permissions were given from the Danish Data Protection Agency (2006-41-6979). Written informed consent was obtained from the patients. Animal care and all experimental procedures were performed under the approval of the Danish Animal Welfare Council (2013-15-2934-00064).

Cells and patient specimens

NGBM_CPH017p4 cells, having a stable expression of luciferase (GBM017_LUC), were used for xenograft generation. Establishment, maintenance and luciferase transduction has previously been described.[15,20] Tumour specimens from 13 GBM patients obtained at primary surgery were randomly chosen and used for the gene expression analysis, and isolated RNA from human microvascular endothelial cells (HMVEC) was used as a positive control. The panel of patient tumours included the patient tumour (GBM017) used for establishment of the neurosphere cell culture NGBM_CPH017p4.

Establishment of a human orthotopic GBM model and experimental design

Six weeks old NMRI (Naval Medical Research Institute) nude female mice were acquired from Taconic Europe (Lille Skensved, Denmark). Following a minimum of one week of acclimatization, mice were injected intracranially with ten µl cell suspension (100,000 cells) of GBM017_LUC as previously described.[15] Mice were injected with cells at week 0 and from week 3, weekly bioluminescence imaging (BLI), MRI and ^{18}F-FET MicroPET combined with computed tomography (CT) were used to monitor tumour growth. Tumour take (TT) was considered as a FET T/B ratio above 1.2 (described in detail below). Mice with confirmed TT were subsequently divided into three groups matched according to FET T/B ratio. Treatment with B20-4.1 (B20) (5mg/kg), B20 (5mg/kg) in combination with TB403 (20 mg/kg) or 0.9% saline solution as control was administered intraperitoneally (i.p.) twice a week to the three groups, respectively.

B20 is like bevazicumab an antibody against VEGF-A, which unlike bevazicumab has affinity for both the human and the murine VEGF-A.[21,22] TB403 (RO5323441) is a humanized monoclonal antibody that binds to both PlGF-1 and PlGF-2 and has affinity for both the murine and the human PlGF-2.[23] B20 and TB403 were kindly provided by Roche (pRED oncology). Treatment was initiated the day after the ^{18}F-FET PET confirming TT (the baseline scan), and the treatment response was monitored after one and two weeks. Survival was the primary end-point, and the survival time was the number of days from confirmed TT until xenografts were sacrificed according to a predefined assessment

score (see S1). Subsequently, the brains were removed from the cranial cavity and used for immunohistochemistry (IHC). Additionally, half of the xenograft tumour was isolated from four mice from each treatment group and used for quantitative real-time polymerase chain reaction (qPCR).

MicroPET/CT imaging

^{18}F-FET was acquired from routine weekly production for clinical use (Rigshospitalet, Copenhagen, Denmark) as previously described.[15] Mice were anaesthetized with Hypnorm/Midazolam (1ml/100g bodyweight) and injected with 7.7±0.2 MBq ^{18}F-FET intravenously (i.v) in the tail vein. In order to prevent hypothermia, mice were placed on an electrical heating-pad during a 10 min PET acquisition, 20-30 minutes post injection of ^{18}F-FET. MicroPET Focus 120 (Siemens Medical Solutions, Malvern, USA) was used for the acquisition of the emission data (see S2 for details). The Inveon Research Workplace (IRW) software (Siemens Medical Solutions) was used for co-registration of MicroPET and MicroCT images. At the location of maximum tracer uptake in the tumour a 3D spherical region of interest (ROI) was placed (ROI_T). In the contralateral normal hemisphere a 4 mm^3 spherical ROI was drawn (ROI_B). ^{18}F-FET uptake was expressed as SUV_{max} in ROI_T and as a T/B ratio ((SUV_{max} in ROI_T)/(SUV_{max} in ROI_B)). *Bioluminescence imaging*

Groups of two to three mice were injected i.p. with 150 mg/kg D-luciferin in phosphate-buffered saline (Perkin Elmer, USA). Subsequently, mice were anesthetized using 2% isoflurane and placed in the IVIS Lumina XR optical imaging system (Caliper Life Sciences, Perkin Elmer, USA), at approximately 5 minutes after D-luciferin injection. Acquisition time was adjusted to optimize the signal without saturating the image while field of view and F-stop were kept constant. Scanning was continued until the peak signal was captured for each mouse. The *Living Image 4.3.2* software on the IVIS system was used for image analysis. A two-dimensional ROI at a fixed size was manually drawn covering the entire skull of the mouse, and total photon flux (photons/sec) in the ROI was measured.

Magnetic Resonance Imaging (MRI)

MRI experiments were performed on a Bruker Biospec 7.0 (Bruker Biospin, Ettlingen, Germany). Mice were anaesthetized using 2% isoflurane and a water heating system, combined with a rectal thermometer, was used in order to maintain body temperature at 36.5-37.5°C. A 30-mm surface coil was fixed covering the skull of the mouse. A TurboRareT2-weighted protocol was used for generation of transverse and coronal images. 8 transverse slices and 12 coronal slices with a thickness of 0.5 mm were acquired using a repetition time (TR) of 2500 ms and an echo time (TE) of 33 ms. The total scan time was 5 minutes and 20 seconds for each orientation. A field of view of 20×20 mm was chosen and sampled into a matrix size of 256×256 mm resulting in a spatial resolution of 0.078. The MRI images were then transferred in DICOM format into the Inveon software (Siemens Medical Solutions) for image analysis. ROIs covering the total tumour area were manually drawn on each slice and a tumour volume was obtained by interpolating the ROIs from all

transverse images and the coronal images, respectively. The total tumour volume was calculated as the mean of the tumour volume in the transverse and coronal images.

Immunohistochemistry

Intact brains were fixed in 4% paraformaldehyde for 24-48 hours at 4°C followed by incubation in 70% ethanol. Primary antibodies used: CD31 (detecting both human and murine CD31, diluted 1:50, Abcam, Cambridge, UK) and Ki67 (detecting human Ki67, diluted 1:100, Abcam, Cambridge, UK) (see S3 for details). Based on the stainings, MVD and Ki67 proliferation index were evaluated (see S4 for details).

Quantitative Real–time PCR

Isolation of RNA, primer design and quantitative Real-time PCR detecting PlGF and VEGFR-1 expression was performed (described in S5).

Statistical analysis

All statistical analyses were performed using GraphPad Prism version 6.0 for MAC OS X (GraphPad Software Inc., USA). All comparisons between the treatment groups were performed using one-way ANOVA assuming Gaussian distribution. P values were adjusted by Sidak's multiple comparisons test. All data are presented as mean ± SEM (standard error of mean) if not stated otherwise. $P < 0.05$ was considered statistically significant. Survival analysis was performed using the Kaplan-Meier method and the log-rank test.

RESULTS

Tumour model characteristics

A total of 35 mice were injected orthotopically with GBM017_LUC cells. Three weeks after tumour cell injection, 32 mice had confirmed TT with a FET T/B ratio above 1.2. One mouse died from anaesthesia before the first evaluation scan was performed, and therefore, TT status was unknown. The remaining 2 mice had confirmed TT 4 weeks after orthotopic injection. A total of 34 mice were included in the treatment study of which 13 mice were included in the control group, 11 mice in the B20 group and 10 mice in the B20+TB403 group. One mouse from the B20+TB403 group was excluded from the final image analysis as tumour symptoms hindered evaluation after one week of treatment.

^{18}F-FET PET imaging of orthotopic GBM xenografts

Figure 1 shows representative ^{18}F-FET MicroPET/CT and MRI images of an orthotopic GBM017_LUC tumour from the control and the B20 group. Here, a difference in the tumour uptake of ^{18}F-FET between the B20 and the control mouse is clear, as a higher signal is observed for the

control group. In contrast, the MRI images are more difficult to assess for possible differences in tumour size. In order to investigate whether the ^{18}F-FET MicroPET/CT could be used quantitatively to detect a response to treatment, in this case B20 and B20+TB403, the ^{18}F-FET uptake in the three groups (relative to baseline) was plotted versus time following TT (Figure 2). The relative T/B ratio was significantly higher after one week of treatment (143±8, n=13 vs. 114±6, n=11; p=0.019) and after two weeks of treatment (190±24, n=5 vs. 116±12, n=8; p=0.018) in the control group as compared to the B20 group (Figure 2A). In contrast, there was no significant difference in the T/B ratio between the B20 and the B20+TB403 group neither after one week of treatment (114±6, n=11 vs. 126±9, n=9; p=0.49) nor after two weeks of treatment (116±12, n=8 vs. 123±19, n=6; p=0.95) (Figure 2A).

We then evaluated whether we also were able to detect a treatment response by evaluating the ^{18}F-FET uptake expressed as maximum standardized uptake values (SUV_{max}). In figure 2B, the mean SUV_{max} of ^{18}F-FET was plotted versus time after TT in the treatment groups. In the B20 group the mean SUV_{max} was significantly lower after one week of treatment (114±4, n=11 vs. 150±11, n=13; p=0.012) and after two weeks of treatment (114±8, n=8 vs. 207±26, n=5; p=0.001) as compared to the control group. Again, when comparing the B20 and the B20+TB403 groups, the results from the evaluation of the T/B ratio were confirmed; as we did not find any significant difference in mean SUV_{max} neither after one week of treatment (114±4, n=11 vs. 131±10, n=9; p=0.38) nor after two weeks of treatment (114±8, n=8 vs. 123±14, n=6; p=0.88).

MRI of orthotopic GBM xenografts

As we were able to detect a treatment response towards B20 monotherapy using ^{18}F-FET MicroPET, we wanted to evaluate if this treatment response was reflected in a difference in the anatomical tumour volume as measured by MRI. However, we found no difference in total tumour volume in the B20 group as compared to the control group neither after one week of treatment (412±63, n=11 vs. 394±54, n=12, p=0.97) nor after two weeks of treatment (768±147, n=8 vs. 800±103, n=5, p=0.98), (Figure 2C). Furthermore, we found no difference between the B20 and the B20+TB403 groups neither after one week (412±63, n=11 vs. 383±54, n=9, p=0.93) nor after two weeks of treatment (768±147, n=8 vs. 804±52, n=6, p=0.97), (Figure 2C).

Bioluminescence of orthotopic GBM xenografts

As results from the FET MicroPET and MRI were conflicting, we evaluated results from quantification of the BLI images, where total flux is a measure of viable tumour cells. Figure 3A shows BLI images of a representative xenograft from the B20 and from the control group for visual comparison, while Figure 3B shows the mean total flux between the three treatment groups. In line with results from the ^{18}F-FET MicroPET, we found a significantly lower mean total flux in the B20 group after two weeks of treatment as compared to the control group (1507±296, n=9 vs. 3296±685, n=9, p=0.03). Contrary, after one week of treatment, there was only a trend towards a significant difference between the B20 and the control group (431±70, n=11 vs. 629±65, n=13, p=0.098). When comparing the B20 group with the B20+TB403, no significant difference was

detected neither after one week of treatment (431±70, n=11 vs. 512±88, n=8, p=0.71) nor after two weeks of treatment (1507±296, n=9 vs. 1305±390, n=6, p=0.96), and the results thereby confirmed the ^{18}F-FET MicroPET data.

Treatment effect on survival

In Figure 4, Kaplan-Meier survival curves are shown. Comparison of the B20 group with the control group using Log-rank test, showed a significant increase in mean survival time (13 vs. 21 days; p=0.04; HR=0.5; 95% CI: 0.13-0.82), while no significant difference in survival was found between the B20 and the B20+TB403 group (21 vs. 16; p=0.30; HR=0.63; 95% CI: 0.2-1.6). 6 mice were censored as they died from anaesthesia before the criteria for euthanasia were fulfilled.

Ki67 labelling index and Micro-Vessel Density (MVD)

As we wanted to investigate if the observed changes in FET uptake, BLI and survival corresponded to molecular markers of proliferation or MVD we performed IHC. Representative pictures from HE, Ki67 and CD31 stained tissue sections are shown in Figure 5A, while figure 5B and 5C shows results from quantification of Ki67 and MVD. In contrast to the results from FET Micro/PET, BLI and survival analysis, but in line with the MRI findings, we found no difference in the Ki67 labelling index neither in the B20 group as compared to the control group (35±1, n=9 vs. 37.5±2; n=11; p=0.34), (Figure 5B) nor in the B20 group as compared to the B20+TB403 group (35±1, n=9 vs. 36.5±1; n=7; p=0.93). However, we found a significant lower MVD in the B20 group as compared to the control group (72±11, n=10 vs. 122±9 n=11; p=0.002), while the MVD was comparable in the B20 and the B20+TB403 groups (72±11, n=10 vs. 68±9 n=7; p>0.99 (Figure 5C).

Quantification of PlGF and VEGFR-1 mRNA expression in xenografts and patient tumours

In order to investigate if the lack of an additional anti-tumour effect of anti-PlGF could be related to the expression level of PlGF and/or VEGFR-1 in the tumour cells, we performed qPCR for PlGF and VEGFR-1 in a small subset of the xenograft tumours and compared the expression to a panel of 13 GBM patients. The gene expression of the tumour samples was normalized to reference genes and scaled to the gene expression in HMVEC, which was adjusted to 1. The relative gene expression is shown in Figure 6A and 6B. As compared to the panel of GBM patients, including the patient tumour from which the GBM_CHP017 cells were established, we found a much lower expression of both PlGF and VEGFR-1 in the xenografts. In addition, no significant difference in the gene expression of PlGF between the B20 group and the control group xenografts was observed (Figure 6C), showing that the gene expression of PlGF was unchanged in response to anti-VEGF (B20) treatment.

DISCUSSION

In the present study, we have used ^{18}F-FET MicroPET in combination with MRI to evaluate a treatment response towards anti-VEGF (B20) monotherapy and towards combined treatment with anti-PlGF (TB403) and anti-VEGF (B20). In contradiction to our hypothesis, we found no significant difference in ^{18}F-FET uptake, MRI, BLI, Ki67 proliferative index, MVD or survival between the B20 and the B20+TB403 groups. Thus, the combination of anti-PlGF and anti-VEGF did not have an additive effect on tumour growth in the GBM017_LUC orthotopic tumour model used in the present study. The efficacy of anti-PlGF has been related to the expression of PlGF and its receptor VEGFR-1.[24] We found a very low expression of both PlGF and VEGFR-1 in the xenografts as compared to the patient tumours, which obviously could explain the lack of efficacy of anti-PlGF. However, it is striking that the tumour specimens from the GBM017 glioma patients had a much higher expression of PlGF and VEGFR-1 as compared to the xenografts. A possible explanation for this is that PlGF and VEGFR-1 observed in the patient tumour is derived from cancer associated stroma cells or endothelial cells and not from the cancer cells. If PlGF and VEGFR-1 primarily is derived from stromal cells in the orthotopic xenograft tumours it is of murine origin and therefore not detectable with the human specific primers. This explanation is supported by recently published data in prostate cancer where PlGF is overexpressed in fibroblasts and undetectable in the prostate cancer cells.[25] Regardless whether there was an undetected stromal contribution of PlGF and/or VEGFR-1 in the present study, we did not detect an effect of adding anti-PlGF therapy to anti-VEGF monotherapy. This is in line with a recent Phase 1-2 study of Bevacizumab and TB403 in patients with recurrent GBM. Response data, time to progression, pharmacodynamics data including MRI did not indicate any additional activity of TB403 compared to Bevacizumab monotheraphy.[26] However, a study has demonstrated especially high expression levels of PlGF in selected hypervascular gliomas[27]. Among the patient tumours examined in this study, we also found two tumours (pt. 2 and pt. 3) with a PlGF level considerable higher than the other patient samples. This supports that anti-PlGF could be effective in certain glioma patients and advocate further investigation of anti-PlGF efficacy.

Others have demonstrated an up-regulation of the gene expression of PlGF in response to anti-VEGF treatment.[28-30] In contradiction to these results, we did not find a significant difference between the B20 and the control group. However, we interpret these results with caution given the small sample size, the use of human specific primers and the very low PlGF gene expression in the xenografts.

In the present study, we additionally have investigated the feasibility of *in vivo* imaging and noninvasively response assessment using ^{18}F-FET Micro/PET and MRI in orthotopic GBM xenografts. We found that it is possible to detect a tumour response towards anti-VEGF (B20) using ^{18}F-FET already after one week of treatment. This is in line with our previous studies where we used ^{18}F-FET MicroPET to evaluate response towards Irinotecan[15] and B20 (unpublished data) in another orthotopic GBM model. In the present study, we also used MRI and demonstrated that the observed tumour response (and increased survival) was not reflected in measurable volume

changes as depicted by MRI. Gadolinium contrast was not used for the MRI scans and it is possible that it would have helped to differentiate between surrounding oedema and true tumour margins and therefore would have resulted in significant MRI results. However, a lack of correlation between tumour volume and contrast enhancement was recently demonstrated,[31] which is in contradiction to this reasoning. It is likely that small changes in viable tumour cells are difficult to visualize on MRI scans where necrosis is a part of the detected anatomical tumour volume. As such, our results therefore indicate that ^{18}F-FET PET is superior to MRI for the detection of anti-VEGF efficacy in GBM xenograft models. This is in line with several clinical studies, where there is increasing evidence for the use of ^{18}F-FET PET as an addition to MRI as ^{18}F-FET PET adds complementary information about tumour growth.[16-19]

In addition to MicroPET and MRI, we also evaluated tumour development using BLI. It is widely accepted that the BLI has a higher sensitivity than MicroPET and MRI,[32] and as such, intracranial gliomas are detectable at a smaller tumour-size using BLI as compared to FET Micro/PET. Therefore it was surprising that we only detected a significant difference in BLI after two weeks of treatment while there after one week of treatment only was a trend towards significance. Although BLI is a very sensitive and well-established method for assessment of tumor-cells[33,34] several limitations have been addressed. Changes in the expression of luciferase, hypoxia, pH and different tumour location may compromise the reliability of BLI as a quantitative measure of viable tumour cells.[33,35]

We evaluated the Ki67 proliferative index as a marker of proliferation and as a molecular indicator of anti-proliferative activity. In contrast to our results from the FET MicroPET, BLI and survival analysis, and therefore supportive of the MRI findings, we were unable to detect a significant difference in the Ki67 proliferative index when we performed IHC at the time of study endpoint. However, it could be speculated that we would have detected a difference in the Ki67 proliferative index if the xenograft brains were analysed at an earlier time point before the brain tumours grew too large. When analysing MVD of the xenograft tumours, we found a highly significant reduction in MVD in the B20 and B20+TB403 groups as compared to the control group. This anti-angiogenic effect is in line with previous studies were B20 and anti-VEGF treatment were evaluated [31,36] and supportive of our results from the FET MicroPET, BLI and survival analysis. Controversy exists whether Bevacizumab has direct anti-cancer activity or if the clinical benefit observed in glioma patients exclusively is caused by effects on the tumour vessels.[36] The latter could be an explanation for the decreased MVD and unchanged Ki67 proliferative index observed in the present study.

Taken together, results from the FET MicroPET, BLI and MVD analysis were all in agreement with the increased survival observed in the B20 treated groups. Thus, as observed in patients, this study shows that ^{18}F-MicroFET PET compared to MicroMRI adds valuable complementary information about tumour growth in orthotopic glioma xenografts. Hence, ^{18}F-FET MicroPET could be a valuable imaging modality for preclinical evaluation of new therapies in orthotopic GBM xenograft models. However, the technique should be combined with GBM models that reflect the diversity of GBM tumours in patients, in order to obtain preclinical results that are transferrable to the clinic.

CONCLUSION

In orthotopic GBM xenografts the combination of anti-VEGF and anti-PlGF did not result in an additive effect on tumour growth or survival. However, anti-VEGF monotherapy increased survival and reduced ^{18}F-FET uptake after one and two weeks of treatment without significant changes in anatomical MRI volume. Therefore, our results indicate that ^{18}F-FET PET is superior to MRI for anti-angiogenic response evaluation. As such, this study supports the additional use of ^{18}F-FET PET in the evaluation of patients with GBM and in preclinical studies as ^{18}F-FET PET might be an early and non-invasive biomarker for detection of anti-angiogenic treatment response or failure.

FUNDING

Danish Cancer Research Foundation; The Danish Cancer Society; Danish National Advanced Technology Foundation; AP Møller Foundation; The Lundbeck Foundation; Novo Nordisk Foundation; Svend Andersen Foundation; The John and Birgitte Meyer Foundation; Danish Research Council; Rigshospitalets Research Foundation.

ACKNOWLEDGEMENTS

We thank Mette Villingshøj for maintaining the cell line and preparing tumour cells for orthotopic transplantation, Janine Erler and Lara Perryman for performing luciferase transducing of the cell line, Babloo Lukram for performing the IHC and radiochemists at The Department of Clinical Physiology, Nuclear Medicine & PET for providing ^{18}F-FET.

REFERENCES

1. Chi AS, Sorensen AG, Jain RK, Batchelor TT. Angiogenesis as a therapeutic target in malignant gliomas. *The oncologist.* 2009; 14(6):621-636.
2. Jain RK, di Tomaso E, Duda DG, Loeffler JS, Sorensen AG, Batchelor TT. Angiogenesis in brain tumours. *Nature reviews. Neuroscience.* 2007; 8(8):610-622.
3. Olsson AK, Dimberg A, Kreuger J, Claesson-Welsh L. VEGF receptor signalling - in control of vascular function. *Nature reviews. Molecular cell biology.* 2006; 7(5):359-371.
4. Bais C, Wu X, Yao J, et al. PlGF blockade does not inhibit angiogenesis during primary tumor growth. *Cell.* 2010; 141(1):166-177.
5. Kerber M, Reiss Y, Wickersheim A, et al. Flt-1 signaling in macrophages promotes glioma growth in vivo. *Cancer research.* 2008; 68(18):7342-7351.
6. Fischer C, Jonckx B, Mazzone M, et al. Anti-PlGF inhibits growth of VEGF(R)-inhibitor-resistant tumors without affecting healthy vessels. *Cell.* 2007; 131(3):463-475.

7. Van de Veire S, Stalmans I, Heindryckx F, et al. Further pharmacological and genetic evidence for the efficacy of PlGF inhibition in cancer and eye disease. *Cell.* 2010; 141(1):178-190.

8. Bagley RG, Ren Y, Weber W, et al. Placental growth factor upregulation is a host response to antiangiogenic therapy. *Clinical cancer research : an official journal of the American Association for Cancer Research.* 2011; 17(5):976-988.

9. Xu L, Cochran DM, Tong RT, et al. Placenta growth factor overexpression inhibits tumor growth, angiogenesis, and metastasis by depleting vascular endothelial growth factor homodimers in orthotopic mouse models. *Cancer research.* 2006; 66(8):3971-3977.

10. Hedlund EM, Yang X, Zhang Y, et al. Tumor cell-derived placental growth factor sensitizes antiangiogenic and antitumor effects of anti-VEGF drugs. *Proceedings of the National Academy of Sciences of the United States of America.* 2013; 110(2):654-659.

11. Eriksson A, Cao R, Pawliuk R, et al. Placenta growth factor-1 antagonizes VEGF-induced angiogenesis and tumor growth by the formation of functionally inactive PlGF-1/VEGF heterodimers. *Cancer cell.* 2002; 1(1):99-108.

12. Yao J, Wu X, Zhuang G, et al. Expression of a functional VEGFR-1 in tumor cells is a major determinant of anti-PlGF antibodies efficacy. *Proceedings of the National Academy of Sciences of the United States of America.* 2011; 108(28):11590-11595.

13. Wen PY, Macdonald DR, Reardon DA, et al. Updated response assessment criteria for high-grade gliomas: response assessment in neuro-oncology working group. *Journal of clinical oncology : official journal of the American Society of Clinical Oncology.* 2010; 28(11):1963-1972.

14. Pope WB, Young JR, Ellingson BM. Advances in MRI assessment of gliomas and response to anti-VEGF therapy. *Current neurology and neuroscience reports.* 2011; 11(3):336-344.

15. Nedergaard MK, Kristoffersen K, Michaelsen SR, et al. The Use of Longitudinal 18F-FET MicroPET Imaging to Evaluate Response to Irinotecan in Orthotopic Human Glioblastoma Multiforme Xenografts. *PloS one.* 2014; 9(2):e100009.

16. Galldiks N, Rapp M, Stoffels G, et al. Response assessment of bevacizumab in patients with recurrent malignant glioma using [18F]Fluoroethyl-L-tyrosine PET in comparison to MRI. *European journal of nuclear medicine and molecular imaging.* 2013; 40(1):22-33.

17. Hutterer M, Nowosielski M, Putzer D, et al. O-(2-18F-fluoroethyl)-L-tyrosine PET predicts failure of antiangiogenic treatment in patients with recurrent high-grade glioma. *Journal of nuclear medicine : official publication, Society of Nuclear Medicine.* 2011; 52(6):856-864.

18. Popperl G, Goldbrunner R, Gildehaus FJ, et al. O-(2-[18F]fluoroethyl)-L-tyrosine PET for monitoring the effects of convection-enhanced delivery of paclitaxel in patients with recurrent glioblastoma. *European journal of nuclear medicine and molecular imaging.* 2005; 32(9):1018-1025.

19. Popperl G, Gotz C, Rachinger W, et al. Serial O-(2-[(18)F]fluoroethyl)-L: -tyrosine PET for monitoring the effects of intracavitary radioimmunotherapy in patients with malignant glioma. *European journal of nuclear medicine and molecular imaging.* 2006; 33(7):792-800.

20. Stockhausen MT, Broholm H, Villingshoj M, et al. Maintenance of EGFR and EGFRvIII expressions in an in vivo and in vitro model of human glioblastoma multiforme. *Experimental cell research.* 2011; 317(11):1513-1526.

21. Liang WC, Wu X, Peale FV, et al. Cross-species vascular endothelial growth factor (VEGF)-blocking antibodies completely inhibit the growth of human tumor xenografts and measure the contribution of stromal VEGF. *J.Biol.Chem.* 2006; 281(2):951-961.

22. Kienast Y, Klein C, Scheuer W, et al. Ang-2-VEGF-A CrossMab, a novel bispecific human IgG1 antibody blocking VEGF-A and Ang-2 functions simultaneously, mediates potent antitumor, antiangiogenic, and antimetastatic efficacy. *Clinical cancer research : an official journal of the American Association for Cancer Research.* 2013; 19(24):6730-6740.

23. Oude Munnink TH, Tamas KR, Lub-de Hooge MN, et al. Placental growth factor (PlGF)-specific uptake in tumor microenvironment of 89Zr-labeled PlGF antibody RO5323441. *Journal of nuclear medicine : official publication, Society of Nuclear Medicine.* 2013; 54(6):929-935.

24. Yao J, Wu X, Zhuang G, et al. Expression of a functional VEGFR-1 in tumor cells is a major determinant of anti-PlGF antibodies efficacy. *Proc.Natl.Acad.Sci.U.S.A.* 2011; 108(28):11590-11595.

25. Zins K, Thomas A, Lucas T, Sioud M, Aharinejad S, Abraham D. Inhibition of stromal PlGF suppresses the growth of prostate cancer xenografts. *International journal of molecular sciences.* 2013; 14(9):17958-17971.

26. Lassen U, Chinot OL, McBain C. Phase I study of anti-PlGF monoclonal antibody (mAb) RO5323441 (RO) and anti-VEGF mab bevacizumab (BV) in patients with recurrent glioblastoma (GBM). [Abstract]. *Journal of Clinical Oncology.* 2013; 31(No 15_suppl).

27. Nomura M, Yamagishi S, Harada S, Yamashima T, Yamashita J, Yamamoto H. Placenta growth factor (PlGF) mRNA expression in brain tumors. *Journal of neuro-oncology.* 1998; 40(2):123-130.

28. Fischer C, Jonckx B, Mazzone M, et al. Anti-PlGF inhibits growth of VEGF(R)-inhibitor-resistant tumors without affecting healthy vessels. *Cell.* 2007; 131(3):463-475.

29. Motzer RJ, Michaelson MD, Redman BG, et al. Activity of SU11248, a multitargeted inhibitor of vascular endothelial growth factor receptor and platelet-derived growth factor receptor, in patients with metastatic renal cell carcinoma. *Journal of clinical oncology : official journal of the American Society of Clinical Oncology.* 2006; 24(1):16-24.

30. Rosen LS, Kurzrock R, Mulay M, et al. Safety, pharmacokinetics, and efficacy of AMG 706, an oral multikinase inhibitor, in patients with advanced solid tumors. *Journal of clinical oncology : official journal of the American Society of Clinical Oncology.* 2007; 25(17):2369-2376.

31. Jalali S, Chung C, Foltz W, et al. MRI biomarkers identify the differential response of glioblastoma multiforme to anti-angiogenic therapy. *Neuro-oncology.* 2014; 16(6):868-879.

32. James ML, Gambhir SS. A molecular imaging primer: modalities, imaging agents, and applications. *Physiological reviews.* 2012; 92(2):897-965.

33. Khalil AA, Jameson MJ, Broaddus WC, et al. The Influence of Hypoxia and pH on Bioluminescence Imaging of Luciferase-Transfected Tumor Cells and Xenografts. *International journal of molecular imaging.* 2013; 2013:287697.

34. Jarzabek MA, Huszthy PC, Skaftnesmo KO, et al. In vivo bioluminescence imaging validation of a human biopsy-derived orthotopic mouse model of glioblastoma multiforme. *Molecular imaging.* 2013; 12(3):161-172.

35. Christoph S, Schlegel J, Alvarez-Calderon F, et al. Bioluminescence imaging of leukemia cell lines in vitro and in mouse xenografts: effects of monoclonal and polyclonal cell populations on intensity and kinetics of photon emission. *Journal of hematology & oncology.* 2013; 6:10.

36. von BL, Brucker D, Tirniceru A, et al. Bevacizumab has differential and dose-dependent effects on glioma blood vessels and tumor cells. *Clin.Cancer Res.* 2011; 17(19):6192-6205.

SUPPLEMENTARY DATA

S1 Monitoring orthotopic glioblastoma xenografts in NMRI mice

Variable	Score
Body Weight Changes	
<20%	0
>20%	3
Physical Appearance	
Normal	0
Lack of grooming	1
Small bites or scratches. Nasal/ocular discharge	2
Serious bites or scratches. Abnormal posture, limb, tremor etc.	3
Unprovoked Behavior	
Normal	0
Minor changes	1
Abnormal, reduced mobility, decreased alertness, inactive	2
Unsolicited vocalizations, self mutilation, either very restless or immobile	3
Behavioral Responses to External Stimuli	
Normal	0
Minor depression/exaggeration of response	1
Moderately abnormal responses	2
Violent reactions or comatose	3
Occipital Tumor	
None	0
Palpable	1
TOTAL SCORE	

Euthanasia of the mouse at

- total score > 5, or
- a score of 3 in any one variable, regardless of the total score.

S2 MicroPET/CT

An energy window of 350-650 keV and a time resolution of 6 ns were set up for the acquisition. The acquired datasets were stored in Listmode before arranging into 2D sinograms. The sinograms were then reconstructed into 256×256×95 image matrices with a voxel size of 0.3×0.3×0.8 mm3 using the maximum a posteriori (MAP) reconstruction algorithm. The intrinsic PET resolution was 1.2 mm full-width at half-maximum. Scatter and attenuation correction were not applied. The quantification unit was provided in Bq/ml. Subsequently, a four minutes CT scan was acquired in order to get anatomical information using a small animal CT scanner (MicroCAT® II system, Siemens Medical Solutions). To quantify the ^{18}F-FET uptake, the standardized uptake values (SUVs) were calculated from the equation: SUV= CT / (Dinj x W). CT is the radioactivity in tissue with the unit Bq/ml, Dinj is the injected dose and W is the weight of the mouse. SUV_{max} was calculated from the voxel with the highest tracer concentration in the ROI. SUV_{mean} was calculated as the mean radioactivity in the ROI.

S3 Immunohistochemistry

After fixation, brains were divided in two by coronal cutting in the incision site, although in the 12 mice which were used for qPCR, the brains were divided before fixation. IHC was performed on formalin-fixed paraffin-embedded tissue, and histological sections (4µM) were stained with hematoxylin and eosin (HE) for normal histological evaluation and with antibodies detecting Ki67 and CD31. All IHC stainings were performed manually and according to the manufacturer's instruction. The AxioScan Z1 slide scanner and the software ZEN 2012 (Carl Zeiss Microscopy, Germany) were used for IHC analysis.

S4 Quantification of MVD and Ki67 proliferative index

The micro-vessel density (MVD) was analyzed treatment-blinded by capturing 4 images at a magnification of ×20 (pixel size: 0.44×0.44 µm, image size: 610×400 µm) covering the regions where the MVD was highest. Subsequently, the microvessels were counted manually on the computer screen using Image J 1.47 software. MVD (microvessels/mm2) of the specimens was estimated as a mean of the MVD in the four analyzed regions. The online available image analysis software ImmunoRatio[1] was used for quantification of the Ki67 proliferation index (percent of DAB-staining area out of the total area). Treatment-blinded and depending on the tumor size, seven to ten images were captured at the magnification of ×40 (pixel size: 0.22×0.22 µm, image size: 310×200 µm) covering the regions in which Ki67 staining was particularly prevalent (hot spots). According to the web-application, camera settings and staining intensity was evaluated and found to be acceptable. The hematoxylin and DAB thresholds were manually adjusted, and results were interpreted with the pseudo-colored images and the original image. The Ki67 proliferation index was estimated as a mean of the Ki67 proliferation index in the 3 regions with the highest Ki67 proliferative index.

S5 RNA extraction, Reverse Transcription and Quantitative Real–time PCR

After resection, tumor specimens from xenografts and patients were snap-frozen and stored in liquid nitrogen. Total RNA from patient specimens was isolated using Trizol reagent (Gibco BRL 15596-018) and Qiagen TissueLyser before RNA purification with the RNeasy Mini kit (Qiagen, Denmark). Total RNA from xenograft tumors was isolated using RNAlater®- ICE (ambion), RNAzol®RT (Molecular Research Center Inc., USA) and PrecellysR-24 (Bertin Techmologies, France) for tissue homogenization. RNA measurements, reverse transcription (RT), primer design and pPCR were performed as previously described[2]. In short, the VEGFR-1 primers were purchased from DNA technology A/S (DNA technology, Denmark), and all other primers were purchased from Sigma-Aldrich (Sigma-Aldrich, USA) and designed to be human-specific. The Brilliant® SYBR®Green QPCR Master Mix (Stratagene) was used and gene expression was quantified on the Mx300P® real-time PCR system (Stratagene). The following thermal profile was used: denaturation for 10 minutes at 95°C followed by 45 cycles of 30 seconds denaturation at 95°C, primer annealing for 1 minute at 60°C and 1 minute extension at 72°C. Subsequently, the PCR product was denatured for 1 minute at 95°C followed by a ramp down to 55°C and a dissociation curve was acquired by a stepwise increase in temperature from 55°C to 95°C with steps of 0.5°C/cycle.

All samples were run in duplicates and included on the same plate using 1 µl of cDNA. To each plate a no-template control (NTC) was included. No reverse transcription control (NoRT) for all samples was tested using the reference genes and PlGF. Quantification of results was based on the computation of target quantification cycle (Cq) values and reference gene Cq values in the qbasePLUS 2.6.1 software (Biogazelle NV, Belgium)[3]. Genes of interest (GOI) were normalized to the arithmetic mean of the expression of the two reference genes peptidylprolyl isomerase A (PPIA) and topoisomerase 1 (TOP1) with a reference target stability of 0.82 (M-value) and 0.28 (CV-value). A default amplification efficacy of 100% was used as all assays were optimized to have efficiencies between 90% and 110%. Results were reported as normalized relative quantities (NRQs).

Primer sequences were PPIA-FP: 5'-cggatttgatcatttggtg-3', PPIA-RP: 5'ccagacaacacacaagac-3', TOP1-FP: 5'-agaggcattgttagtttagtg-3', TOP1-RP: 5'-cctacagttgattaaaagggaa-3', PlGF-FP: 5'-ctcacactttgccatttg-3', PlGF-RP: 5'-actctgtatgtgtctcttag-3', VEGFR1-FP: 5'-ggctctgtggaaattcagc -3', VEGFR1-RP: 5'-gctcacactgctcatccaaa-3'.

Supplementary References

1. Tuominen VJ, Ruotoistenmaki S, Viitanen A, Jumppanen M, Isola J. ImmunoRatio: a publicly available web application for quantitative image analysis of estrogen receptor (ER), progesterone receptor (PR), and Ki-67. *Breast cancer research : BCR.* 2010; 12(4):R56.

2. Nedergaard MK, Kristoffersen K, Michaelsen SR, et al. The Use of Longitudinal 18F-FET MicroPET Imaging to Evaluate Response to Irinotecan in Orthotopic Human Glioblastoma Multiforme Xenografts. *PloS one.* 2014; 9(2):e100009.

3. Hellemans J, Mortier G, De PA, Speleman F, Vandesompele J. qBase relative quantification framework and software for management and automated analysis of real-time quantitative PCR data. *Genome Biol.* 2007; 8(2):R19.

FIGURES

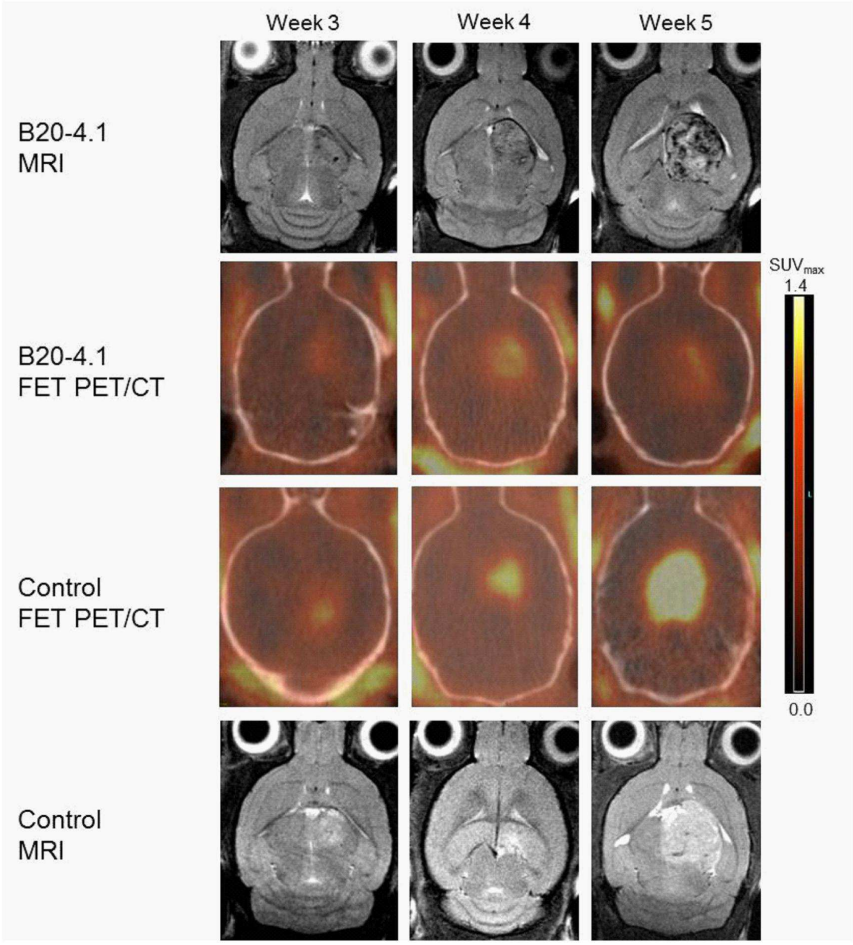

Figure 1: MRI and fused ^{18}F-FET MicroPET/CT images showing tumour progression 3-5 weeks after tumour cell injection. Transverse views through the brain of a mouse from the B20-4.1 group and a mouse from the control group. Scale bar: 0-1.4 SUV_{max}.

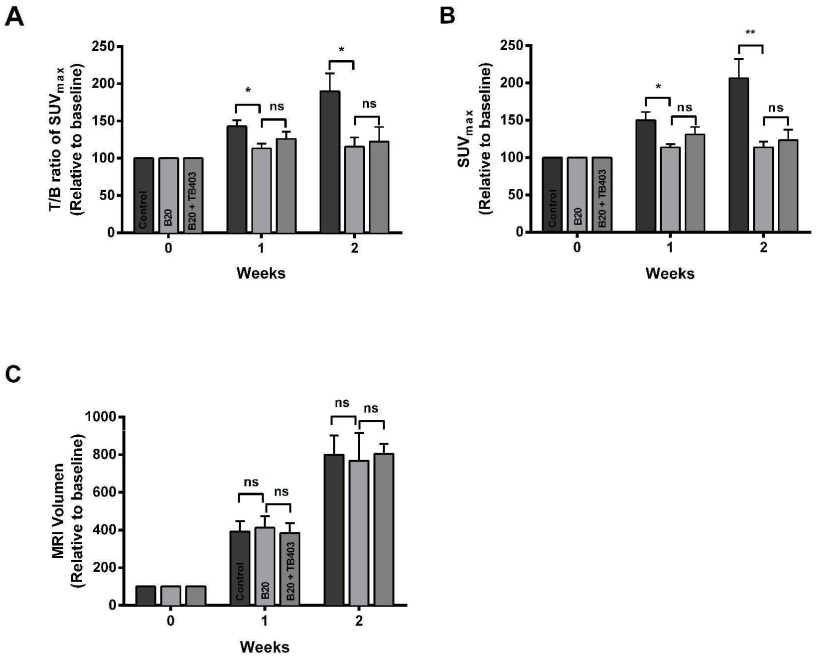

Figure 2: ^{18}F-FET uptake in the treatment groups expressed as A) T/B ratio and B) SUV_{max}. C) MRI volume in the treatment groups. All values are expressed as mean ± SEM relative to baseline (week 0) after 1 week of treatment in the control (n=13), the B20 group (n=11) and in the B20+TB403 (n=9); and after 2 weeks of treatment in the control (n=5), the B20 group (n=8) and in the B20+TB403 group (n=6). *p<0.05, **p<0.01.

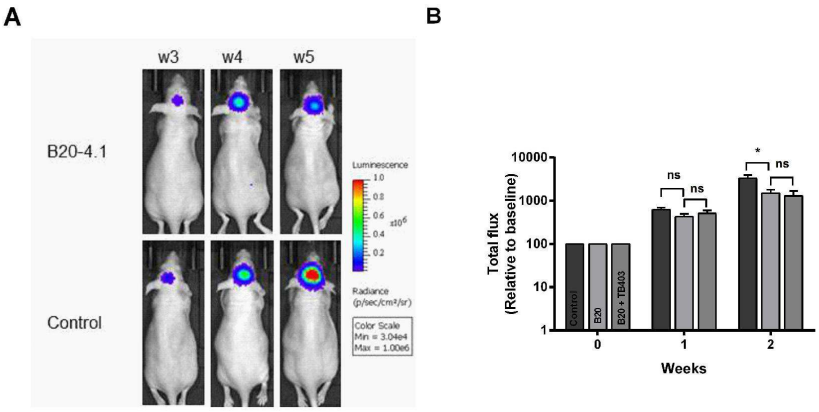

Figure 3: A) Representative images of bioluminescence 3-5 weeks after tumour cell injection showing tumour progression in a B20-4.1 mouse and a control mouse. B) Quantification of total flux relative to baseline (week 0). Values are expressed as mean ± SEM after one week of treatment in the control (n=13), the B20 group (n=11) and the B20+TB403 group (n=8); and after two weeks of treatment in the control (n=9), the B20 (n=9) and the B20+TB403 group (n=6). *p<0.05.

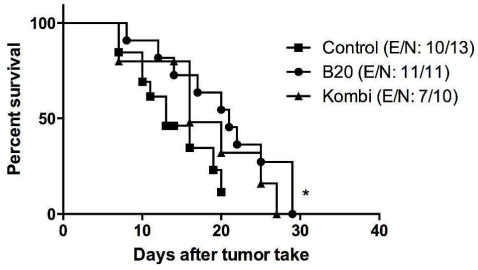

Figure 4: Kaplan Meier survival curves from tumour take. Control group vs. B20 group, p=0.04 (determined by log-rank test). E: events, N: number of animals.

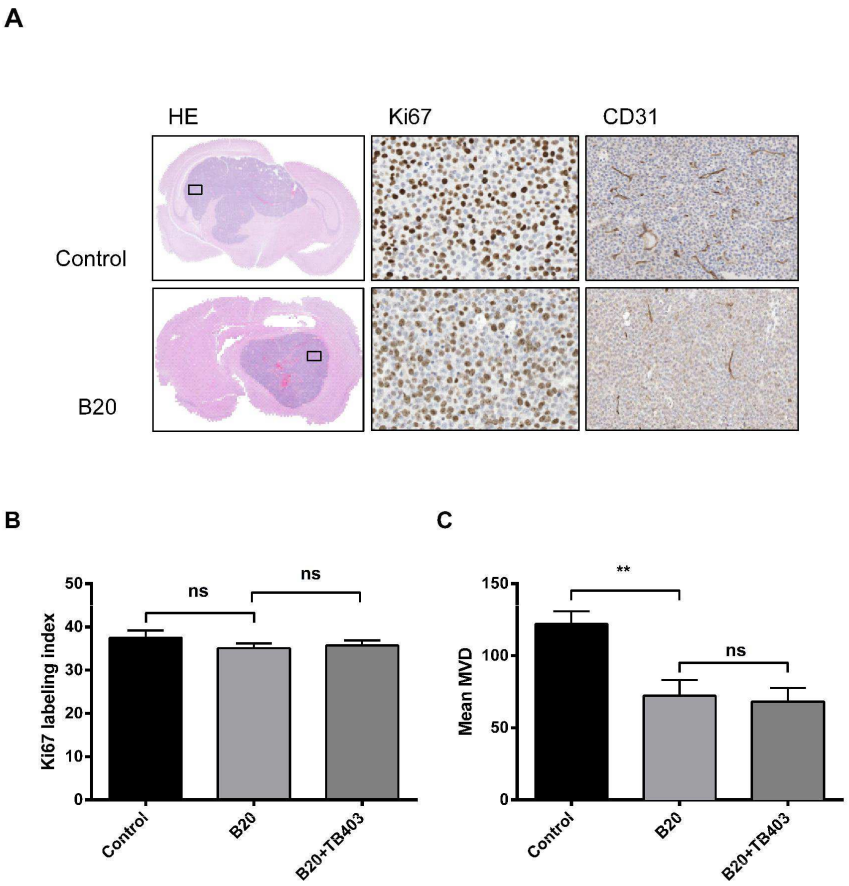

Figure 5: A) Representative IHC images of HE and high magnification of Ki67 (40x) and CD31 (20x). B) Ki67 proliferation index and C) MVD in the control group (n=11), the B20 group (n=10) and the B20+TB403 group (n=7). Mean ± SEM, **p<0.01.

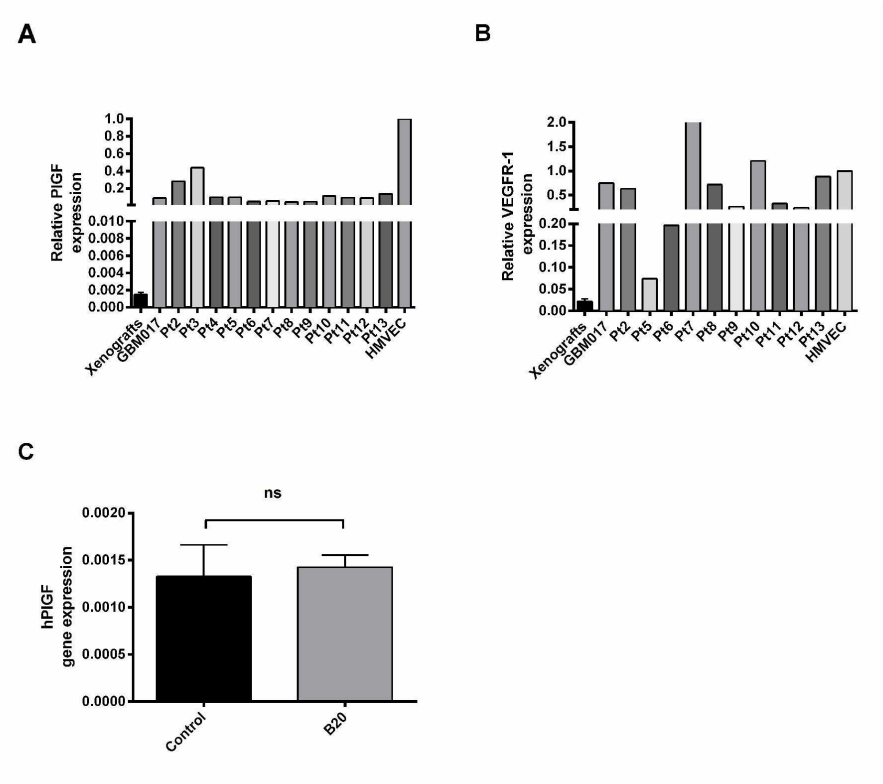

Figure 6: Gene expression of A) PlGF and B) VEGFR-1 in xenografts and a panel of GBM patients including patient GBM017. Values in xenografts are expressed as mean ± SEM (n=12). C) Xenograft gene expression of PlGF in the control group (n=4), the B20 group (n=4). All genes are normalized to reference genes and are relative to human HMVEC.